CHARACTERIZATION OF FIBER REINFORCED EPOXY MATRIX COMPOSITES WITH SINTERED BRONZE AND GRAPHITE FILLERS

Thesis

Submitted in partial fulfillment of the requirements for the degree of

DOCTOR OF PHILOSOPHY

By

NITINCHAND RAMKRISHNA PATIL

Reg.No.121187ME12P04

DEPARTMENT OF MECHANICAL ENGINEERING,

NATIONAL INSTITUTE OF TECHNOLOGY KARNATAKA,

SURATHKAL, MANGALORE - 575025

APRIL, 2019

D E C L A R A T I O N

I hereby *declare* that the Research Thesis entitled **"CHARACTERIZATION OF FIBER REINFORCED EPOXY MATRIX COMPOSITES WITH SINTERED BRONZE AND GRAPHITE FILLERS"** which is being submitted to the **National Institute of Technology Karnataka, Surathkal** in partial fulfillment of the requirements for the award of the Degree of **Doctor of Philosophy** in **Mechanical Engineering** is *a bonafide report of the research work carried out by me.* The material contained in this Research synopsis has not been submitted to any University or Institution for the award of any degree.

Register No. – **121187 ME12P04**

Name of the Research Scholar: NITINCHAND RAMKRISHNA PATIL

Signature of the Research Scholar:

Department of Mechanical Engineering

Place: NITK-Surathkal

Date:

C E R T I F I C A T E

This is to *certify* that the research Thesis entitled **"CHARACTERIZATION OF FIBER REINFORCED EPOXY MATRIX COMPOSITES WITH SINTERED BRONZE AND GRAPHITE FILLERS"** submitted by **Mr. NITINCHAND RAMKRISHNA PATIL** (**Register Number: 121187 ME12P04**) as the record of the research work carried out by him, is *accepted as the Research Thesis submission* in partial fulfillment of the requirements for the award of degree of **Doctor of Philosophy**.

Dr. Prasad Krishna
Professor
Department of Mechanical Engineering
(Research Supervisor)

Dr. Shrikantha S. Rao
Professor and Head
Department of Mechanical Engineering
(Chairman – DRPC)

Dedicated to

My beloved Parents

&

Teachers

ACKNOWLEDGEMENT

This thesis reflects the results of the last five years' work. I have been associated with many people during this work. All these people supported me as and when I approached them. It is an honor and pleasant opportunity to be able to express my gratitude to all of them.

I express my sincere and heartfelt gratitude to my supervisor **Prof. Prasad Krishna** for his support and encouragement. I am fortunate to get his continuous motivation and inspiring me during this work. I am obliged to thank him for providing me the opportunity to pursue my research work.

I am thankful to Prof. K. Uma Maheshwar Rao, Director, NITK, Surathkal, for being an inspiration during his tenure. I am grateful to Prof. Shrikantha S. Rao, Head of the Department of Mechanical Engineering for his help and cooperation. I acknowledge the encouragement and support of Prof. Narendra Nath S., former HOD and the Professors of Department of Mechanical Engineering, NITK, Surathkal

I would like to express my sincere gratitude to Dr. Anandhan Srinivasan, Associate Professor, Dept. of Metallurgy and Material Science, NITK and Dr. Srikanth Bontha, Department of Mechanical Engineering, NITK and Research Progress Assessment Committee members for their suggestions and generosity shown during this research work.

I extend my sincere thanks to all the nonteaching staff, administrative staff and the fellow research scholars of the NITK, Surathkal for their co-operation and wholehearted support.

I express my deep sense of gratitude to Dr. A. M. Gadade, faculty and Tribology Laboratory in-charge at Army Institute of Technology, Pune, for arranging the pin on disc wear test setup as and when required to carry pin on disc wear test.

I am very much thankful to Executive trustee and Secretary of PNES, Pune, for their support and encouragement. I extend my sincere regards to Prof. J. B. Dafedar, Principal, NK Orchid college of Engineering and Technology, Solapur.

I would also like to express my sincere thanks to my colleagues Dr. S.S. Metan and Dr. B. K. Sonage for their motivation and kind support. I would like to thank Mr. Metkari and Mr. Jadhav, workshop instructor for their valuable help during fabrication of pressure die moulding machine and test specimens.

My heartfelt emotions go to my parents, wife and children. This work is possible because of their patience and love. The strong inspiration and support of my dear parents forced me to complete this task of research.

Finally, I would like to mention my better-half, Sapana and sons Yashraj, Pruthviraj for bearing with me during this research work.

<div align="right">

Mr. Nitinchand Ramkrishna Patil
Research Scholar,
NITK, Surathkal.

</div>

ABSTRACT

The characterization of new materials is essential to fulfill the industrial demand these days. Extensive research work in the field of material science and metallurgy is going on across the world. Development of composite material is the area of interest of the researchers and laboratories. Composite material is developed by combining two or more dissimilar materials and the resultant composite exhibits superior properties. The composite materials are popular in various engineering applications like automobiles, aircraft structures and sporting goods. Polymer Matrix Composite has widespread applications due their advantages like high wear resistance, low coefficient of friction, low density, high strength to weight ratio and low cost.

In this study an attempt is made to develop polymer matrix composite material for tribological application. The major requirement of material for tribological application is its high wear resistance and low friction coefficient. To achieve these requirements sintered bronze and solid lubricant, graphite is selected as filler material. Epoxy resin is selected as matrix material because of its low shrinkage, high strength and high adhesive strength properties. Epoxies can be formulated with other materials. Reinforcement provides the strength and stiffness to the composites. Short/chopped glass fiber is used as reinforcing element because of their low cost, high strength, high impact resistance and good chemical resistance. The fillers used are sintered bronze and graphite

The present study focuses on processing, characterization and study of friction and wears behavior of epoxy matrix composite. The experimental investigation is carried out for mechanical and tribological characterization. In mechanical characterization, properties such as density, tensile strength and modulus, flexural strength and modulus, hardness and impact strength are estimated. The use of fiber and fillers showed enhanced mechanical properties of the composites. Tribological characterization is carried out to estimate coefficient of friction and specific wear rate using pin on disc wear setup as per ASME standards. The micrographs of worn pin surface and its debris are carried out to study wear mechanism of the composites. The decrease in specific wear rate of the composites is observed for increase in sliding distance and sliding velocity.

Adaptive Neuro Fuzzy Inference System (ANFIS) Simulink model is used predict the wear rate of the composite. The results show 98% accuracy in prediction of wear rate. The polymer matrix composite developed in this study is used in bearing application (roller and race) and the contact pressure is calculated analytically. Finite Element Method is used to validate the results of contact pressure at the area of contact. The FEA results are very much close to the analytical results.

Key words: *Polymer Matrix Composite (PMC), Tensile and Flexural Strength, Epoxy resin, Fillers-Graphite and Bronze, Reinforcement- Glass fiber, Friction and Wear, Design of Experiment (DOE), Adaptive Neuro Fuzzy Inference System (ANFIS), Contact Pressure.*

CONTENTS

LIST OF FIGURES

ix

LIST OF TABLES

NOMENCLATURE

$\rho_m,$	Density of Matrix Material
ρ_g	Density of Graphite Filler
ρ_f	Density of E-GassFiber
$\rho_b,$	Density of Bronze Filler
ρ	Density (gm/mm^3)
E*	Effective elastic modulus (N/mm^2)
F	Load Applied (N)
Δm	Mass loss (gm)
ρ_{me}	Measured Density (gm/mm^3)
F_n	Normal load (N)
v	Poisson Ratio
P	Pressure (N/mm^2)
V_s	Sliding velocity (m/s)
L	Span Length of the Sample (mm)
τ	Shear Stress
t	Time (sec)
t_s	Thickness of Sample (mm)
ρ_{th}	Theoretical Density (gm/mm^3)
V_c	Total Volume of Composite
V_v	Void fraction
$V_m,$	Volume of Matrix Material
V_g	Volume of Graphite
V_f	Volume of E-Glass Fiber
$V_b,$	Volume of Bronze
W_s	Wear rate
b	Width of the Sample (mm)

ABBREVATIONS

Al$_2$O$_3$	Alumina
ANFIS	Adaptive Neuro Fuzzy Inference System
ANN	Artificial Neural Network
ANOVA	Analysis of Variance
CNF	Carbon Nano Fiber
DOE	Design of experiments
FE	Finite Element
FEA	Finite Element Analysis
FEM	Finite Element Method
FIS	Fuzzy Inference System
GE	Glass Fabric–Epoxy
GFRP	Glass Fiber Reinforced Polymer
MMC	Metal matrix Composite
MoS$_2$	Molybdenum Disulphide
MWCNT	Multi Wall Carbon Nano Tube
OA	Orthogonal Array
PA12	Polyamide 12
PA66	Polyamide 66
PEEK	Poly-Ether-Ether-Ketone
PEI	Polyetherimide
PMC	Polymer matrix Composite
PTFE	Polytetrafluoroethylene

RMSE	Root Mean Square Error
RoHM	Rule of Hybrid Mixture
ROM	Rule of Mixture
S/N ratio	Signal to Noise Ratio
SCF	Short Carbon Fiber
SEM	Scanning Electron Microscope
SGF	Short Glass Fiber
SiO_2	Silicon Dioxide
3D	Three Dimensional
SnS_2	Tin Sulfide
TGA	Thermogrevimetric Analysis
TiO_2	Titania
WC	Tungsten carbide
XRD	X-Ray Diffraction

CHAPTER 1

INTRODUCTION

1.1 GENERAL

There exist more than 50,000 materials to engineers for manufacturing and developing the different applications. Materials like brass, copper and cast iron are available for many years where as advanced materials like composites, ceramic and steels are developed materials (Michael and David 2002).The development of new material is the continuous process in search of economical and environment friendly material. With the advancement in technology, the conventional material needs to be replaced due to number of design constraints and due to specific design requirement like low density and high strength. Hence development of new materials with special properties is the area of interest for the researchers across the globe. It was observed that the composites serve the purpose of low density and high strength. The composite materials are very much popular in various engineering applications like automobiles, marines, sporting goods and aircraft structures.

A composite material is developed by combining two or more dissimilar materials so that the resulting composite exhibits a major part of the properties of the elemental phases without undergoing chemical reaction and maintaining the interface between them. The continuous phase which surrounds the other phase is termed as matrix and the discontinuous phase is called as the reinforcement, if it leads to improvement in mechanical property else called as filler. (Agrawal J. P. 1999). Figure 1.1 show possibilities of combinations of number of materials i.e. metal, polymer and ceramic to form composites. However polymers and polymer composites have replaced the metals because of their ability to tailor the desired requirement by combining the best properties of the materials. This was possible because of various advantages of polymer such as economical, effortless processing, flexible design, rapid manufacturing and tailor-made properties over conventional materials. Amongst the number of polymer matrices, thermoset polymer possesses high strength, good

thermal stability and wears resistance. This blend of properties allows use of epoxy resin in polymer based tribological applications. For these purposes, epoxy resin can be compounded with reinforcement like glass or carbon fiber and inorganic fillers. The properties like friction and wear resistance, tensile strength, compressive strength, dimensional stability and toughness can be improved by addition of fillers in polymeric matrix composites. In addition to above epoxy resin helps in cost reduction.
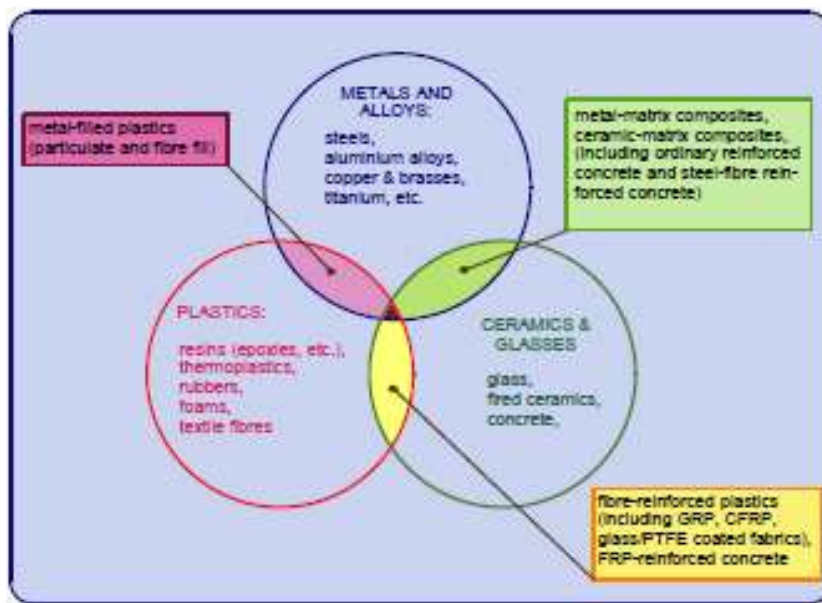
Figure 1.1 Classes of engineering materials showing the evolution of composites (Bryan Harris 1999)

1.2 MOTIVATION AND BACKGROUND

There is extensive study of mechanical and tribological properties of polymer composites filled and reinforced with both natural and inorganic fibers. Extensive study of epoxy matrix composites with solid lubricant is reported by researchers due to its demand in industrial applications. Addition of PTFE, MoS_2 and graphite resulted in variation in properties of epoxy composites. The friction and wear study of PTFE, graphite, Molybdenum disulphide (MoS_2) and Tin Sulphide (SnS_2) of epoxy matrix composite is reported and the reduction in wear rate is observed for only PTFE (Jacobs O. et al. 2004). The tribological performance can be improved by 5–25 wt% of PTFE along with 5–30 wt% of graphite (Zhang X. et al. 2008).The tribological

behavior of polyethylene for 10 wt% of MoS_2 showed increased wear resistance for both abrasive wear and sliding conditions (Pettarin V. et al. 2010). Kumar Hemath et al. (2017) reported 0.002 mm^3/m of the rate of wear for epoxy filled with graphite and aluminium 10 wt% for the speed of 900 rpm. Many researchers found that the solid lubricant only cannot improve the friction and wear behaviour of bare polymer. They found that the fiber reinforcement govern the friction, wear and strength of composites. Addition of 10% glass fiber resulted highest wear resistance. (Bijwe J. and Indumati J. et al. 2004). The enhanced friction and wear properties of glass fiber reinforced-epoxy composites can be achieved by graphite as filler (Suresha B. et al. 2007). Joshi H.C. et al. (2010) reported 4 fold increases in Vickers hardness and 8 fold decreases in moisture absorption rate for 32 vol% glass fibers composite. Sayer Metin (2014) discussed mechanical and flexural properties of glass epoxy composites filled with ceramic particle. The influence of particle size, ceramic fillers and weight fraction on the load carrying capacity of the composites was observed in this study. The addition of boron carbide (10 wt%) showed 42% increase in critical buckling load of composite.

The polymer matrix composites were used as alternate bearing material. There is need to study contact stress behaviour between the rolling and sliding elements. Many researchers have studied the contact stress behaviour and gave solution mathematically and numerically. Merwin J. E. and Johnson K. L. (1963) gave approximate solution of rolling contact deformation mathematically. Balley D. M. and Sayles B. S (1991) developed theoretical technique to determine the subsurface stress field within real rough surfaces subjected to both normal and tangential loads. Cho Young-Tae et al. (2006) studied fretting fatigue in particle reinforced composites under uniaxial tensile loading and under contact stress using FEM. Few researchers used the ANFIS model to study certain behaviour of the material. Ramesh C. S. et al (2014) developed ANFIS Model to estimating sliding wear. They found the accuracy in the range of 90.28% and 91.7 %. Alambeigi Farshid et al. (2016) found that the wear behaviour can be predicted with great accuracy using artificial intelligence techniques such as ANN, FCM, and ANFIS.

1.3 RESEARCH PROBLEM

There is a need to develop alternating materials for better tribological properties without harming environment and with emphasis on economic aspect. The sole aim of this research is to characterize the epoxy composites reinforced with fiber and filled with graphite and sintered bronze and to develop the polymeric-tribo engineering material. In this study the mechanical and tribological characterization of glass fiber reinforced, graphite and sintered bronze filled polymeric composite is carried. However, the replacement of metallic materials by polymers often needs detailed information about its strength in tension, shear, impact and bending along with friction and wear test. The mechanical characterization is carried out to know the strength in static loading conditions. The friction and wear are the basic failure mechanisms of the moving machine elements besides corrosion and fatigue. The friction is caused between the load carrying sliding machine elements. The sliding friction leads to the wear of the machine element and can result in the failure in many cases. Because of the strength, chemical resistance and self-lubricating ability of polymers, they can be chosen as sliding material in many applications of machine construction. It will help the designer to select this material for appropriate applications.

Contact stress analysis for the developed polymer composite is carried by both analytical model and finite element analysis using ANSYS. A cylindrical roller, rolling in hollow cylinder is considered to study contact stress behaviour. The analytical model was developed for cylinder rolling in another cylinder as in case of rolling contact bearing. The results of analytical model for contact stress are verified by developing finite element model using ANSYS workbench. It is observed that the results of analytical model and ANSYS are very close. To predict the wear rate of the composite an Adaptive Neuro Fuzzy Inference System (ANFIS) Simulink model is used. The ANFIS Simulink model gave 99 % accuracy compared to experimental results.

1.4 ORGANIZATION OF THESIS

The remaining thesis is organized as follows

Chapter 2   Contains the extensive literature review which highlights the results of research work by various investigators. This chapter covers research work on polymer matrix composites, tribological study of composites, Contact stress analysis.

Chapter 3   Deals with the materials and methods used to achieve the objectives of the research work. It describes the fabrication and characterization of the composites. It elaborates Taguchi orthogonal array, ANFIS Simulink model and FEA.

Chapter 4   Includes the mechanical characterization of the composites under study

Chapter 5   Describes the wear and friction behaviour of the composites under study and studies the effect of control parameters on wear rate. It discusses ANOVA results, TGA and XRD analysis of the pin specimen debris. It shows the prediction results of ANFIS Simulink model.

Chapter 6   Describes the analytical contact pressure between the roller cylinder and flat surface. It discusses the results of FEM for contact pressure and compares it with analytical results.

Chapter 7   Provides the conclusion and summary of the research work, outlines the major observation from experimental and analytical study. It provides the future scope of this research work.

CHAPTER 2

LITERATURE REVIEW

The literature review outlines the detailed background of the research work presented in this thesis and its relevance to the present study. The research studies undertaken by the researchers related to mechanical and tribological characterization, prediction of friction and wear behavior using artificial intelligence techniques and contact stress simulation using FEM tools of reinforced polymer matrix composites are presented here. This literature review is limited to the reviews of:

- Mechanical characterization of reinforced PMC
- Friction and wear of particulate filled PMC
- Tribology of fiber reinforced PMC
- Friction and wear of hybrid PMC
- Wear test by Taguchi OA
- Artificial Intelligence technique- ANFIS
- FEM simulation of contact stresses

The summary and the research gap of the previous investigations are given at the end and are followed by the objectives of the present research work.

2.1 MECHANICAL CHARACTERIZATION OF REINFORCED PMC

Most of the researchers reported the mechanical properties of the PMC reinforced with natural, glass and carbon fiber along with different filler particulates. It is observed that the combination of matrix type, filler and reinforcement has great influence on mechanical behavior of PMC. Other factors like volume percentage, modifying agents and curing cycle that govern the mechanical properties of PMC are also reported. Use of submicron inorganic filler indicates significant improvement in the thermoset polymer performance (Bondioli Federica et al. 2006). Strength and toughness of particulate composite depend on particle size, particle/matrix adhesion and particle loading but particle/matrix adhesion is most effective and the stiffness

depends mostly on particle loading (Fu Shao-Yun et al. 2008). Guo Qing Bing et al. (2010) reported mechanical and tribological study of epoxy composites filled with lubricant oil-loaded microcapsules, surface grafted nano-SiO$_2$ and discontinuous carbon fibers and observed balanced mechanical properties.

Joshi H. C. et al. (2010) investigated experimentally and using rule of mixture (ROM) the thermal, mechanical and wear resistance behaviour of glass fiber-epoxy composites filled with borosilicate glass powder and found the close agreement between the experimental and ROM values except for coefficient of thermal expansion. Varga C. S. et al. (2010) found remarkable improvement in mechanical properties of polyester by reinforcing chopped glass fiber whose surface is modified by additives. They reported 38.9% and 21.9% improvement in tensile and flexural properties respectively. There is a high potential for increasing the fatigue life of GFRP under mechanical loading by incorporating the nanoparticles. Boger Lars et al. (2010) investigated fatigue life of glass fiber reinforced fumed SiO$_2$ and MWCNT nano-filled epoxy composites and reported 16% increase in inter fiber fracture strength that lead to increased high cycle fatigue.

Improvement in tensile strength and reduction in impact strength of short glass fiber reinforced polyamide-6 was reported by Li Du-Xin et al. (2010). They also observed the use of glass fiber is effective in reducing the friction and wear of the composites. The use of PMC in structural materials has been increasing significantly because filled and glass fiber reinforced epoxy composite showed increased compressive and impact strength (Singhal Manoj 2010). Mechanical and dry sliding wear study of epoxy-Titania (TiO$_2$) homogeneous and functionally graded composites were reported by Siddhartha et al. (2011). They found dramatic improvement i.e. 91% increase in impact strength for 10 wt% TiO$_2$ of functionally graded composite over homogeneous one. The effect of surface modification of aluminium powder on mechanical and wear properties of epoxy composites was reported by Kim Sung Soo et al. (2012). They observed tensile modulus and strength were 9% and 12% greater over untreated aluminum filler. Hassan S. B. et al. (2012) developed eco-composite by making use of agro waste and reported enhanced tensile strength and modulus for higher wt% of carbonized maize stalk particles with polyester composites but found reduced impact strength.

7

Siddhartha and Gupta Kuldeep (2012) compared mechanical and abrasive wear behaviour of bi-directional and chopped E-glass fiber reinforced epoxy composites and found improved tensile strength of epoxy composites with bi-directional glass fiber whereas epoxy composites with chopped E-glass fiber showed superior wear performance over bi-directional fiber. Mohanty Akash and Srivastava V. K (2012) investigated mechanical properties of short glass/carbon fiber reinforced epoxy composites filled with alumina nano particle and found improved compressive strength of glass fiber with 2% alumina nano particles whereas hybrid composites showed remarkable strengthening effect. Flexural properties of treated (6% NaOH) and untreated kenaf fiber-epoxy composites were reported by Yousif B. F. et al. (2012) and observed 36% increase in flexural strength for treated over untreated kenaf-epoxy composite.

Raju Bhadrabasol Revappa et al. (2013) investigated mechanical and tribological behavior of glass fiber reinforced epoxy composites filled with alumina (Al_2O_3) experimentally and found raise in tensile strength for 7.5 wt% of filler addition, beyond 7.5 wt%, it was marginal. It was also reported that the addition of Al_2O_3 with glass epoxy has improved abrasive wear to great extent. Shivamurthy B. K. et al. (2013) investigated mechanical and sliding wear behavior of glass fabric/graphite/epoxy composites and observed the optimum mechanical and wear performance of composites for 3 wt% of graphite. Sudheer M. et al. (2013) studied abrasive wear behavior and mechanical properties of epoxy composites with MoS_2 filler, with and without glass fiber mat and reported detrimental effect on flexural strength over tensile properties. It is obvious from the results that addition of MoS_2 brought down wear rate and further reduction in wear was observed with glass fiber reinforcement.

The effect of SiO_2 on mechanical and dry sliding wear of glass epoxy composites was studied by Anjum Naveed et al. (2013) and reported improved flexural strengths, impact strengths, hardness and density of the composite and the wear rate reported was almost 40% lower than unfilled composite. Zhang Yongli et al. (2013) studied tensile and interfacial properties of natural and synthetic fibers and found the enhanced mechanical properties with increase in glass fiber content. Glass fiber epoxy composites containing ceramic whisker and solid lubricant graphite was developed by

8

Sudheer M. et al. (2014) to study mechanical and wear performance. The addition of graphite showed increase in strength and wear properties. Sayer Metin (2014) investigated experimentally and numerically the elastic properties of E-glass fiber reinforced epoxy composites filled with ceramic particles and reported that the particle weight fraction and particle sizes influence the elastic modulus and load carrying capacity. The increase in critical buckling load carrying capacity reported was 42% for 10 wt% of boron carbide composites.

Raja Satheesh R. et al. (2014) reported elastic properties of polymer composites impregnated with fly ash and reinforced with glass fiber and found maximum hardness, tensile and flexural strength for 30 wt% of glass fiber without fly ash but on the addition of fly ash, above properties showed maximum values for 10 wt%. It was concluded that addition of fly ash along with fiber enhanced the mechanical behaviour of the composites. Detomi Anine et al. (2014) described influence of ceramic particles on flexural behavior of epoxy composites reinforced with glass fiber and observed 110% improvement in flexural strength for the micromechanical configuration with ceramic particle located at upper side and found 10 wt% of silica particles to obtain the same. Omrani Emad et al. (2015) reported enhanced bending strength and modulus of carbon fiber epoxy composites and also found improved tribological properties because of carbon fiber reinforcement.

Saba N. et al. (2016) described dynamic mechanical properties of oil palm nano filler/kenaf/epoxy hybrid nano composites and found increased storage modulus and loss modulus values due to good fiber-matrix bonding. Yesgat A.L. and Kitey R. (2016) investigated effect of glass particle (milled and spherical) filler geometry and volume fraction on fracture mechanism and flexural properties of epoxy composites and reported higher flexural modulus and fracture toughness for milled-fiber with increased filler volume fraction, whereas spherical particles reinforcement showed better flexural strength.

Effect of high graphite filler loading on strength and wear behaviour of epoxy composites was studied and it leads to high elastic modulus materials and increased brittle behavior of the composites (Baptista R. et al. 2016). Various micro and nano fillers were added to improve the tensile strength, thermal and wear resistance of

9

polymer composites (Abenojar J. et al. 2017). Jo Hyu Sang and Lee Gyo Woo (2017) investigated thermal and mechanical characteristics of silica reinforced epoxy composites and observed improved mechanical strength and elastic modulus by 8-10% and 51-55% respectively at the same time there was reduction in ductility by 34%.

Natural fiber reinforced composites are gaining attention of industry over glass and carbon fibers. India has large production of rice husk, stalk, baggase, jute, coconut fibers and hemp. Investigation of mechanical properties of glass and sugarcane reinforced fiber epoxy composites was carried and it was found that addition of natural fiber with chopped glass fiber improved mechanical properties to a great extent. (Kumar Hemath et al. 2017). Khan Ziaullah et al. (2017) used treated bamboo fibers of varying length to study fracture behavior of randomly reinforced epoxy composites experimentally and numerically and reported higher fracture toughness for the fiber length of 25mm. Matykiewicz D. et al. (2017) studied thermal conductivity and elastic behavior of epoxy matrix composites with basalt fibers and powder and the hybrid effect showed improved stiffness and thermal resistance of epoxy composites. Mahato Kishore Kumar et al. (2017) compared the effect of loading rate of thermal shocked glass fiber- epoxy composites on tensile strength and modulus and observed that ultimate tensile strength for all loading is higher for thermal shock conditioned (TSC) composites over RT specimens. It was also noticed that the tensile modulus was insensitive to the loading rate and fiber-matrix interfacial bonding in case of TSC was better as compared to RT composites.

Torres Rubens Bagni et al. (2017) investigated elastic properties of glass fiber reinforced silica/cement epoxy composites and found 67% increase in compressive modulus for 5 wt% of cement particles on the other hand an increase in number so layers from 7 to 11 reported 56.5% increase in composite stiffness. Rafiq Ahmad et al. (2017) reported 23% improvement in peak load and 11% increase in stiffness for 1.5 wt% of nano-clay in glass fiber reinforced epoxy composites. Kwon Dong-Jun et al. (2017) used SiC and SiO_2 nanoparticles to study elastic and thermal behaviour of epoxy composites reinforced with glass fiber and found that SiC-epoxy showed better thermal resistance over SiO_2-epoxy composites because SiO_2 induces weak hydrogen bonding due to oxygen. The reduction in tensile strength from 20% to 50% was

reported for thermal aging of day 1 to day 6. Hung Pui-yan et al. (2018) demonstrated low velocity impact response of hybrid (carbon and glass) fiber epoxy composites and found minimum damage of hybrid composites with carbon fiber layer at top and bottom surface because the flexural strength depends on the strength of bottom layer.

Sepe R. et al. (2018) presented mechanical properties of surface treated hemp fiber reinforced epoxy composites and the results show improved mechanical characteristics of the composites for silane treated fibers. Bazrgari D. et al. (2018) observed increased bending strength and impact strength for 3 vol% of Al_2O_3 nanoparticles whereas reduction in wear was observed for 1 vol% of Al_2O_3/epoxy composites. Ulus Hasan et al. (2018) investigated static and dynamic response of $CaCO_3$ nanoparticle filled epoxy/carbon fiber composites and found 48%-47% increase in tensile and flexural strength for 2 wt% of $CaCO_3$ respectively.

2.2 FRICTION AND WEAR OF PARTICULATE FILLED PMC

Polymer composites been filled with micro-particles and nano particles to have specific properties is well known practice in the field of development of materials. It is also been used to control density, reduce cost, control thermal expansion and thermal conductivity and to improve elastic and wear properties. The wear resistance can be reduced by addition of particle fillers (Xing X.S. and Li R.K.Y. 2004) and depends on its content, particle size, interfacial adhesion of filler and matrix, uniform dispersion and also depends on the wear test condition like sliding speed, sliding velocity, normal load and temperature.

Large numbers of particulate fillers (graphite, MoS_2, Al_2O_3, SiC, TiO_2, SiO_2, $CaCO_3$ and PTFE) has been used to reduce the wear and to enhance the frictional coefficient of the epoxy matrix composites for last few decades. Li Xiubing et al. (2004) discussed wear mechanism of graphite and MoS_2 filled epoxy composites and found that graphite filler reduces the friction coefficient and increased the wear resistance to a great extant. On the other hand MoS_2 showed increase in wear resistance only and do not have any influence on the friction coefficient because of formation of MoO_3. However addition of graphite more than 30 vol% showed increased wear rate of the epoxy composites. Bhagyashekar M. S. and Rao R. M. (2007) investigated friction

and wear study of graphite and SiC filler epoxy composites and found superior wear resistance characteristics of graphite-epoxy compared to SiC-epoxy composites. Composites with 0 to 5% filler showed sudden reduction in wear loss and thereafter showed gradual wear till 40% of filler loading which indicated stabilization of wear. Tribological behaviour of nano (CuO) and micro (PTFE) particle filled epoxy composites was investigated by Larsen et al (2008) and observed that the coefficient of friction is independent of CuO, but addition of PTFE showed 35% reduction. Addition of CuO with PTFE beyond 0.4 vol% showed increased wear rates and concluded that the effect of addition of particles is to stabilize the transfer film in case of epoxy composites.

The solid lubricant filled PMC showed increased wear resistance under abrasive and sliding wear circumstances (Pettarin V. et al., 2010). It was found that MoS_2 helped in dissipating the heat generated on surface melting of polymer that lead to reduce the wear. The adhesive wear mechanism was observed under sliding condition wherein a uniform adherent transfer film was formed on the counter surface. Luo Y.et al. (2010) investigated effect of grafting of filler on tribological performance of epoxy composites using dry ring-on-block wear tester and found lowered friction coefficient and improved sliding wear resistance. Lower percentage (7%) Glycidylmethacrylate grafted nano-Si_3N_4 filler showed better dispersion due to separation of agglomerated nanoparticles. Yang Yu-lin et al. (2010) reported tribological behaviour of expanded graphite filled PTFE matrix composites and results reveal 15 wt% of nano EG-PTFE composite improved 31.6 times the wear resistance as compared to neat PTFE composites. The transfer film on counter surface prevents the damage of metal substrate along with reducing friction coefficient and wear rate. Chauhan Santram and Thakur Sunil (2012) investigated friction and wear characteristics of cenosphere filled vinyl ester composites and reported reduced friction coefficient and wear rate for 2, 6, 10 and 15 wt% cenosphere-vinyl ester composites when normal load and sliding speed is increased.

Jin Hongyun et al. (2013) reported the influence of spherical silica powder on friction and wear properties of phenolic matrix composites and reported enhanced friction coefficient for irregular and surface treated spherical silica whereas increased wear resistance was observed for only surface treated spherical silica. Wang Shibo et al.

(2013) studied friction and wear behavior of PTFE composite filled with hexagonal boron nitride (h-BN) and poly (phenyl p-hydroxybenzonate) (PHBA) and reported increased hardness and thermal diffusivity increased but decreased tensile and impact strength. About 15 times reduced wear rate was observed for 20 wt% of both PHBA and h-BN-PTFE composites. Bhagat Subita and Verma Pardeep Kumar (2013) studied effect of graphite on epoxy matrix composites and concluded that the particle filler dispersion condition, particle size and aggregate structure greatly control the properties of the composites. The XRD study showed decreased amorphosity and increased crystallinity with increase in graphite content.

The dry sliding friction and wear study of zirconium oxide (ZrO_2) filled poly (methyl methacrylate) (PMMA) composites were carried out by Akinci A. et al. (2014) and reported that the friction coefficient and wear rate depends largely on sliding speed, applied load and filler percentage. The increase of ZrO_2 up to 30 wt% showed decreased trend in wear rate for increased load and sliding speed. Atuanya C. U. et al. (2014) carried thermogravimetric analysis (TGA) and pin-on-disc wear test and concluded that addition of filler enhanced both wear resistance and thermal decomposition temperature due to uniform distribution of the filler particles. Sliding speed and applied load showed key part in the composite wear. You Yi-Lan et al. (2014) described influence of solid lubricants (TiO_2, MoS_2, and PTFE) on tribological behavior of polyamide 6 nano-composites and reported improved wear resistance due to increased adhesion between transfer film and counter surface. The test parameters, applied load and sliding velocity has no effect on the friction coefficient whereas increase in load lead to increased wear rate and decreases with increased velocity. Shen J. T. et al. (2015) studied friction and wear performance of PTFE and SiO_2 filled epoxy composites and observed friction coefficient of 0.095 and wear rate of 8.4×10^{-7} mm^3/Nm for 12.5 wt% of PTFE for 2000 m of sliding distance.

Tahir Noor Ayuma et al. (2016) investigated tribological behavior of palm kernel activated carbon epoxy composites and concluded that the composite has the ability of self-lubricating property at temperature below 90^0C. Karami Pooria and Shojaei Akbar (2017) studied dry sliding tribological behavior of nano-diamond containing carboxylic group (ND-COOH) filled polyamide 6 (PA6) and found decreased friction coefficient and specific wear by around 60% and 30% respectively for 1 wt% of the

13

ND-COOH and suggested that ND particles can be used as self-lubricant, heat conductors at contact surface and reinforcement of polymer composites.

2.3 TRIBOLOGY OF FIBER REINFORCED PMC

The fiber reinforcement has major influence on the mechanical (strength and stiffness) and tribological (friction and wear) properties of the PMC because of its large aspect ratio that helps to transfer shear stress between the matrix and the reinforcement. The reinforcing fibers carry the load and the surrounding matrix holds them together and helps to transfer the load and protect them from environmental changes like temperature and humidity. Larsen Thomas Ø. et al. (2007) investigated the role of glass and aramid-carbon fibers epoxy composites on tribological behaviour of the PMC and reported that the glass fibers are superior to the carbon and especially aramid fibers because of it higher compressive stiffness and strength. The friction coefficient was reduced by 35% by substituting the glass fiber weave with carbon-aramid weave. Yousif B.F. and El-Tayeb (2008) carried wet friction and wear characteristics of chopped glass reinforced polyester composites using pin-on-disc and block-on-ring techniques and concluded that the chopped glass fibers orientations and test parameters significantly influence the friction and wear behaviour of the PMC, whereas the wet test resulted in the rough counter surface in both test techniques. Davim Paulo J. and Cardoso Rosaria (2009) studied effect of carbon and glass fiber reinforcement on friction and wear behaviour of (poly-ether-ether-ketone) PEEK and observed increased friction coefficient and specific wear rate with the increased sliding speed. PEEK-carbon fiber composite resulted lesser friction coefficient whereas PEEK-glass fiber showed lesser specific wear rate.

Friction and wear study of carbon nano fiber (CNF) reinforced (high density polyethylene) HDPE composites was reported by Xu Songbo et al. (2012). They observed reduced friction coefficient and increased micro hardness of the nanocomposites with the addition of CNFs. The use of silane coating of CNF (0.5 wt%) showed 35% reduction in the wear rates. Kim Sung Soo et al. (2012) investigated tribological properties of short glass fiber reinforced polyamide 12 (PA12) and reported that the 30 wt% glass fiber content has great influence on friction

and wear resistance as compared to its orientation. The glass fiber helped to increase the strength and prevented the deformation of the soft PA12 matrix. Nirmal Umar et al. (2012) investigated the adhesive wear and frictional performance of bamboo fiber reinforced epoxy (BMBFRE) composite and the results showed excellent wear resistance for anti-parallel oriented fibers whereas the friction coefficient was increased by 44% at low sliding velocity because of the thin layer of shield which prevents debonding of the fibers. Zhao Gai et al. (2013) evaluated effect of reinforcements on friction and wear of fiber reinforced polyimide composites under dry sliding conditions and concluded that the fiber breaking, matrix fracture and fiber-matrix debonding are the major mechanisms of PMC wear. It was reported that use of fibers into polyimide matrix under dry sliding conditions resulted improved wear resistance.

Effect of dry and wet sliding conditions of epoxy composites reinforced with carbon fiber were compared by Dhieb H. et al. (2013). They found large degradation of anti-parallel sliding due to debonding and breaking of the carbon fibers over sliding in parallel and perpendicular directions. Agrawal Sandeep et al. (2016) reported tribological properties of epoxy resin reinforced with glass fiber and discussed the comparative results under dry, oil-lubricated and inert gas (argon)sliding conditions and found maximum value of friction coefficient for inert gas sliding and lowest for oil lubricated sliding due to transfer film. It was concluded that the sliding velocity and normal load govern the rate of wear to a great extent. Venkata Krishna K. and, Kanny K. (2016) investigated the effect of surface modification of kenaf fiber reinforced epoxy composites using amino acids. The surface was modified by glutamic acid (acid) and lysine (base). The results showed improved tensile properties in both the cases because of amino acid treatment that improved fiber matrix interfacial adhesion. Shuhimi Fairuz Fazillah et al. (2016) compared dry sliding tribological performance of oil palm fiber-epoxy and kenaf fiber-epoxy composites and reported reduced friction coefficient and increased wear on increased temperature for both the composites. It was reported that the existence of a thin lubricating layer of matrix resin and low shear strength are responsible for lower friction coefficient.

2.4 FRICTION AND WEAR OF HYBRID PMC

Self-lubricating characteristics of the polymer make them special class of material and do not need external liquid lubrication for its function. However there are some thermal related limitations like lower thermal stability, conductivity, diffusivity and high thermal expansion coefficient restricts its use under high load and speed. Hence the fiber and particulate reinforcement are used to develop mechanical, thermal and tribological properties in PMC. Bijwe J. and Indumati J. (2004) studied the influence of glass fibers and solid lubricants (PTFE, MoS_2 and graphite) on oscillating wear of polyetherimide (PEI) composites and observed that addition of glass fiber showed 5-6 times improved wear resistance with no effect on friction coefficient. However the addition of three lubricants showed 10-17 times improvement in friction and wear performance of PEI composites. Kishore P. et al. (2005) reported comparative study of rubber and graphite filled glass-epoxy composites and observed that for all combinations of load and velocity, the graphite filled glass fiber-epoxy composites showed lower friction coefficient.

The influence of SiC and graphite on the tribological behavior of glass fabric reinforced epoxy composites with varying load and sliding velocity was reported by Suresha B. et al. (2006). They observed lower friction coefficient for graphite filled composites irrespective of increased load and sliding velocity whereas composites with SiC filler exhibited maximum wear resistance. Zhang Hui et al. (2007) reported tribological wear resistance of short carbon fiber (SCF) reinforced epoxy composites using both a block-on-ring and a pin-on-disk wear tests and found that increase in fiber length improved wear resistance by 3 times and concluded that the addition of graphite flake and nano-TiO_2 improved wear resistance because of formation of thin lubricating film on the opposite surface. Larsen Thomas Ø. et al. (2008) studied the effect of glass fiber weave reinforcement and PTFE-nano-CuO particle addition on tribological behavior of epoxy matrix composites for different contact pressure and sliding velocity. They found 35% reduction in friction coefficient by replacing glass fiber with carbon/aramid weave. The addition of PTFE/nano-CuO showed no effect on friction coefficient and little effect on wear. Sua Feng-Hua et al. (2008) reported tribological behaviour of TiO_2 filled glass/PTFE composites and observed that

addition of 4% TiO$_2$ showed reduced wear rate but increased friction coefficient of hybrid glass/PTFE composites under dry sliding condition and not suitable for wet (oil or water) condition. SEM images showed formation of transfer films on counter surface for unfilled and filled composites but filled composites exhibited bonding strength between transfer film and counter surface hence increased wear resistance.

Friction and wear properties of fiber reinforced polyimide composites filled with MoS$_2$ and carbon was investigated by Zhang X. R. et al. (2008) and they observed that an increased wt% of MoS$_2$ enhanced wear resistance and reduced friction coefficient not only because of anti-shear ability of MoS$_2$ but because of the worn debris that formed the lubricating film when the load is increased. Guo Qing Bing et al. (2009) investigated sliding wear behaviour of carbon fiber reinforced epoxy matrix composites filled with grafted hybrid nano-SiO$_2$ and found that the hybrid composite (4 wt% nano-SiO$_2$ and 6 wt% carbon fiber) resulted lowest friction and wear rate due to rapid development of thin lubricating film. The grafted filler reacted with the epoxy and enhanced the filler and matrix adhesion of PMC. Chang Li and Friedrich Klaus (2010) reported effect of nano-filler (graphite and PTFE) on short glass fiber reinforced epoxy/polyamide 66 (PA66) composites and found positive effect of graphite and PTFE nano fillers on friction and wear. It was concluded that the short fibers decrease wear rate and increase load sustaining ability of the composites to a great extent. The use of solid lubricant graphite and PTFE led to formation of continuous transfer film and resulted in decreased/stabilized friction coefficient. The nano fillers helped in reducing the adhesion thus acted as spacers. Guo Qing Bing et al. (2010) optimized the friction and wear properties of epoxy composites through hybrid filling and found improved tribological and balanced mechanical properties. The oil loaded microcapsules resulted reduced wear rate and friction coefficient due to oil released during sliding. Mohan N. et al. (2011) reported abrasive wear behaviour of glass fabric–epoxy composites filled with tungsten carbide (WC) and tantalum niobium carbide (Ta/NbC)) and found decreased specific wear rate for filled GE composites.

The tribological behaviour of PTFE filled GF polymer composites under oil and graphite mixed oil conditions were experimentally investigated by Kharde Y.R. and Saisrinadh K. V (2011). They found that the friction coefficient and specific wear rate

significantly affected by load and surface conditions. Both COF and specific wear rate was reduced at higher load and velocities due to formation of micro thin layer of transfer film. Hence the composites offer high resistance to wear at higher loads. Zhang G. et al. (2012) studied the effect of SiO_2 nanoparticles on friction and wear behaviour of short carbon fiber epoxy composites filled with graphite flake when sliding against rough and polished counter surface and found significant reduction in the friction and wear rate as compared to sub-micron particles. The grooves of rough counter surface were responsible to form transfer film whereas in case mirror finish counter surface the transfer film forms only after the counter surface undergo scratches this was observed for the sub-micron particle composites.

Friction and wear study of silicon carbide and graphite filled glass–epoxy (G–E) composite were reported by Basavarajappa S. and Ellangovan S (2012). They observed the good wear resistance for filled glass–epoxy composites due to formation of thin lubricating film which further reduces the frictional heating. It was noticed that the addition of filler improved the binding strength between the fiber and matrix. The load applied and sliding distance showed negligible change in wear rate as compared to sliding velocity. Sudheer M. et al. (2013) reported effect of the MoS_2 filler epoxy-fiber composites and observed significant reduction in specific wear rate and enhanced mechanical properties. The flexural property was reported an increase of 32% for MoS_2 filled glass fiber epoxy composites. The presence of solid lubricant, MoS_2 helped to reduce the wear rate even at high loads because MoS_2 particles act as a barrier for large scale deformation.

Tribological behaviour of hybrid epoxy composites filled with solid lubricant under water lubricating conditions was investigated by Gao C. P. et al. (2016). The reinforcing element used was short carbon fiber (SCF) and short glass fiber (SGF) and the fillers used were graphite, SiO_2 and PTFE. It was demonstrated that carbon and glass fiber enhanced the wear resistance of the composites due to their high abrasion resistance but concluded that SCF is more suitable reinforcement under water lubricated condition over SGF. The addition of graphite with SCF-EP showed remarkable reduction in friction coefficient because of uniform tribo-film developed on the counter face due to laminar structure of graphite. Qi Huimin et al. (2016) studied impact of counterpart material on tribological performance of epoxy

composites filled with SCF and graphite and SiO_2 and found that the counterpart material play important role in material transfer and formation of tribo / transfer film. Addition of SiO_2 resulted in improved load carrying capacity of the transfer film during friction process. It was concluded that the oxidation resistance of counterpart influence the formation of lubricating transfer film. Song Fuzhi et al. (2016) investigated effect of glass fiber and MoS_2 on tribological performance of SCF reinforced PTFE composites and found that either glass fiber or MoS_2 on their own could not improve tribological performance but the hybrid filling showed best tribological behaviour with highest pressure-velocity limits of 9.5 MPa m/s at 1 m/s and 15 MPa m/s at 2 m/s.

Friction and wear behavior of carbon /PTFE - epoxy composites filled with graphite and MoS_2 under heavy load and oil lubricating conditions was studied by Sun Yousong et al. (2016). They observed 40%, 91% and 64% reduction in the friction coefficient, wear volume and temperature rise of the 6 yarns PTFE reinforced composites respectively over without PTFE composites. It was noted that addition of PTFE reduced frictional heat and temperature rise this resulted in reduced friction and wear rate of the composites. The combination of carbon (low wear resistance) and PTFE (higher wear resistance or anti-wear property) fabric helped each other to overcome their limitations. Zhang Ligang et al (2016) discussed effect of silica nano particles (SiO_2) on tribological behaviour of epoxy composites reinforced with CNT, SCF and SGF and found 40% reduction in wear rate for the SiO_2/CNT/EP composites due to development of thin lubricating film whereas SiO_2/SCF/EP composite resulted 91.9% reduction in wear rate due to its load carrying ability. The formation of transfer film of solid lubricant was observed after the addition of graphite filler which in turn helped to reduced friction and wear. The reduction in friction coefficient and wear rate was 34% and 67% respectively for the combination SiO_2/SGF/EP/Gr/PTFE. It was observed that the silica based transfer film could not be formed due to abrasive nature of SGF and therefore it was advised not to use hard nano-particles in the SGF reinforced epoxy composites.

Tribological behaviour of glass fiber reinforced epoxy composites filled with solid lubricants and silica under oil lubricated conditions was reported by Zhao Fuyan et al.

(2016). The SGF reinforcement showed remarkable decrease in tribological behavior of epoxy composites due to its high load carrying capacity, resistance to abrasion and ability to form tribo film. It was noticed that the addition of 10% SGF reduced friction coefficient of epoxy by 67.42% and wear rate by 87.34% and found no change when SiO_2, graphite and PTFE were added. The tribological mechanism of epoxy composites reinforced with SGF under oil lubricating condition is shown in Figure 2.1. Zhang Ligang et al. (2017) reported friction and wear performance of PTFE/SiO_2 filled polyoxymethylene (POM) composites reinforced with SCF, aramid particles (AP) and SGF and found synergetic effect of AP with PTFE and SiO_2 nanoparticles as compared to SCF and SGF.
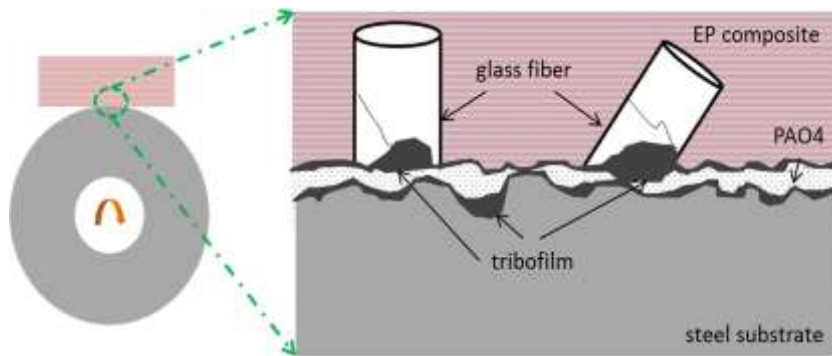
Figure 2.1 Tribological Mechanism of SGF Reinforced Epoxy Composites Under Oil Lubricated Condition. (Zhao Ligang et al. 2016)
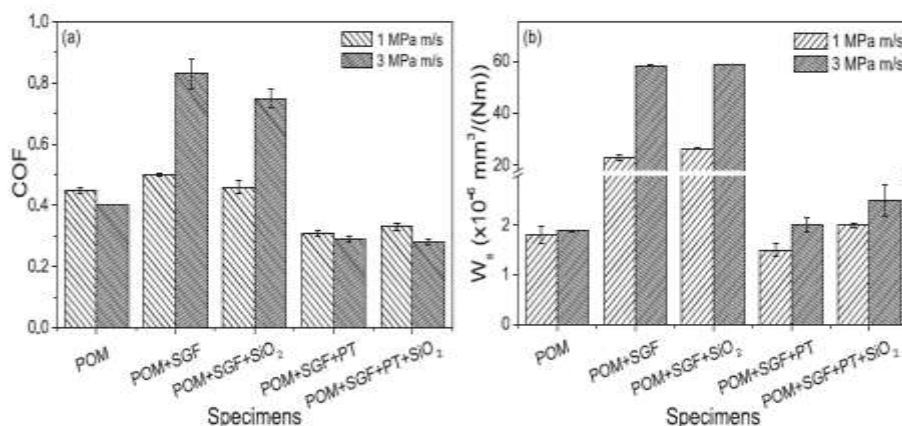
Figure 2.2 Friction Coefficient and Wear Rate of POM Composites. (Zhang Ligang et al. 2017)

The POM/AP/PT combination showed highest wear resistance due to the formation of high bonding transfer film. Figure 2.2 indicate the results of friction coefficient and wear rate of POM composites.

Friction and wear behaviour of carbon fiber reinforced PEEK composites filled with oxide nano-particles at a low FV (force $\times$ speed) condition was reported by Guo Lihe et al. (2017). They observed dramatic improvement in friction and wear properties for hard nano-particles SiO_2 and ZrO_2 at FV condition of 30 to 300 N m/s, however ZrO_2/SCF/PEEK combination showed excellent self-lubricating ability under severe loading condition at FV values of 100 to 300 N-m/s. The schematic illustration of tribo film formation due to ZrO_2 is shown in Figure 2.3.
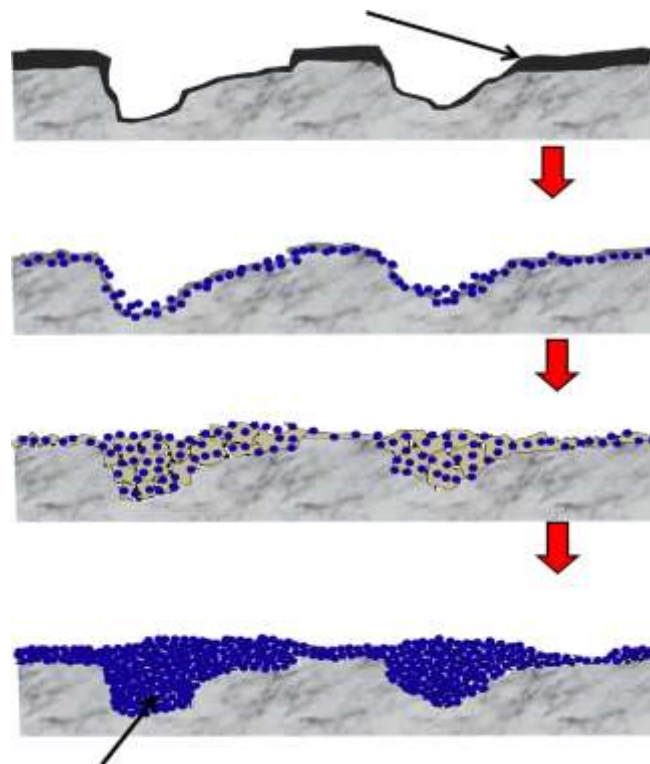
Figure 2.3 Tribo-Film showing Effect of ZrO_2 Nano-Particles. It carries Iron oxide, ZrO_2 and Remnant PEEK. ZrO_2 Nano-Particles are seen in blue dots (Guo Lihe et al. 2017)

Zhao Fuyan et al. (2017) investigated the effect of ZnS particle on SCF and SGF reinforced polyimide composite under oil lubricated condition and found that SGF reinforcement is more effective in reducing friction and wear of the composite than SCF reinforcement. The hybrid composite ZnS/SGF/PI under lubricated condition

showed excellent friction and wear performance. Figure 2.4 indicate the effect of sliding speed on the friction coefficient and wear rate. It was observed that in case of lubricated condition the SGF reinforced composite exhibited superior tribological performance than SCF because of the higher abrasive resistance of SGF and presence of oil molecules led to mitigation of the abrasiveness caused by SGF
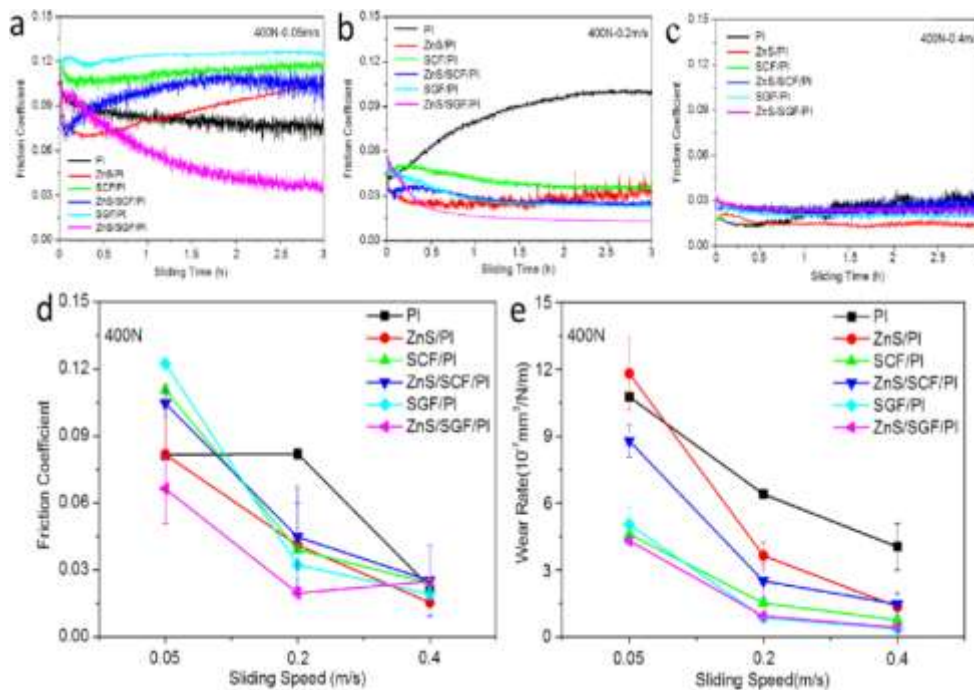
Figure 2.4 Effect of Sliding Speed on Friction Coefficient and Wear Rate (Zhao Fuyan et al. 2017)

2.5 FRICTION AND WEAR OF PMC BY TAGUCHI METHOD

Basavarajappa S. et al. (2009) studied the effect of filler on dry sliding wear behaviour of PMC using Taguchi experimental design and observed that the inclusion of SiC and Graphite in glass epoxy composites enhanced the wear resistance of the composite greatly. L_{27} orthogonal array and analysis of variance (ANOVA) were used to investigate the influence of process parameters on the wear of these composites. ANOVA indicated applied load (p=51.40%), sliding distance (p=20.2%), sliding speed (p=4.52%) and the interaction of sliding speed and sliding distance (p=4.5%) influence the wear significantly. Biswas Sandhyarani and Satapathy Alok (2009) studied red mud filled glass fiber reinforced epoxy composites using L_{27} (3^{13})

orthogonal design and found that red mud content, erodent temperature, stand-off distance, impingement angle and impact velocity respectively significant factors to minimize the erosion rate. The peak erosion rate was observed for the 60^0 impingement angle for all composite. Addition of red mud filled glass epoxy composite exhibited improved erosion wear performance.

Effect of fillers on erosive behaviour of glass polyester composites using $L_{27}(3^{13})$ Taguchi orthogonal design were investigated by Patnaik Amar et al. (2010). The results showed the combinations of factors which produces minimum wear of composites as shown in Figure. 2.5. The control factor which influences the wear performance was analysed by ANOVA and for fly ash composite.
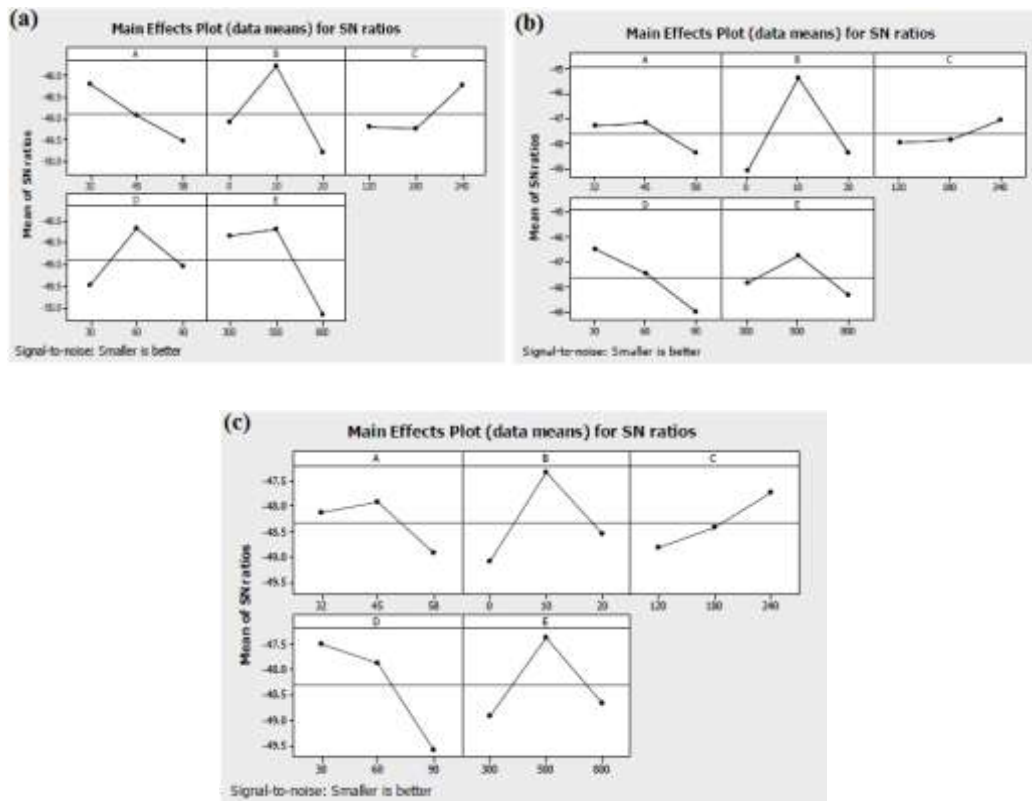
Figure 2.5 Influence of Control Parameter (a) Composite Filled with Fly Ash (b) Composite Filled with Al₂O₂ (c) Composite Filled with Sic (Patnaik Amar et al. 2010)

Subbaya K. M et al. (2012) studied multiple response optimization of three body abrasive wear behaviour of graphite filled carbon-epoxy composites using grey-based

23

Taguchi method and observed that 10 wt% graphite filled carbon-epoxy composite showed lowest wear volume for all abrading distances and loads. It was revealed that filler content, abrading distance, and applied load are the significant factor in order for minimum wear. Ismail Mohammed et al. (2012) investigated carbon fabric reinforced epoxy (C-E) composites filled with fly ash cenosphere (CSP) and observed that the erosion rate increased with increased impact velocity. It was reported that the filler content, impact velocity, impingement angle, erodent size and erosion time were the significant factors which influence the erosive wear process. Optimization of polymer composite preparation using mix level of Taguchi robust design was reported by Aziz Mohamed et al. (2012) and reported that the addition of filler quantity was the parameter which influences the tensile strength and neutron absorption mostly. It was observed that the factors governing the tensile strength and neutron absorption are dispersant, filler loading, filler size and mixing time.

The specific wear rate of glass filled PTFE composites using ANN and Taguchi method was reported by Varade B.V and Kharde Y.R (2012) and they found that 25% of graphite and PTFE showed minimum wear. ANN results showed satisfactory prediction accuracy. Agarwal Gaurav et al. (2013) carried out parametric optimization and abrasive wear study of SiC filled chopped glass fiber reinforced epoxy composites using L_{25} Taguchi orthogonal array. The S/N ratio for the factors were computed by selecting smaller is better characteristics and is given in equation 2.1, where S/N is signal to noise ratio, y is observed data and n is number of observations.

$$\frac{S}{N} = -10 \log \frac{1}{n}(\sum y^2) \tag{2.1}$$

It was reported that addition of up to 10 wt% SiC resulted in reduction of void fraction and specific wear rate. The significant factor responsible for wear reduction observed was particle size followed by filler content, sliding distance, normal load and sliding velocity. The S/N ratios for various factors is shown in Figure 2.6

Tribological behaviour of epoxy composites filled with WS_2 particulates were investigated by Shaikh M. H. et al. (2013). They used a pin-on-disc wear test under dry sliding conditions for the investigation. A plan of experiments, based on the Taguchi technique, was performed because it eliminates the need for repeated experiments and thus saves time, material and cost. The most predominant factor

responsible for specific wear observed was filler content and is shown in Table 2.1. The SEM images of the tested samples showed abrasive, adhesive and ploughing wear mechanisms. Bagci Mehmet and Imrek Huseyin (2013) optimized the testing parameters for erosion of glass fiber reinforced epoxy composites using Taguchi orthogonal array L_{36} ($2^2.3^3$) and observed the reduction in wear rate by addition of boric acid particles. The ANOVA results showed the material i.e. boric acid particles (52.51%) as most significant factor affecting erosion rate.

Rao Sudarshan K. et al. (2013) investigated the abrasive wear behavior of Carbon/Epoxy composite. They reported S/N ratios of 21.2275 and 21.6499 for predicted and experimental value.
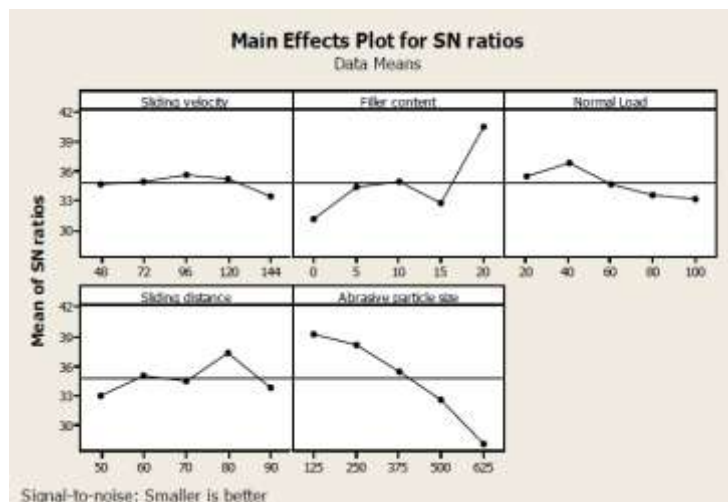
Figure 2.6 S/N Ratios For Various Control Factors. (Agarwal Gaurav et al. 2013)

Table 2.1 Signal to Noise Ratio Response Table For Wear Rate (Shaikh M. H. et al. 2013)

Level	Sliding velocity (A)	Normal Load (B)	% Filler content (C)	Sliding distance (D)
1	80.47	79.84	70.5	79.37
2	76.54	76.83	81.27	80.36
3	80.85	**83.8**	82.73	**81.27**
4	**82.6**	79.99	**85.96**	79.47
Delta	6.06	6.97	15.46	1.9
Rank	3	2	1	4

Naveed Anjum et al. (2013) investigated effect of SiO_2 on wear

Naveed Anjum et al. (2013) investigated effect of SiO_2 on wear behaviour and strength of glass epoxy composites and found that the inclusion of SiO_2 leads to increase in hardness, flexural, and impact strengths. The results showed increased wear volume with increase in sliding distance, load, and sliding velocity. The sliding distance was the most significant factor followed by applied load, sliding velocity and SiO_2 loading influencing the dry sliding wear rate. It was concluded that the de-bonding and fiber breakage at higher loads and speeds constitute the wear mechanisms.

Effect of natural fibers like Sisal, Banana, Roselle and their hybrid combinations were studied by Chandramohan, D. and J. Bharanichandar (2013). They have investigated use of epoxy matrix for the application of automobile accessories and reported the optimum mixing of fiber and resin by using Taguchi method. The hybrid natural fiber reinforced epoxy composites indicated better performance. Benham A. et al. (2013) optimized the polymer composite material for a wind turbine blade using grey based Taguchi technique and reported that 5 wt% of SiC improved the mechanical properties of the composite. Bobbili Ravindranadh and Madhu (2016) discussed the wear study of epoxy based, E-glass/MWCNT and MWCNT composite. Orthogonal array L_{16} was used to study the effect of control factors on the wear and ANOVA was carried out to record the response. The study reported that addition of MWCNTs helped in reducing the specific wear rate and friction coefficient. The worn surface analysis was carried out by Scanning electron microscopy (SEM).

2.6 ARTIFICIAL INTELLIGENCE TECHNIQUE- ANFIS

ANFIS is a combination of two soft computing methods of ANN and fuzzy logic system (Jang 1993). Many researchers used ANN, FUZZY and ANFIS to predict the mechanical and tribological behaviour of reinforced polymer composites. Sagba A. et al. (2009) reported modeling and prediction of abrasive behaviour of poly oxy methylene using response surface method and neural network and found increased wear loss with increase in applied load and sliding distance. Singh Bhoopal et al. (2012) discussed adaptive neuro-fuzzy inference system to predict thermal

conductivity of polymer matrix composites and reported good agreement with experimental results. The different blocks of FIS was described and is shown in
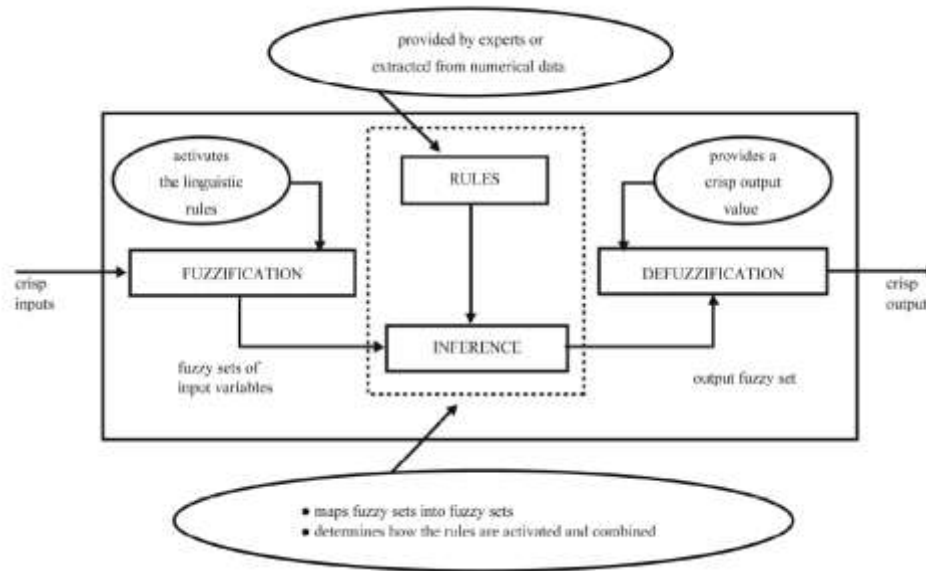
Figure 2.7 Fuzzy Inference System (Singh Bhoopal **et al. 2012**)

Figure 2.7. It was concluded that use of hybrid learning procedure helped the architecture to refine fuzzy if-then rules. Mesbahi Ali et al. (2012) predicted specific wear rate of epoxy nanocomposites filled with PTFE, graphite, SCF and nano-TiO_2 using ANFIS and reported that ANFIS is powerful tool to model the specific wear rate. It was found that ANN and ANFIS can predict specific wear rate in epoxy composites with good accuracy. Sugeon fuzzy model was used to generate fuzzy rules and Genfis3 was used to generate FIS. Petkovic Dalibor et al. (2012) estimated mechanical properties of conductive silicon rubber using ANFIS and predicted stress-strain variation during compression test. It was concluded that approximation of any nonlinear functions can be matched and chaotic time series can be predicted by ANFIS. Fuzzy Logic Toolbox of MATLAB was used to develop ANFIS model as shown in Figure 2.8. Gupta Vikrant et al. (2014) predicted effective thermal conductivity of polymer matrix composites filled with different fillers using ANFIS and results showed very low root mean square error (RMSE) values reflecting in predicting accuracies of physical properties. It was noticed good agreement between predicted and experimental results.
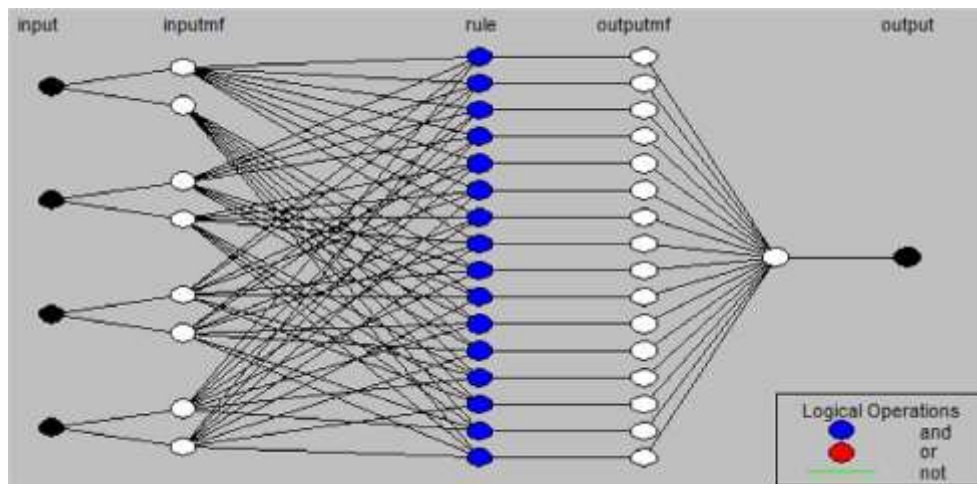
Figure 2.8 ANFIS Structure with Four Inputs and 2–2–2–2 MFs Combination
(Petkovic Dalibor et al. 2012)

Ramesh C. S. et al. (2014) estimated sliding wear behaviour of Carbon fiber reinforced Al6061 composites using ANFIS and the results indicate close agreement with the experimental results. The predicting accuracy for 10 wt% of carbon fiber was 90.28% whereas for 5 wt% it was 91.7%.

Bakar Syamsiah et al. (2015) reported role of input selection using ANFIS to predict the physical properties of degradable composites and found high predicting accuracy for all the input selection. It was noticed that ANFIS model demonstrate high capability of identifying relevant input variables. Alambeigi Farshid et al. (2016) predicted the wear behaviour of sinter hardened steel parts by developing artificial neural networks (ANNs) approach, adaptive neural-based fuzzy inference system (ANFIS) technique, and fuzzy clustering method (FCM) models and reported performance comparison of different techniques as shown in Table 2.2. Sliding distance, cooling rate, type of powder and applied load were input parameters selected for pin on disc wear test. Wear rate of Al-SiC, MMC was predicted by Vijayakumar S. and Karunamoorthy L. (2016) using ANFIS model and found good agreement with experimental results and mathematical model. It was reported that ANFIS can give 99.9% accuracy in predicting experimental data.

Table 2.2 Performance Comparison of Different Techniques

(Alambeigi Farshid et al. 2016)

	ANN Method	C-means method	ANFIS method
RMSE training	4.21×10^{-4}	3.84×10^{-4}	1.23×10^{-7}
RMSE test	3.98×10^{-4}	0.0016	9.19×10^{-4}
R^2 training	0.9912	0.9933	1
R^2 test	0.9911	0.7103	0.9053
Training time (s)	34	52	65

Alimam H. et al. (2016) developed ANN and ANFIS models to predict abrasive wear behaviour of 3105 Aluminium alloy with polyurethane and reported precision and accuracy in prediction of abrasive wear of a coated specimen. The comparison between predicted and experimental data of mass loss was reported and is shown in Figure 2.9.

2.7 FEM SIMULATION OF CONTACT STRESSES

Many machine elements like gears, bearings and cams has interacting surfaces and often support load on small surface area. Hence high amount of the contact pressure and stresses are induced leading to failure of component by overloading, wear, rolling
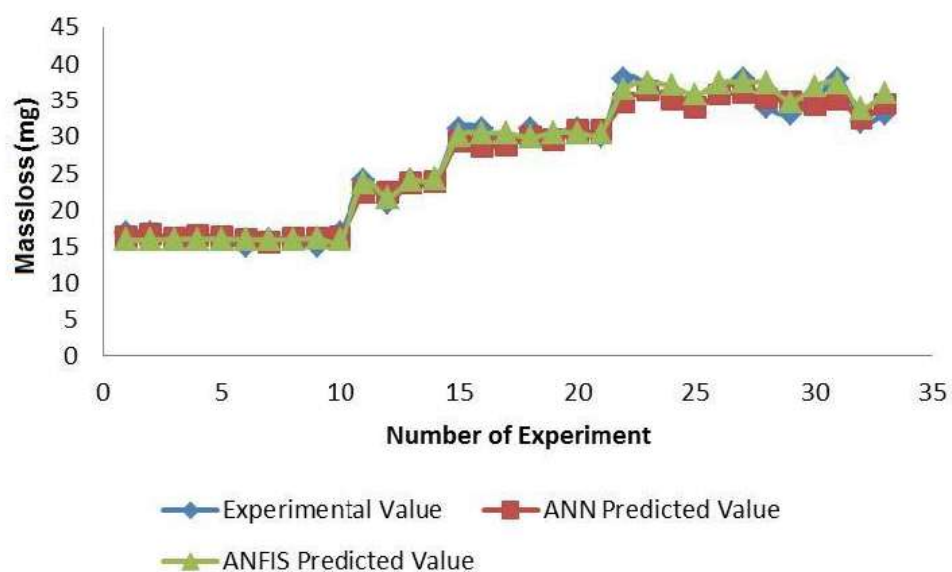
Figure 2.9 Experimental and Predicted Values for Mass Loss (mg).
(Alimam H. et al. 2016)

contact fatigue, seizure and loss of tolerance (Dwyer-Joyce, 1997). Ihara T. et al. (1986) reported finite element analysis of contact stress and strain in an elastic film on a rigid substrate considering load in axial direction and compared the results with Hertz solution. It was found that as the ratio d/H (depth of penetration/thickness of elastic film) increases the maximum shear stress also increases and become uniform at high values of d/H ratio. Bourdon et al. (1999) discussed methodology of modeling the nonlinear behaviour of ball and roller bearings to predict the mechanical load and strain distribution. The analytical model was developed to express the load in terms of stress on inner ring to compute the corresponding displacement of more complex cases like flexible rings.

Tibor Goda et al. (2002) developed FE micro models to determine contact stress and strain of steel asperity sliding on fiber reinforced polymer composite and found high shear loading of matrix and stresses at fiber matrix interface leading to debonding of the fiber. A FE micro model was developed t represent the original body as shown in Figure 2.10. The normal and tangential forces act on a fixed bottom model as shown in Figure 2.10 (b). The macro contact model consists of 8 node solid elements and node to node contact elements; the entire model have 27454 solid elements and 156 contact elements as shown in Figure 2.11. It was concluded that the calculated contact stress and strains were very close to real condition.

Cho Young-Tae et al. (2006) investigated fretting damage of particle reinforced composites due to crack and surface contact using two dimensional elastic finite element analysis. Matrix and reinforcement were modeled by eight nodes solid element and analysed by FEM analysis program commercially available. Numerical analysis result showed stress concentration at the particle and matrix interface. A three dimensional semi-analytical model for elastic plastic sliding contacts considering Coulomb's law was presented by Daniel Nelias et al. (2007) and found reduced computing time as compared to finite element method (FEM). The variational principle and discrete convolution fast Fourier transform (FFT) for acceleration were used to obtain the contact problem. The results obtained by the model was validated with finite element code ABAQUS.
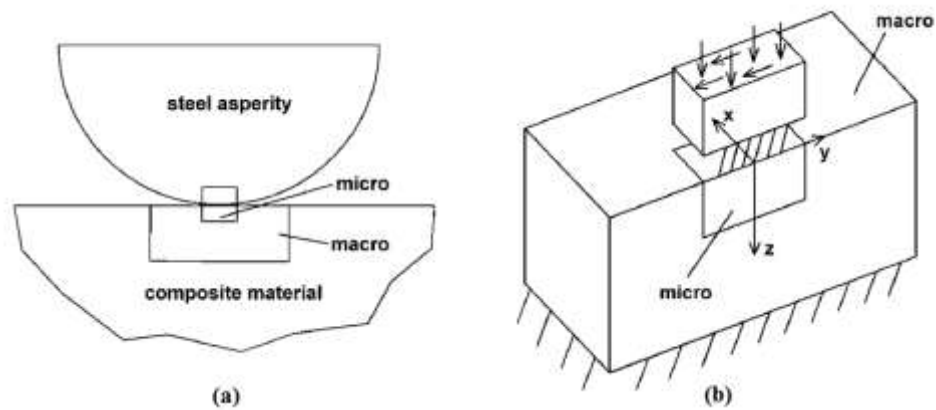
Figure 2.10 (a) Global Model (b) Macro/Micro Models With Contact Elements.
(Tibor Goda et al., 2002)
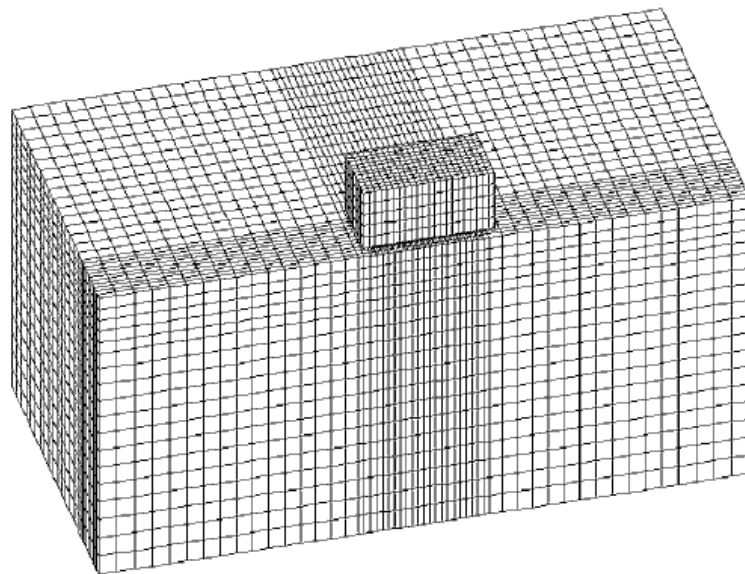
Figure 2.11 FE Mesh of the Contact Macro-Model. (Tibor Goda et al., 2002)

Scarcella Jeffrey A. (2008) compared contact stress developed between roller bearing elements with smooth and rough surface profiles and found less than 2% difference in the results of theoretical and FEA contact stresses. The planer surface was considered as cylinder having large radius i.e. infinite radius for analytical calculations. The analyses were carried considering two dimensions and the depth was considered infinite. The values of load are considered as 'per unit width' and hence the unit of the force or load is N/mm.
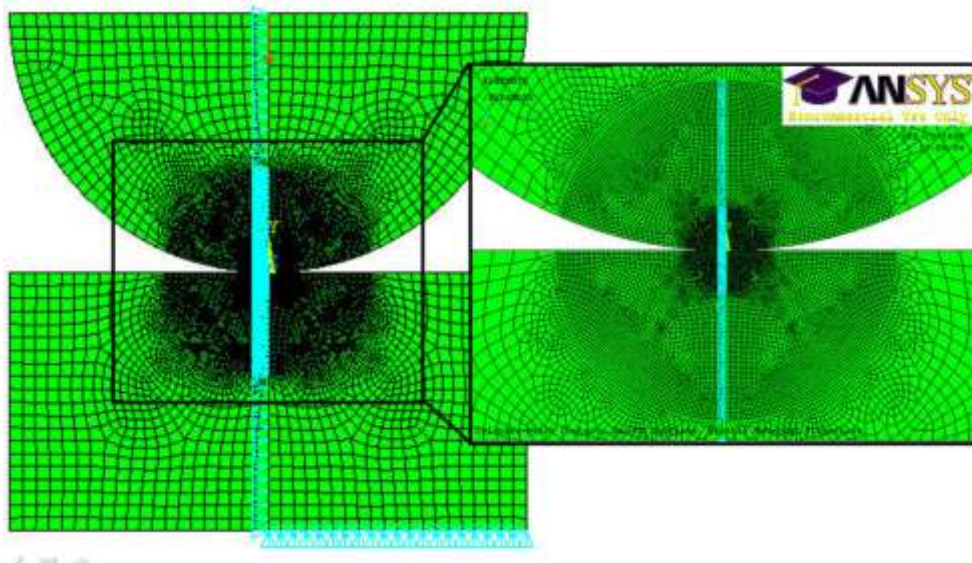
Figure 2.12 Elastic FE Model, Smooth Cylinder and Block. (Scarcella Jeffrey A.2008)

A finite element model and its mesh were developed with 8142 quadrilateral elements having element size 0.03 mm is shown in Figure 2.12. The results showed maximum contact pressure of 410 MPa which was less by 1% as compared to theoretical one and is shown in Figure 2.13.

Hu Zhong and Mohammad Robiul (2012) evaluated the strength and predicted the failure of SCF reinforced nylon spur gear using finite element modeling and reported that nylon gears manufactured by injection molding provides higher strength and better performance. The spur gear was modeled by 3-D, 8 node homogeneous structural solid element, SOLOD 185, considering isotropic steel or nylon or transverse isotropic short carbon fiber reinforced nylon material properties. The surface to surface contact was modeled by 3-D target segment, TARGE170, and 3-D contact element, CONTA174. The unreinforced gear showed maximum deformation and longer contacting duration due to lower stiffness whereas SCF reinforced gear showed much smaller strain due to high stiffness.

Finite element analysis of contact stresses between two cylinders were carried by Brezeanu Ligia Cristina (2013) and found the much higher stress concentration at the area of contact. The three dimensional modeling of two cylinders was carried using

ALGOR V16 FEMPRO software and is shown in Figure 2.14. The maximum stress distribution was reported at the area of contact considering section perpendicular to the axis of cylinders and is shown in Figure 2.15. Fayyad Sayel M. (2013) presented analysis and simulation of contact stress of convex contact area of a punch and flat surface reported higher deformation with friction than without friction. 3-D modeling and meshing of the punch and flat surface was carried using solid work simulation without considering friction and is shown in Figure 2.16 and the stress distribution was simulated and is shown in Figure 2.17.

It was concluded that for the self-similar contact the properties are independent of the boundary condition and valid for linear, nonlinear, isotropic and anisotropic material. Purushothaman Prabhakar and Thankachan Prashanth (2014) used finite element analysis to validate the Hertz contact stresses and found the difference of 10% in the results. This difference in the results is attributed to the approximation made in 3-D modeling of cylinder wherein a full cylinder is approximated in to two semi cylinder. The element selected for modeling was solid 8 node 82 (Plane 82) and TARGE 169. The surface to surface contact was modeled using CINTA175 and is shown in Figure 2.18. The contact stresses were simulated and is shown in Figure 2.19. It was reported that 1049 N compressive load on the upper cylinder resulted in 0.044 mm deformation using FEM technique compared to analytical value of 0.048.

Brahmam D.Veera et al. (2016) investigated contact stress analysis of fly ash graphite reinforced aluminium matrix hybrid composite spur gear using FEM. 3-D modeling of spur gear was done by CREO 2.0 and is shown in Figure 2.20. The values of contact stress obtained analytically and by FEM reported are very close with maximum 5% error.
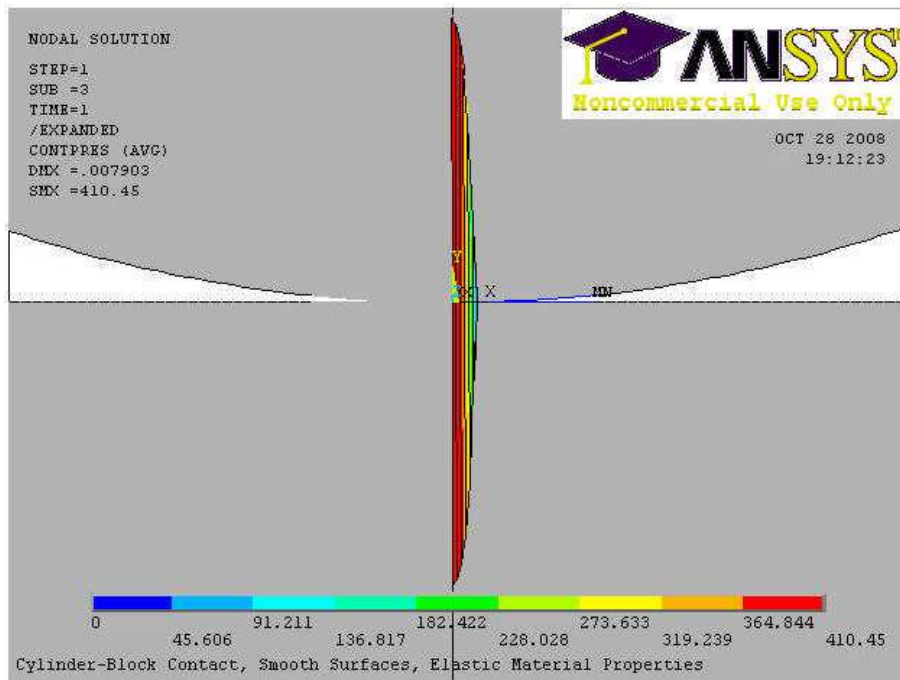
Figure 2.13 Contact Pressure Distribution, Elastic Cylinder & Block (Scarcella Jeffrey A. 2008)
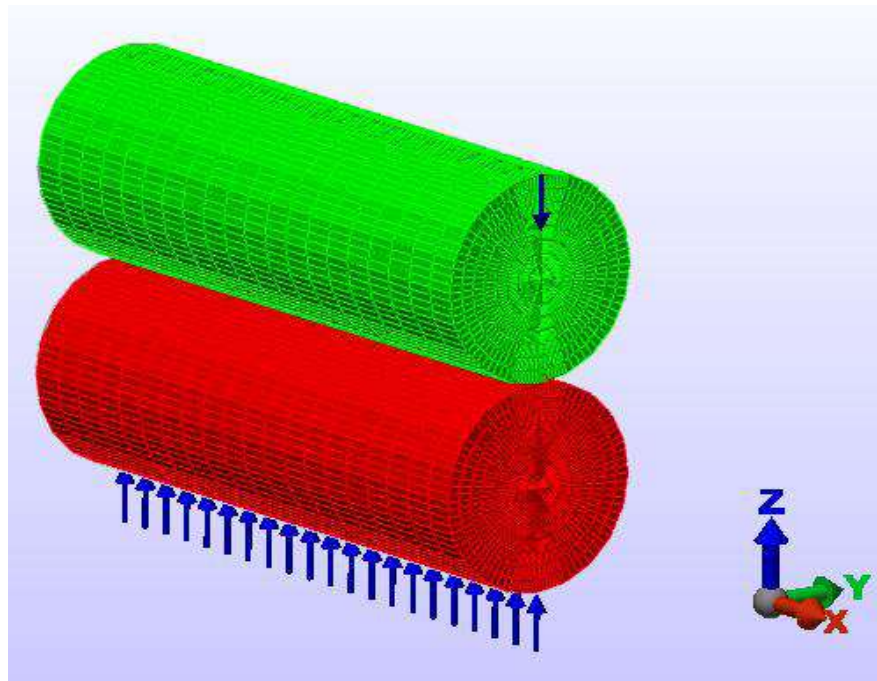
Figure 2.14 Contact between Two Cylinders with Parallel Axes: Modeling and Meshing (Brezeanu Ligia Cristina 2013)
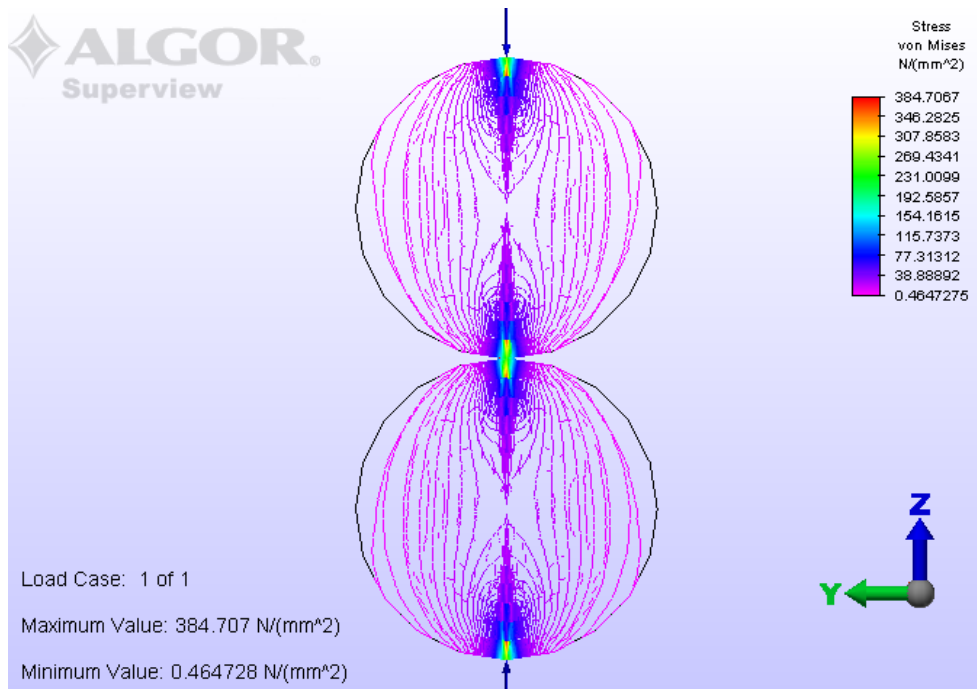
Figure 2.15 Von-Mises Stress Distribution in Cross-Section Area of Two Cylinders (Brezeanu Ligia Cristina 2013)
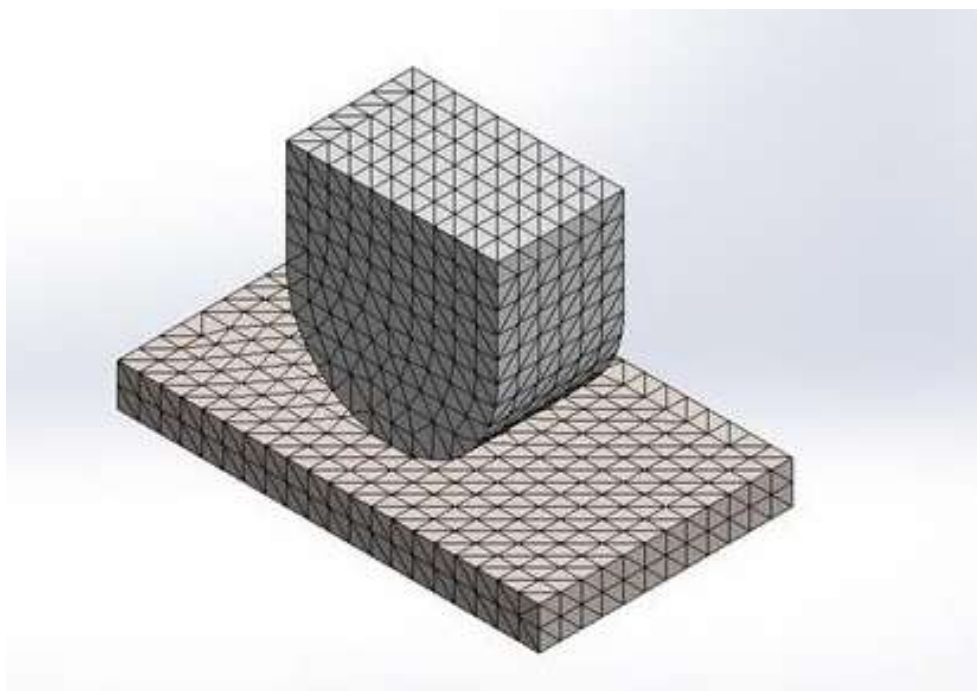
Figure 2.16 Meshing of Two Contact Bodies (Fayyad Sayel M. et al. 2013)
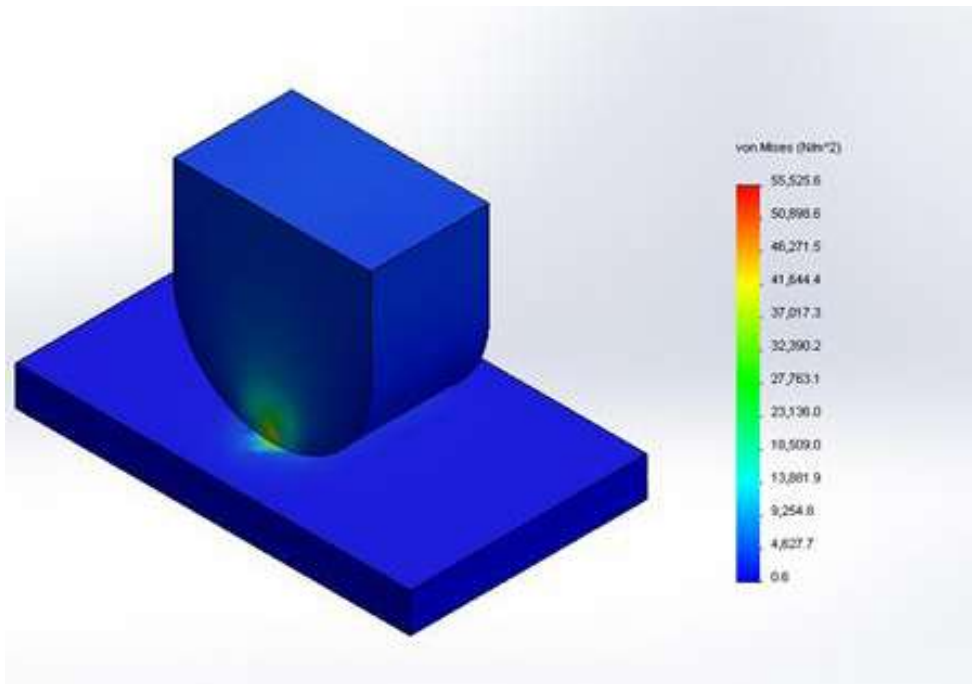
Figure 2.17 Von-Misses Stress Distribution (Fayyad Sayel M. et al. 2013)
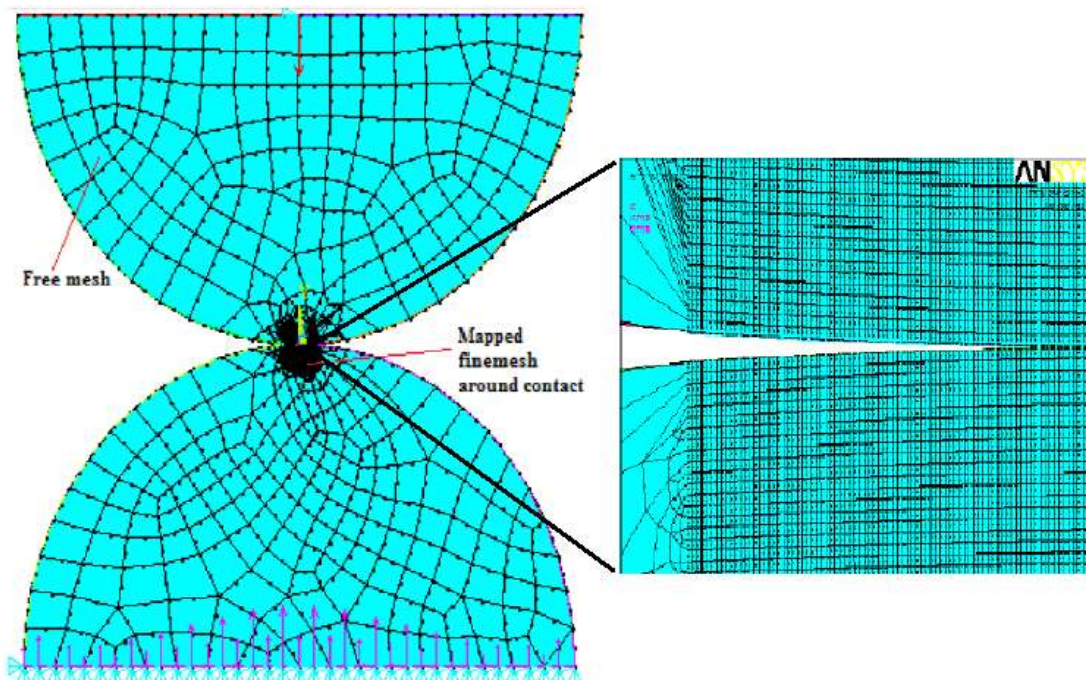
Figure 2.18 Mesh Generated for FE Analysis (Purushothaman and Thankachan 2014)

DISPLACEMENT
STEP=1
SUB =2
TIME=1
DMX =.044324
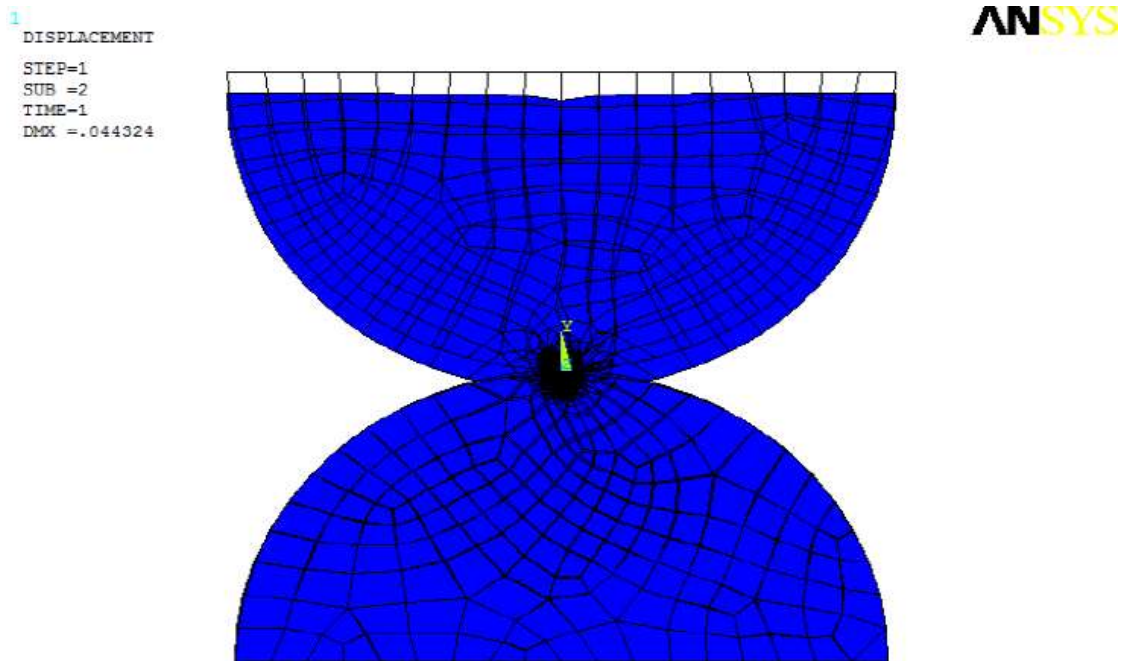
Figure 2.19 Displacement Result of Analysis (Purushothaman and Thankachan 2014)
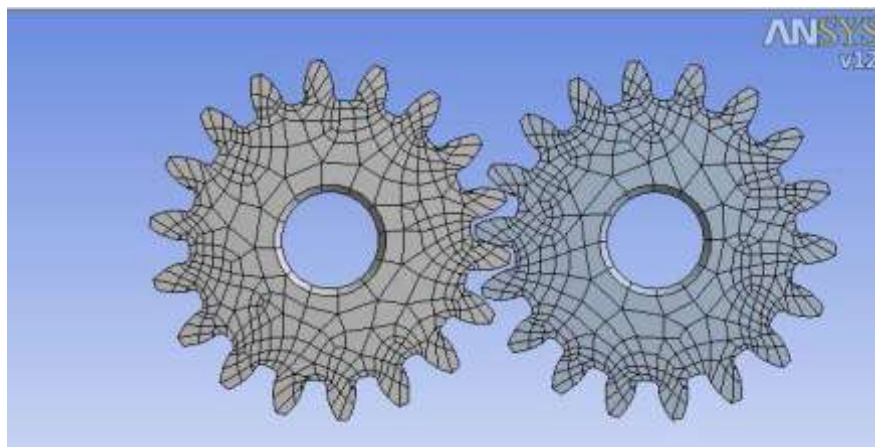
Figure 2.20 Meshing of Spur Gears (Brahmam D.Veera **et al. 2016)**

2.8 RESEARCH GAP

1. Development of low cost and environment friendly reinforced polymer matrix composites having self-lubricating properties is very much needed.

2. Use of sintered bronze (copper & tin) and graphite is not studied with epoxy polymer matrix composites, though tin enhances hardness on dissolving in

copper. It also cements lead, copper and graphite into a single, strong compound.

3. Mechanical characterization of filled and reinforced PMC for antifriction material is very rare.

4. Simulation model to predict the wear rate of polymer composites is not much demonstrated in published literature.

5. Contact stress analysis of filled and reinforced PMC is not much addressed analytically and numerically.

2.9 OBJECTIVE OF THE RESEARCH

Evaluation of mechanical properties experimentally such as: tensile strength, flexural strength, tensile modulus, hardness and impact strength and using Rule of Hybrid Mixture (RoHM)

1. To study the friction and wear behavior of glass fiber reinforced epoxy matrix composite with graphite and sintered bronze particulate filler.

2. To identify the significant control factors and their interactions predominantly influencing the friction and specific wear rate of the composites using Taguchi experimental design.

3. To predict the specific wear rate using ANFIS Simulink model.

4. To study contact stress between the roller and flat plate of PMCs (developed in this study) analytically and validating the results of contact pressure using ANSYS workbench.

CHAPTER 3

MATERIALS AND METHODS

3.1 INTRODUCTION

The extensive literature review of polymer matrix composites (PMC), design of experiment (DOE) by Taguchi Orthogonal Array and Artificial Intelligence techniques (ANFIS) is carried out to decide the research methodology for this study. A six step methodology is decided in the present study to achieve the set objectives. Figure 3.1 shows the outline of the work methodology. The glass fiber reinforced polymer matrix composites filled with graphite and sintered bronze for tribological application was developed by carrying mechanical and tribological characterization. Mechanical characterization is carried to find out the tensile and flexural strength, impact strength and hardness of the composites. Tribological characterization is carried to find out the friction and wear behavior of the composites using pin on disc wear teat. The specific wear rate was predicted using ANFIS Simulink model. Finally contact stress analysis of two mating cylinder in contact was carried to investigate the practical application of PMC in bearing application.
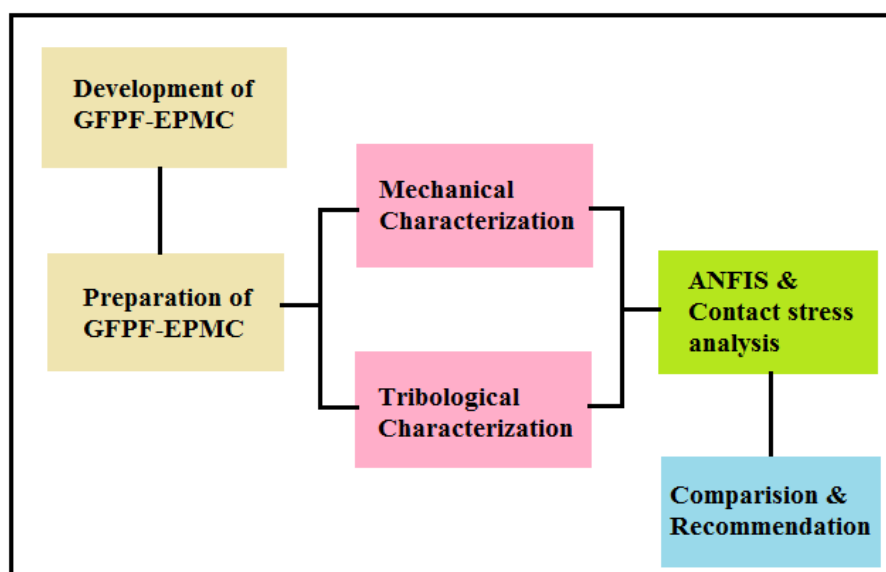
Figure 3.1 Outline of the Methodology

3.2 CONSTITUENT MATERIALS

To develop the polymer matrix composite for tribological application, the matrix, reinforcement and filler are selected considering the available literature. Commercially available epoxy resin CY230 was selected as a matrix and chopped E-glass fiber was used as reinforcement. The fillers, graphite and sintered bronze (95% Cu – 5% Sn) were also obtained from local vendors in Maharashtra, India (Patil and Prasad 2015). The curing agent selected was HY951. The particle size of graphite and sintered bronze fillers specified by the manufacturer is 20 and 47 microns respectively, and the length of chopped glass fiber is 6 mm. The densities of the materials provided by manufacturers are listed in Table 3.1.

All the constituent materials are taken in volume percentage for developing the PMC. After deciding the materials and its volume percentage, the mould was designed to fabricate test specimens of thickness 3 mm using hand lay-up technique. The constituent materials selected are epoxy resin as matrix material, glass fiber as reinforcing element and fillers as graphite and sintered bronze.

Table 3.1 Density of Materials Used In the Composite

Sr.No.	Material	Size in micro-meter	Density (g/cc)
1	Epoxy resin	-----	1.1383
2	E-Glass fiber	14	2.62
3	Graphite	20	2.15
4	Sintered Bronze (95% Cu-5%Sn)	47	6.4

All the constituent materials are taken in volume percentage for developing the PMC. After deciding the materials and its volume percentage, the mould was designed to fabricate test specimens of thickness 3 mm using hand lay-up technique. The constituent materials selected are epoxy resin as matrix material, glass fiber as reinforcing element and fillers as graphite and sintered bronze.

3.2.1 Matrix material-Epoxy resin

Composite materials are classified based on the matrix materials as polymer matrix composite (PMC), Metal Matrix Composite (MMC) and Ceramic Matrix Composite (CMC). Cost effectiveness, ease of processing, less tooling and excellent properties at room temperature attracts the researchers for its selection. The matrix material playimportant role of binding the fibers and fillers together and protect them from chemical and environmental attack. The matrix material helps in transferring the load to the fibers thus it prevent the premature failure of the composites.

Polymer matrices are classified in to thermoset and thermoplastics. Thermosets are monomers having low viscosity and molecular weight. These monomers get converted in to three dimensional cross linked structures on curing and are infusible and insoluble. The cross linking occurs either due to exothermic heat of reaction or by external heating. As the curing progresses, the cross linking accelerates and further heating accelerates cross linking till the polymer matrix is fully cured.
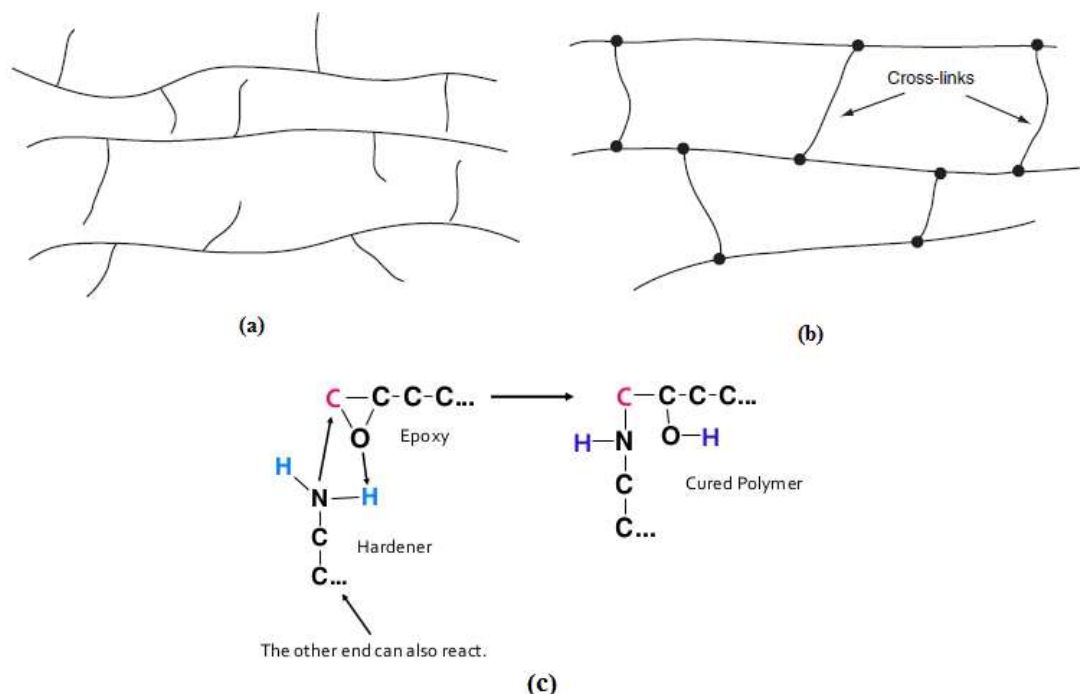
Figure 3.2 Cross Linking in (a) Thermoplastic Polymer (b) Thermoset Polymer (c) Hardener (Mallick 2007).

The schematic representation of cross linking in thermoplastic and thermoset polymer is shown in Figure 3.2. (Mallick 2007). The rigidity and thermal stability of thermoset resin depends on number of cross linking developed on curing. Thermoset composite matrices include epoxies, vinyl esters, polyimides, phenolics and polyesters. Epoxy resin is the most common matrix material used for high performance composite materials because of its low shrinkage, high strength and high adhesive strength properties. Epoxies can be formulated with other materials or can be mixed with other epoxies to get specified performance. The molecular structure of epoxy resins shown in Figure 3.3 is based on the epoxy group.

Diglycidyl ether of Bisphenol A (DGEBA) is the most widely used type of epoxy having a three member ring of two carbon atoms and one oxygen atom is shown in Figure 3.4. Epoxy based composites can be used at room temperature and elevated temperatures and can operate well up to 500F Epoxy resin needs the curing agent and the ratio of epoxy and curing agent depends on the application.
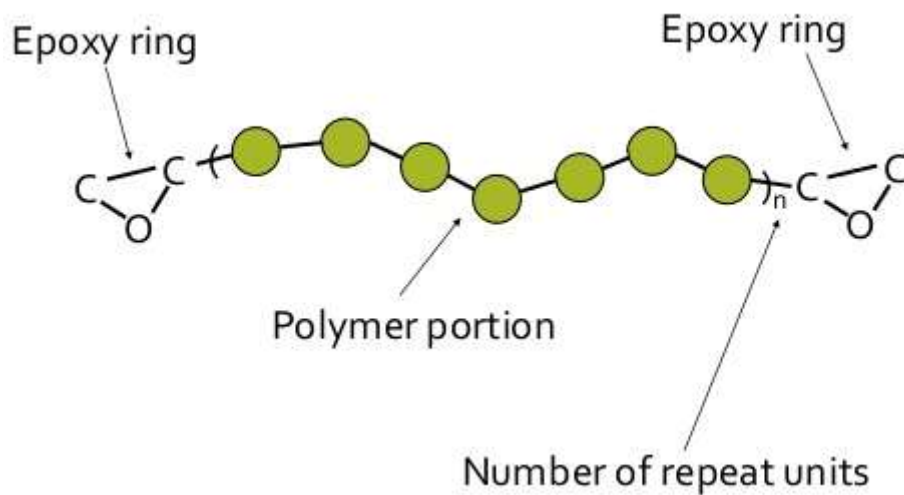
Figure 3.3 Basic Epoxide Group
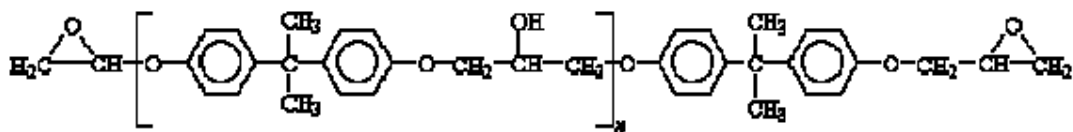
Figure 3.4 Structure of DGBEA

Polyamides, melamine formaldehyde, polyamines and polysulfide are the types of curing agents used with epoxy resin. The properties like strength, corrosion resistance and wear resistance depend on curing agent and the curing cycle employed. The following are the few advantages of epoxy matrix over other resins (Karal 2007). Epoxy exhibits wide range of properties with the help of number of starting materials, curing agents and modifiers

1. Epoxy exhibits higher strength retention under sustained loading as compared to polyester and vinyl ester
2. Epoxy has low shrinkage and low creep properties
3. Epoxy matrix exhibits good chemical resistance
4. Epoxy matrix exhibits excellent adhesive property with fillers and fibers.

3.2.2 Reinforcement-Glass fiber

Reinforcements are important elements of polymer composites and provide the necessary strength and stiffness to the PMC. The reinforcements commonly used are glass, carbon, aramid and boron fibers. These fibers are available in different forms i.e. continuous, chopped, fabric, stapled and woven. Chopped fibers are best suited for the composites manufactured by injection molding and compression molding. Glass fibers are used extensively in polymer matrix composites for reinforcement because of their low cost, high tensile strength, high impact resistance and good chemical resistance (Campbell).

The most used glass fibers in composites are E-glass, S-2 glass and quartz. E-glass fiber is most commonly used as reinforcing element in polymer matrix composites because of its high tensile strength, modulus and low cost. The diameter of chopped glass fiber is in the range of 5 to 25 micrometer and length can be varied as per the requirement 0.125 to 2 inches. Table 3.2 shows fiber types and their properties and the composition and properties of the most common type of glass fibers are shown in Table 3.3.

Table 3.2 Fiber Types and Their Properties (Suresha B. et al, 2006)

Fiber	Advantages	Disadvantages
Aramid	High tensile strength and toughness	Hygroscopic, less interfacial strength
Carbon	High strength and stiffness	Moderate cost
Graphite	High stiffness	Low strength and high cost
E, S-Glass	High strength and low cost	Low stiffness, short fatigue life, high temperature sensitivity

Table 3.3 Mechanical Properties and densities of Various Glasses. (Bunsell and Renard)

Glass type Composition (wt%)	E	S	R	C	D
SiO_2	54	65	60	65	74
Al_2O_3	15	25	25	4	-
CaO	18	-	9	14	0.2
MgO	4	10	6	3	0.2
B_2O_3	8	-	-	5.5	23
F	0.3	-	-	-	-
Fe_2O_3	0.3	-	-	-	-
TiO_2	-	-	-	-	0.1
Na_2O	-	-	-	8	1.2
K_2O	0.4	-	-	0.5	1.3
Properties					
Density	2.54	2.49	2.49	2.49	2.16
Strength (20^0C) (GPa)	3.5	4.65	4.65	2.8	2.45
Elastic modulus (20^0C) (GPa)	73.5	86.5	86.5	70	52.5
Failure strain (20^0C) (%)	4.5	5.3	5.3	4	4.5

3.2.3 Filler -Graphite (Solid lubricant)

Graphite is naturally occurring minerals comprised solely of the element carbon and has a high melting temperature (3,000 °C). Graphite is composed of interconnected hexagonal rings of carbon atoms wherein the carbon atoms are loosely bound (Van Der Walls force) in layers making it one of the softest materials and hence used in friction material composite as a lubricant. These lattice are individual very rigid but each is able to slide easily over adjacent layer. It is a medium temperature (180–260 °C) lubricant and can bring down the friction to the required level and in humid conditions, graphite exhibits lower friction coefficient (μ). Amorphous graphite is formed by the thermal metamorphism of coal and its very fine particle size and low degree of crystalline order make it appear amorphous. Inclusion of graphite in polymer composites brings down the friction coefficient and enhances the thermal conductivity considerably. It exhibits lubricating properties by filling and smoothing of uneven surfaces because it acts as solid lubricant. It also offers resistance to oxidation and cyclic temperature stress. The chemical structure of the graphite is shown in Figure 3.5.
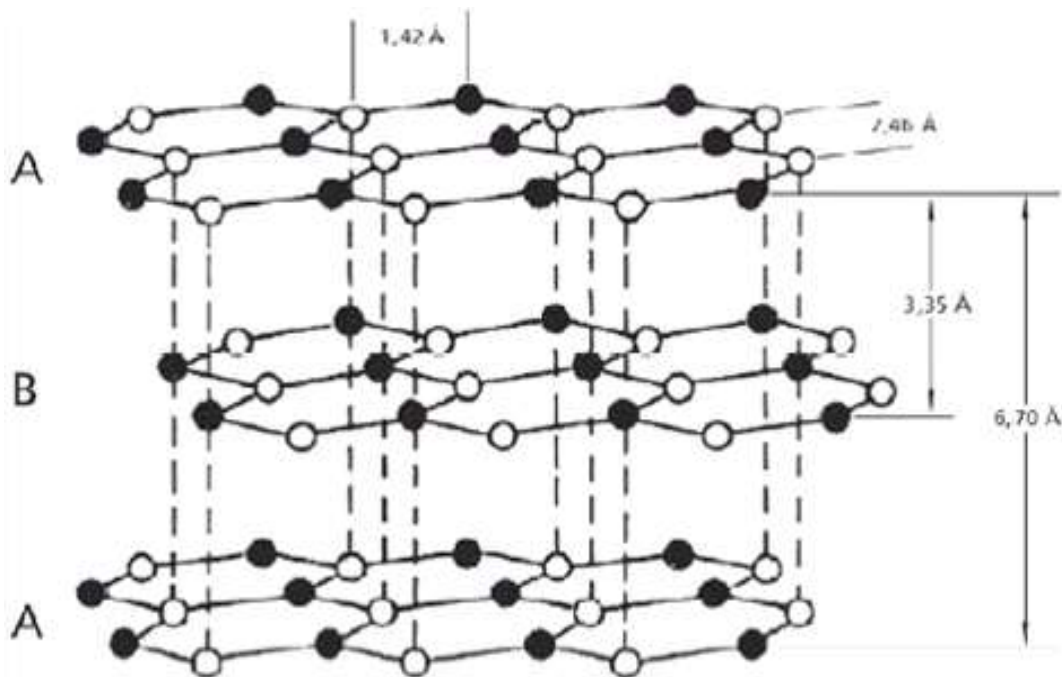
Figure 3.5 Crystal Structure of Graphite

3.2.4 Filler -Sintered Bronze

Bronze is an alloy consisting of copper as base material and tin as the main additive but arsenic, phosphorus, aluminum, manganese, and silicon can also be used to produce alloy of different properties. The additives make the copper hard and tough. There are many bronze alloys available, but in this research the bronze used consists of 95% copper and 05% tin. The bronze possesses the favourable properties like wear resistance, corrosion resistance and antifriction ability. It has also very low metal on metal friction.

3.3 DEVELOPMENT OF COMPOSITION

Polymer Matrix Composition is decided based on a rigorous literature survey. Many researchers used the varying proportion of the fiber reinforcement and fillers. Also the proportions are taken in volume percentage. Table 3.4 show compositions of E-Glass fiber reinforced graphite and sintered bronze particulate filled epoxy composite for mechanical characterization. The composition which exhibits optimum mechanical properties is used to fabricate the test specimens for tribological characterization i.e. pin on disc wear test. As wettability of fiber is important in the reinforced polymer composites (Mallick 2007), the volume percentage of matrix epoxy is fixed to 60. The study of volume % of glass fiber on strength is carried out by many researchers and found the best results for 10 vol% to 20 vol%. Graphite filler is extensively used by researchers to study its tribological behaviour. It was observed that the graphite filler is varied between 5 vol% to 20 vol%. Keeping in view the various aspects mentioned above. An attempt is made to develop the fiber reinforced PMC filled with bronze and solid lubricant graphite for tribological application. The study of copper-tin alloy (bronze) and solid lubricant (graphite) as filler in PMC is not undertaken previously. So the volume % of bronze is selected randomly to make total vol% as 100. Hence to develop an alternating material for the sleeve bearings, combination of graphite and sintered bronze is made with epoxy matrix. To optimize the composition three classes of PMC is decided.

Table 3.4 Composition of PMC for Mechanical Characterization

Sr. no	Designation	Composition (vol %)			
		Resin	Glass Fiber	Graphite	Bronze
1	10F/10G/20B	60	10	10	20
2	10F/15G/15B	60	10	15	15
3	10F/20G/10B	60	10	20	10
4	15F/5G/15B	65	15	5	15
5	15F/10G/10B	65	15	10	10
6	15F/15G/5B	65	15	15	5
7	20F/5G/15B	60	20	5	15
8	20F/10G/10B	60	20	10	10
9	20F/15G/5B	60	20	15	5

The preparation of the composite mixture is done as per the method shown in Figure 3.6. The epoxy resin and hardener is mixed in the ratio 100:15 (own judgment) by weight (volume percentage is converted into weight while preparing the composition mixture) in a glass flask initially by mechanical stirrer followed by magnetic stirrer. The fillers i.e. Graphite and Sintered Bronze particulates are sonicated for about one and half hour separately and then added in above mixture of matrix and stirred on magnetic stirrer for half an hour. E-Glass fiber is washed by acetone and dried before mixing with the matrix material for improving the interfacial strength of fiber with matrix material. The dried glass fibers at last are mixed with matrix and particulate filler by mechanical stirrer for about 1 hour. Total 9 compositions are prepared to fabricate test specimens for mechanical characterization as shown in Table 3.4.
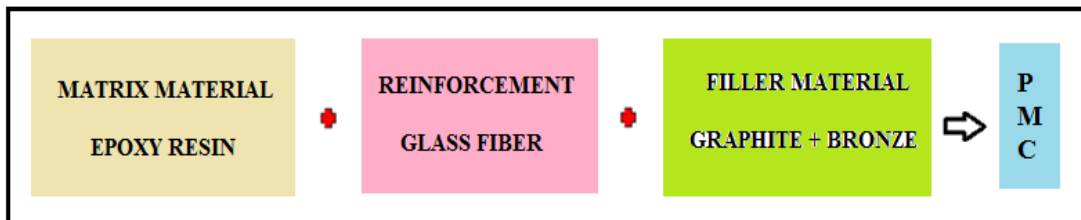
Figure 3.6 Preparation of Composite

The epoxy resin and E-Glass fiber volume percentage is fixed as 60/10, 65/15 and 60/20 for three class of composites. The mixture of composite is stirred gently for 1 hour to ensure complete homogeneous mixing. The mixture is then poured into a pressure die mould coated with a release agent to manufacture the sheets to fabricate the test specimens for mechanical characterization.

3.4 MECHANICAL CHARACTERIZATION

The fabrication of the test specimen is carried out by pressure die moulding method. The test specimens for mechanical and tribological characterization are fabricated. The method of fabrication for both specimens is same except its shape and size. The dimensions of the test specimen are decided by considering ASTM standards as shown in Table 3.5.

To evaluate mechanical characteristics of composites, there are many tests need to be carried out. In this work tensile, flexural, impact, hardness and density tests only are carried out. Apart from above tests, XRD and TGA analysis are also carried. These tests disclose enough characteristics of the developed composites which are to be used as antifriction material in the application of bush bearings.

3.4.1 Fabrication of Test specimen

To fabricate the test specimens for mechanical testing, a moulding box is designed and developed. In a single set of mould, twenty specimens are planned (4 test and its 5 replicates) and a rectangular sheet of composite is fabricated. In all, three moulding boxes are designed and developed for three compositions. The moulding boxes are developed from 10 mm thick acrylic sheet. The spacers are selected so as to achieve moulding thickness of 3 mm. To apply external pressure while curing, the moulding clamp is designed and manufactured. This clamp holds the moulds in proper position and applies sufficient pressure to remove voids.

The composite mixture of composition is prepared separately in a glass flask. The mixture is then poured into a mould cavity of the pressure die mould which is coated

with a release agent (oil). It is allowed to cure in the pressure die moulding at designed temperature to complete the cross linking of the polymer.

The fabricated test specimens are shown in Appendix I, of only two compositions. Curing of the composite sheets of test specimen is carried in the muffle furnace at different temperature and for different duration. The following curing cycle is followed and the same cycle is repeated for all the samples of mechanical specimen and tribological test specimens (Patil and Prasad 2015).

i.   1hr at 110^{0}C with mould under clamp pressure.

ii.   24 hours at room temperature.

iii.   Post curing 30 minutes at 160^{0}C followed by

iv.   12 hours curing at room temperature.

3.4.2 Mechanical Test Plan

Several mechanical tests those are required to be carried out to know the mechanical properties of the polymer matrix composite. Table 3.6 shows the tests planned and the equipment used to carry the various tests. The tensile and flexural strength is important property of the material which indicates the ability of the material to sustain the externally applied load without undergoing tensile failure or bending failure. Hardness and impact strength is also important properties of the material which decides the application of the developed materials. The density of the material is estimated by rule of hybrid mixture (RoHM).

Table 3.5 ASTM Standards and Dimensions of the Test Specimen

Sr. No	Characteristic to be Investigated	Dimensions	ASTM Standard used
1	Tensile Strength	150x12.5x3 mm	ASTM D-3039
2	Flexural strength	90x12.5x3 mm	ASTM D-790
3	Impact strength	125x12.5x3 mm	ASTM D-256
4	Hardness	20x20x3 mm	ASTM D-785
5	Specific Wear rate	Ø12 x 25 mm	ASTM G-99

Table 3.6 Mechanical Test, ASTM Standard and Equipment

Sr. No	Characteristic to be Investigated	Test set up to be Used	ASTM Standard used
1	Tensile	UTM	ASTM D-3039
2	Flexural strength	UTM	ASTM D790
3	Impact strength	Izod Impact Test	ASTM D 256
4	Hardness	Rockwell Hardness test	
5	Density	Archimedes Principle	RoHM

3.4.3 Tensile Test

The flat test specimens of size 150mm x 12.5 mm x 3 mm as shown in Appendix B is used to carry tensile test. For holding these specimens in the jaws of cross head of UTM, the ends are firmly glued with tabs. These tabs protect the specimen from any kind of damage at the time of loading. The tensile tests are performed according to the ASTM D-3039, on the universal testing machine (Appendix III) at the cross head speed of 2mm/min. The test results give tensile strength and tensile modulus of the composites. The test is repeated on four replicate composite samples and the mean value of tensile strength and modulus is reported.

3.4.4 Flexural Test

The flat test specimens of size 90 mm x 12.5 mm x 3 mm is used to carry three point flexural tests in universal testing machine. The flexural strength of the composite is the ability of material to withstand maximum tensile stress before bending failure. The span length of 50 mm and the cross head speed of 2 mm/min are maintained for the flexural loading. The test is repeated on four replicate composite samples and the mean value of flexural strength and modulus is reported. The theoretical flexural strength of the composite specimen is computed using the equation 3.1.

$$\text{Flexural strength} = \frac{3FL}{2bt_s^2} \ (\text{N/mm}^2) \tag{3.1}$$

Where, F is the maximum load applied (N)

L is the span length of the sample (mm)

b is the width of the sample (mm)

t_s is the thickness of sample (mm)

The theoretical inter laminar shear strength of the composite is calculated using the equation 3.2

$$\text{Inter laminar Shear Strength} = \frac{3F}{4bt} \ (\text{N/mm}^2) \tag{3.2}$$

3.4.5 Impact strength

The impact test measures a materials resistance to impact from a swinging pendulum. The tests are performed according to ASTM D256 using AIT-300EN (Fasne test equipment Pvt., Ltd.) to measure the energy required to break the test specimen. The dimensions of the test specimen as per ASTM D-256 are 64 mm x 12.7 mm x 3.2 mm. The average results obtained for five test specimens are taken for each composite. The depth under the notch of the specimen is 10 mm. The dial indicator of Izod impact testers indicates the impact energy of the composite specimens and is recorded directly in Joules (J) (Patil and Prasad 2015).

3.4.6 Hardness test

Vickers micro-hardness (HV) of the PMC is measured. A pyramid-shaped diamond indenter is pressed against polished composite surfaces for 30 seconds using a load of 200 gm. The Rockwell hardness tester (Meta test instruments Pvt., Ltd.) is used to measure the hardness of composites. The average results obtained for five different locations are taken for each sample (Patil and Krishna 2015).

3.4.7 Density and Void fraction

The theoretical density of the composites is computed by rule of hybrid mixture using the equation 3.3. The PMC developed consists of matrix, fiber reinforcement and graphite and bronze fillers so the equation for theoretical density is modified accordingly. Actual density is measured by Archimedes Principle of simple water immersion technique.

$$\rho_{th} = \rho_m V_m + \rho_f V_f + \rho_g V_g + \rho_b V_b \ \ (g/cc) \tag{3.3}$$

Where,

$(\rho)_{th}$ is theoretical density,

ρ_m, ρ_b, ρ_g and ρ_f are densities of matrix material, bronze, graphite and E-glass fiber respectively.

V_m, V_b, V_g and V_f are volume fraction of matrix material, bronze, graphite and E-glass fiber respectively

The volume fraction of voids (V_v) is computed using the theoretical and measured density using equation 3.4

$$\text{Void fraction } (V_v) = \frac{(\text{Theoretical density} - \text{Measured density})}{\text{Theoretical density}}$$

$$(V_v) = \frac{(\rho_{th} - \rho_{me})}{\rho_{th}} \tag{3.4}$$

3.5 THERMOGRAVIMETRIC ANALYSIS

Thermal gravimetric analysis is technique to study the stability of the composite under the constant heating. The heat supplied is increased gradually and the temperatures are measured at various % mass loss. The loss of mass may be due to number of chemical phenomena such as absorption, sublimation, vaporization, oxidation, and decomposition. This information of the mass loss at certain degrees of temperature describes the stability of the composites. For example: filler content in polymers; carbon black in oils; ash and carbon in coals, and the moisture content of many substances (NPTEL, 2016). Thermogravimetric analysis of three composites (F20/G5/B15, F20/G10/B10 andF20/G15/B5) is carried out to study the stability of the composite at elevated temperatures.

3.6 XRD ANALYSIS

X - ray diffraction (XRD) technique is used for the study of polymer structure and different phases of the composites. It uses x-rays to investigate and quantify the crystalline nature of materials by measuring the diffraction of x-rays from the planes

of atoms within the material. XRD offers a direct means of determining the orientation characteristics of composites. The XRD pattern of three composites consisting of glass fiber, graphite powder, epoxy resin and sintered bronze. These composites are 20F/5G/15B; 20F/10G/10B and 20F/15G/5B remaining is epoxy matrix. The number indicate vol% of fiber, graphite and bronze respectively.

3.7 TRIBOLOGICAL CHARACTERIZATION

The test specimens for tribological characterization are fabricated from the composite which has exhibited best mechanical properties. The mould is designed to fabricate pins using pressure die moulding technique. The pins of diameter 15mm and length 100mm are fabricated using pressure die moulding. The test specimens of size Ø12 mm x 25 mm length are machined as per the ASTM standard for pin on disc wear test. These tests are planed according to Taguchi orthogonal array L_{27}. The Taguchi experiment is repeated twice and the average results are reported.

The friction and wear characteristics plays very important role in the applications of bush bearing. Hence friction and wear test was carried out on pin on disc wear test setup.

3.7.1 Composition for Tribological characterization

The polymer composition for tribological characterization is selected on the basis of the Mechanical characterization carried in this study. The composition which exhibited best mechanical characterization is shown in Table 3.7. The tribological characterization aims at assessment of friction and specific wear rate of the composite using pin-on-disc tribotester. Polymer structure, dispersion of fillers and surface characterization also are part of tribological characterization. Table.3.8 shows different tests that are carried out to analyze surface of the composite pin before and after the test and the worn out debris.

3.7.2 Pressure Die Mould

The pressure die moulding set up is designed and developed to fabricate the test pins for pin on disc wear test. The hydraulic circuit diagram of the setup is shown in

Table 3.7 Composition of PMC for Tribological Characterization

Sr. No.	Designation	Composition (vol %)			
		Resin	Glass Fiber	Graphite	Bronze
1	20F/5G/15B	60	20	5	15
2	20F/10G/10B	60	20	10	10
3	20F/15G/5B	60	20	15	5

Table 3.8 Tribological Test, ASTM Standard and Equipment

Sr. No	Characterization	Test set up	ASTM Standard
1	Friction and Specific Wear rate	Pin on Disc tribotester	ASTM G-99
2	Polymer structure	Optical Microscope	--
3	Worn surface	SEM	--
4	Worn debris	SEM	--

Appendix IV. It consists of a pump, DA cylinder, 4/2 lever operated valve and oil sump. A single 4/2 valve can be used to apply pressure and to release it. A maximum pressure of 100 kg/cm^2 can be applied by the setup. The DA cylinder used has the capacity of 70 kg/cm^2. Appendix V shows photograph of the developed setup.

3.7.3 Mould for Cylindrical Pin

The design and development of the mould is done considering the dimensions of the test pin. As per ASTM G 99, the pin dimension varies between 8 mm to 25 mm. In this work the pin diameter selected is Ø12 mm and length 25 mm. To get pin diameter of 12 mm, it is decided to get mould of diameter 15 mm. Also as the tests are planned according to Taguchi OA L$_{27}$, the total number of pins required is 27.

The mould is so designed that its length is kept 115 mm to produce 3 pins from a single mould. Figure 3.7 shows detailed drawing of pin mould. As the test specimen is in cylindrical shape, a hollow cylindrical mould is developed. A MS polished bar of

outer diameter 45 mm and length 140 mm is used to develop the mould for pin fabrication as shown in part no 1. The assembly drawing of whole pin mould is shown in Figure 3.8

3.7.4 Wear Test Pin Specimens

The pin on disc wear tests is planned according to Taguchi Orthogonal Array L_{27} with replicate of two, so the total number of pins fabricated is 81. Table 3.7 shows the elemental content of the test specimen. The composition of composite consists of glass fiber, graphite and sintered bronze. The glass fiber content was kept constant as 20 volume percentage and the fillers, graphite and sintered bronze are varied between 5 vol% to 15 vol% in a step of 5 vol% (Patil and Krishna 2017).

In this study, all the specimens used are fabricated considering ASTMG-99 standards of test specimens by pressure die moulding Technique. The mixture of composite is stirred for about 60 minutes before pouring in the mould cavity. The homogeneous mixture was poured into the mould cylinder and the hydraulic pressure is applied by double acting (DA) cylinder of pressure die moulding setup. Figure 3.9 shows the fabricated test specimen pins.
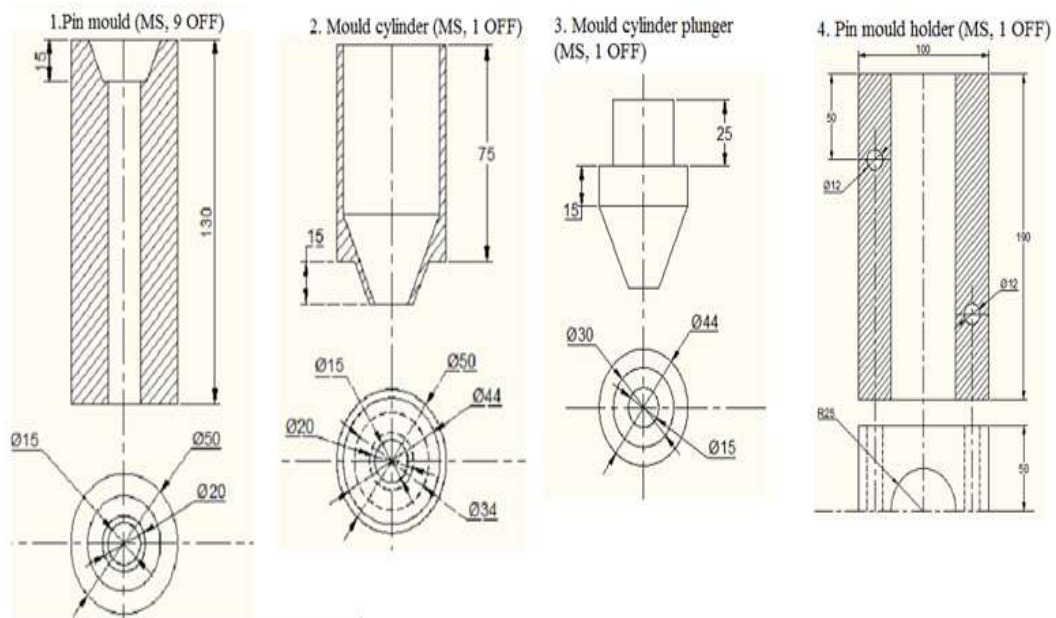
Figure 3.7 Detailed Drawing of Pin Mould
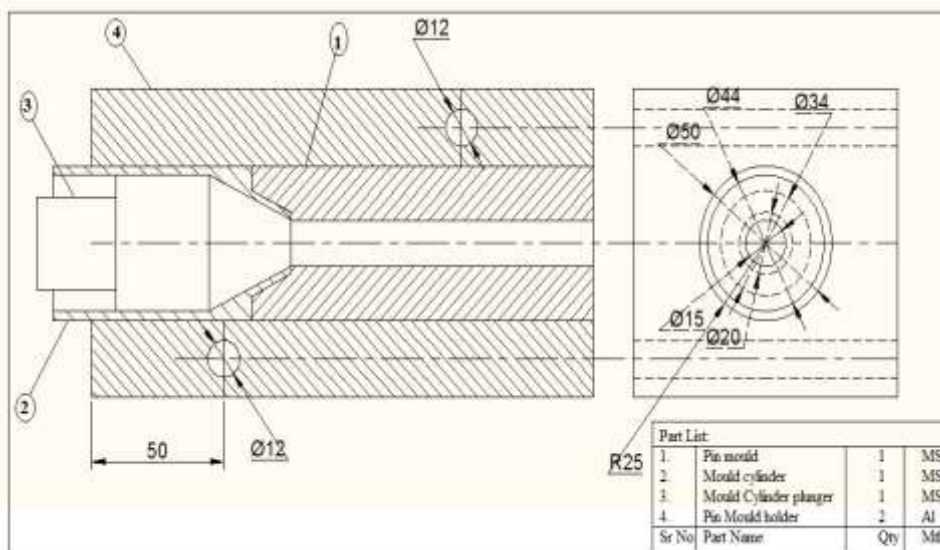
Figure 3.8 Assembly Drawing of Pressure Die Mould

3.7.5 Pin on Disc Wear Test

A pin-on-disk wear test setup (supplied by DUCOM) is used for estimating the sliding specific wear rate or loss at dry conditions as per ASTM G-99. The pin on disc experimental set up is shown in Figure 3.10. The counter rotating disc is made of steel having grade EN-32 and hardness 72 HRC, its surface roughness is 0.6 Ra. The holding jaw holds the specimen and the disc is rotated with the help of motor with different speeds. The normal force on the pin is applied through weights. For measuring the weight of sample pin, (before and after the test is performed) an electronic balance with an accuracy of 0.0001gm is required. The difference between the initial and final weight gives the measure of sliding wear loss.

Figure 3.9 Test Specimens for Pin on Disc Wear Test

The tests are conducted as per Taguchi Orthogonal Array L27. The sliding velocities considered for the test are 210, 260 and 320 cm/sec. The normal force used for the test is 20N, 30N and 40N. The material loss from the composite surface is directly taken from the setup display which is in micrometer. The specific wear rate can also be computed using the equation 3.5

$$W_s = \frac{\Delta m}{\rho t V_s F_n} \tag{3.5}$$

Where,

W_s is the specific wear rate

Δm is the mass loss in the test duration (gm)

ρ is the density of the composite (gm/mm^3)

t is the test duration (sec).

V_s is the sliding velocity (m/sec)

F_n is the average normal load (N).

The wear test is performed on wear and friction monitor, according to Taguchi Orthogonal Array L$_{27}$. The tests are carried out considering 4 factors each at three levels as shown in Table 3.9. As per the sliding velocity the time required to cover the sliding distance is estimated using empirical relationship (Patil and Prasad 2017). The distance between the centers of the pin and the center of the disc is kept fixed to 50mm. The pin-on-disc apparatus gives us the accurate readings of all the data points for Wear, Frictional Force and Co-efficient of Friction.

Figure 3.10 Pin on Disc Wear Test Setup (AIT, Pune)

3.7.6 Taguchi Orthogonal Array $L_{27}(3^{13})$

To assess the influence of numbers of input factors on the behaviour of outcome by conventional experiments is tedious and time consuming task. Design of experiment by Taguchi method provides the tool to model and analyze the output and the factor influencing it. The selection of control factor is the most important stage in the design of experiment. Therefore, the variables having no effect on output must be identified at first while selecting the control factors.

The tests are conducted as per the orthogonal array L_{27} given in Table 3.10. The experiments are carried out as follows: sliding distance (A) is assigned to first column, filler content (B) to second column, sliding velocity (C) to fifth column and normal load (D) to ninth column. Interaction $(A \times B)_1$ and $(A \times B)_1$ are assigned to third and fourth column respectively. Similarly $(B \times C)_1$ and $(B \times C)_2$ are assigned to sixth column and 7 respectively. $(A \times C)_1$ and $(A \times C)_2$ are assigned to eighth and eleventh column respectively to estimate interaction between the normal load (B) and filler content (C). The remaining columns are assigned to error columns respectively.

Table 3.9 DOE: Levels of the Variables

Control Factors	Levels			
	I	II	III	Units
A: Sliding distance	2000	4000	6000	meter
B: Filler content	5	10	15	vol%
C: Sliding velocity	210	260	320	cm/s
D: Normal load	20	30	40	N

In this study sliding distance, filler content, sliding velocity and normal load are the four parameters with three levels, are considered. The column and row of Table 3.10 represents test parameters and test condition respectively. The output of the experiment is transformed into signal-to-noise (S/N) ratios. As the pin on disc wear test is conducted to find wear resistance, the output must be smaller. Hence smaller is

better characteristics is selected for the analysis of the results. It can be calculated by logarithmic transformation of the loss function equation 3.6.

Smaller is the Better Characteristic:

$$SN_s = -10 \log \left(\frac{1}{n} \Sigma_{i=1}^{n} y_i^2 \right) \tag{3.6}$$

Where,

   n is the number of observations, and

   y is the observed data.

The linear graph as shown in Figure 3.11 is used to identify the factors and interactions.

3.7.7 Scanning Electron Microscope (SEM)

Scanning electron microscope (SEM) is used to analyze the worn surfaces of the composites test specimen pin and the worn out debris to study the wear track, self-lubricating film formed and to identify the constituent element which undergo maximum wear. Worn surface pin and worn out debris are mounted on stub and are sputter coated with gold prior to SEM examination. The surfaces of the samples are examined directly by scanning electron microscope.

3.8 ARTIFICIAL INTELLIGENCE SIMULINK MODEL

Neural networks have been successfully applied across an extraordinary range of problem domains and in areas like engineering, medicine, physics, biology, geology, and finance. The neural network is capable of modeling the human brain. Neural network are interesting because of its potential use in prediction of the output of a system or test results.

Artificial neural networks (ANNs) differ over the traditional model based methods in its non-linear data driven self-adaptive approach. ANNs has an ability to learn and identify the correlated patterns between input data sets and corresponding target values. ANNs can be used to predict the output of new independent input data after training the algorithm. The adaptive nature of these networks is unique feature wherein learning by example is replaced by programming while providing solution to

the problems. Because of this uniqueness it is most popular for the problems of unknown patterns and the data for training is available.

Table 3.10 Taguchi's Experimental Design: Orthogonal array for L27 (3^{13})

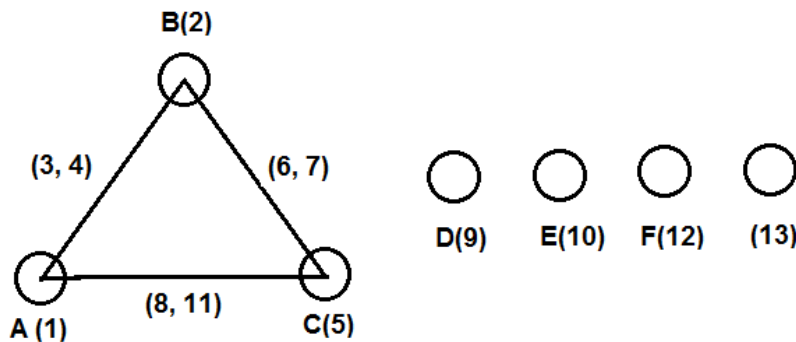| $L_{27}(3^{13})$	1	2	3	4	5	6	7	8	9	10	11	12	13
	A	B	$(A \times B)_1$	$(A \times B)_2$	C	$(B \times C)_1$	$(B \times C)_2$	$(A \times C)_1$	D		$(A \times C)_2$		
1	1	1	1	1	1	1	1	1	1	1	1	1	1
2	1	1	1	1	2	2	2	2	2	2	2	2	2
3	1	1	1	1	3	3	3	3	3	3	3	3	3
4	1	2	2	2	1	1	1	2	2	2	3	3	3
5	1	2	2	2	2	2	2	3	3	3	1	1	1
6	1	2	2	2	3	3	3	1	1	1	2	2	2
7	1	3	3	3	1	1	1	3	3	3	2	2	2
8	1	3	3	3	2	2	2	1	1	1	3	3	3
9	1	3	3	3	3	3	3	2	2	2	1	1	1
10	2	1	2	3	1	2	3	1	2	3	1	2	3
11	2	1	2	3	2	3	1	2	3	1	2	3	1
12	2	1	2	3	3	1	2	3	1	2	3	1	2
13	2	2	3	1	1	2	3	2	3	1	3	1	2
14	2	2	3	1	2	3	1	3	1	2	1	2	3
15	2	2	3	1	3	1	2	1	2	3	2	3	1
16	2	3	1	2	1	2	3	3	1	2	2	3	1
17	2	3	1	2	2	3	1	1	2	3	3	1	2
18	2	3	1	2	3	1	2	2	3	1	1	2	3
19	3	1	3	2	1	3	2	1	3	2	1	3	2
20	3	1	3	2	2	1	3	2	1	3	2	1	3
21	3	1	3	2	3	2	1	3	2	1	3	2	1
22	3	2	1	3	1	3	2	2	1	3	3	2	1
23	3	2	1	3	2	1	3	3	2	1	1	3	2
24	3	2	1	3	3	2	1	1	3	2	2	1	3
25	3	3	2	1	1	3	2	3	2	1	2	1	3
26	3	3	2	1	2	1	3	1	3	2	3	2	1
27	3	3	2	1	3	2	1	2	1	3	1	3	2

Figure 3.11 Linear Graph for L$_{27}$

3.8.1 Artificial Neural Networks

 A neural network consists of a set of connected cells: the neurons. The neurons receive impulses from either input cells or other neurons and perform some kind of transformation of the input and transmit the outcome to other neurons or to output

60

cells. The neural networks are built from layers of neurons connected so that one layer receives input from the preceding layer of neurons and passes the output on to the subsequent layer. A neuron is a real function of the input vector (y_j.....y_k). The output is obtained as

$$f(x) = f a_i + [\sum_{n}^{k} W_{ij} \times Y_j] \tag{3.7}$$

Where f is a function, typically the sigmoid (logistic or tangent hyperbolic) function. A graphical presentation of neuron is shown in the Figure3.12. Mathematically a Multi-Layer Preceptor network is a function consisting of compositions of weighted sums of the functions corresponding to the neurons.

Feed-forward networks are especially useful in function approximation when a set of inputs and outputs is all that is known of the system, which is the situation in this study. Feed-forward networks have their neurons arranged in layers. These layers have connections to the layers either side, as shown in Figure 4.13. As described by (Graham, 2006) Figure 3.13 shows a network with 'p' inputs and 's' outputs. There are two layers of hidden neurons, 1 and 2, with 'q' and 'r' neurons in each, respectively. In designing a feed forward neural network, it is necessary to determine heuristically the combinations of the number of hidden layers and the number of neurons in each to obtain the optimum combination. Common notation for the number of layers in a network is described as being the number of hidden layers plus the output layer, since these are the layers that process the information.
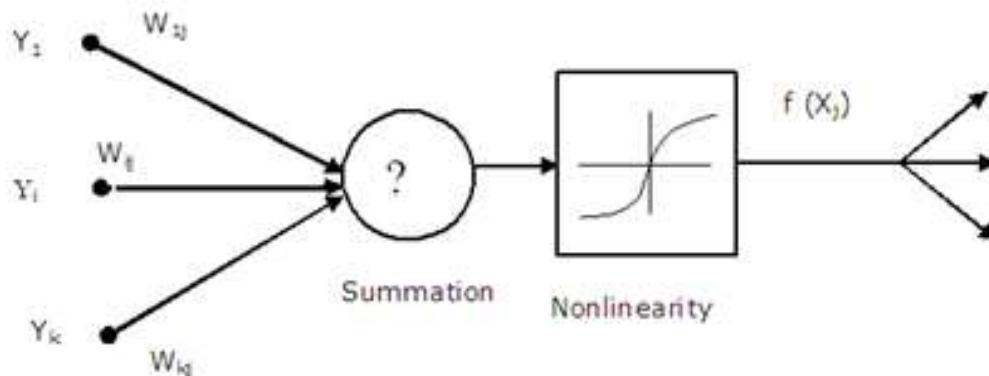
Figure 4.12 Structure of Neuron
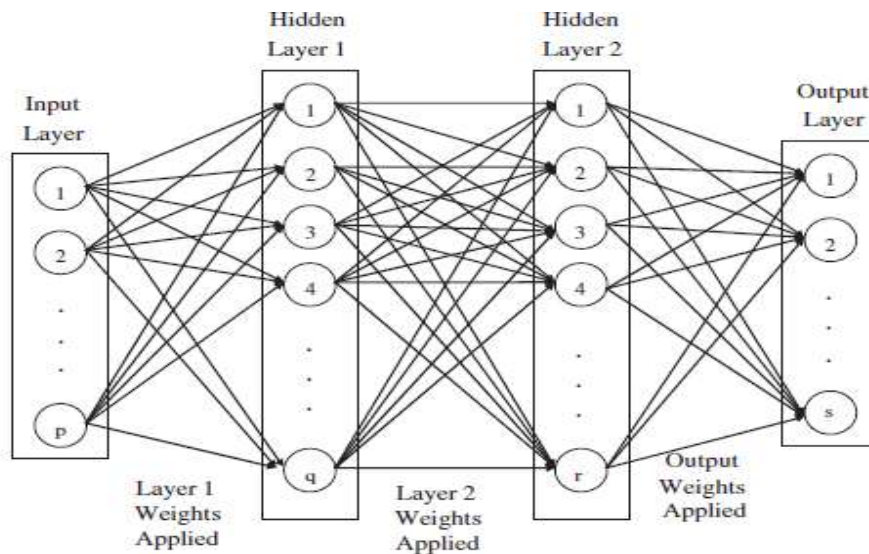
Figure 3.13 Feed-Forward Back Propagation Neural Network Architecture

3.9 ADAPTIVE NEURO-FUZZY INFERENCE SYSTEM (ANFIS)

Modern intelligent techniques are popular amongst the researchers in recent years. Many studies were carried out to take benefits of artificial neural networks (ANN) and fuzzy inference system. The combination of neuro-fuzzy system displays the generalization capabilities of ANN and the decision-making ability of fuzzy systems. The fuzzy logic plays important role in the intelligent systems by self-tuning the parameters through a learning technique. Adaptive Neuro- Fuzzy Inference System (ANFIS) is based on Takagi–Sugeno fuzzy inference system. The integration of networks and fuzzy logic in a single framework displays the benefits of both. The nonlinear functions are approximated by set of fuzzy If and Then rules. ANFIS is considered to be a universal estimator (Alambeigi Farshid et al., 2016)

3.9.1 Fuzzy Inference System

It is also known as fuzzy-rule-based system. FIS has three major elements namely basic rules consisting of fuzzy logic rules If-Then, membership function and reasoning fuzzy inference techniques. Figure3.14 shows FIS composed of (i) a rule base having fuzzy If-Then rule (ii) data base which defines membership function (iii)

Decision making wherein it performs inference operation (iv) Fuzzification interface which transforms the crisp inputs into degrees of match with linguistic values and (v) defuzzification interface which transforms the fuzzy results into a crisp output (Singh Bhoopal et al, 2012). Takagi–Sugeno, Mamdani, and Tsukamoto are the types of FIS (Cheng et al. 2005) but Takagi–Sugeno model of FIS is widely used in the application of ANFIS method.
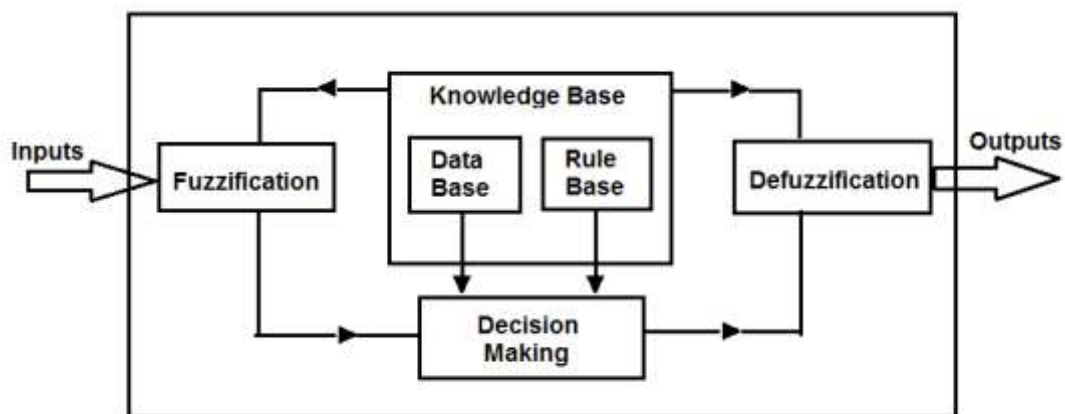

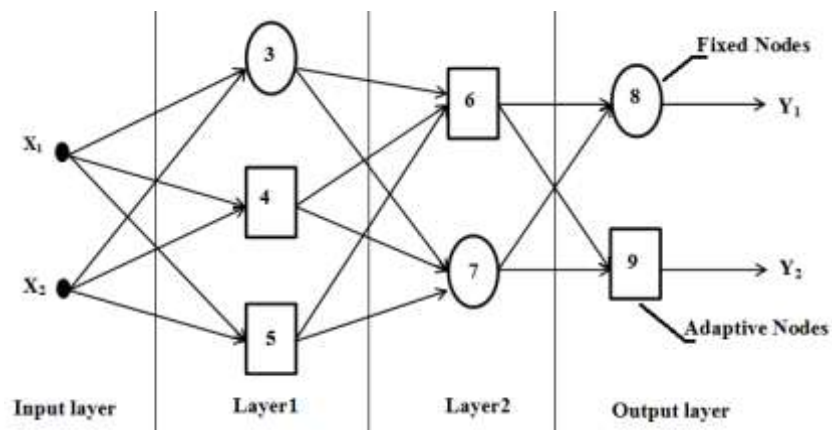**Figure 3.14 Basic Fuzzy Inference System (FIS)**

Figure 3.15 Adaptive Network

3.9.2 Adaptive Network

Adaptive network is feed-forward neural network having multiple layers as shown in Figure 3.15 This network use supervised learning algorithms during the learning process. In adaptive network the number of adaptive nodes is directly interconnected

63

without any weight value between them. The network node has different function and tasks in terms of signals and parameters that controls the output of the network. The error in the output of an adaptive network is controlled by the learning rule used in the nodes. The learning algorithm used for basic adaptive network is gradient descent or back propagation and the chain rule.

3.9.3 ANFIS Architecture

As described by W. Suparta and K.M. Alhasa in chapter 2 of the book *Modeling of Tropospheric Delays Using ANFIS*, the architecture levels and the nodes are given as follows. Figure 3.16 (a, b) shows the fuzzy reasoning mechanism for Takagi–Sugeno model and ANFIS architecture. For simplicity, assume that there are two inputs x and y, and one output f. Two rules are used in the method, "If-Then" for Takagi–Sugeno model, as follows:

Rule 1 = If *x* is *A₁* and *y* is *B₁*   Then $f_1=p_1x+q_1x+r_1$

Rule 2 = If *x* is *A₂* and *y* is *B₂*   Then $f_2=p_2y+q_2y+r_2$

Where,

A_1, A_2 and B_1, B_2 are the membership functions of each input *x* and *y* (part of the premises), and

p_1, q_1, r_1 and p_2, q_2, r_2 are linear parameters in part-Then (consequent part) of Takagi–Sugeno fuzzy inference model.

ANFIS architecture as shown has five layers. The first and fourth layers contain an adaptive node, while the other layers contain a fixed node.

Layer 1: Every node in this layer adapts to a function parameter. The output from each node is a degree of membership value that is given by the input of the membership functions. For example, the membership function can be a Gaussian membership function (equation 3.8), a generalized bell membership function (equation 3.9), or another type of membership function

$$\mu_{Ai}(x) = \exp\left[-\left(\frac{x-c_i}{2a_i}\right)\right]^2 \tag{3.8}$$

$$\mu_{Ai}(x) = \frac{1}{1+\left|\frac{x-c_i}{a_i}\right|^{2b}} \tag{3.9}$$

$$O_{1,i} = \mu_{Ai}(x), \quad i = 1,2 \tag{3.10}$$

$$O_{1,i} = \mu_{Bi-2}(y), \quad i = 3,4 \tag{3.11}$$

Where μ_{Ai} and μ_{Bi-2} are the degree of membership functions for the fuzzy sets A_i *and* B_i, respectively, and $\{a_i, b_i, c_i\}$ are the parameters of a membership function that can change the shape of the membership function. The parameters in this layer are typically referred to as the premise parameters.

Layer 2: Every node in this layer is fixed or non-adaptive and the circle node is labelled as P. The output node is the result of multiplying of signal coming into the node and delivered to the next node. Each node in this layer represents the firing strength for each rule. In the second layer, the T-norm operator with general performance, such as the AND, is applied to obtain the output

$$O_{2i} = w_i = \mu_{Ai}(x) \times \mu_{Bi}(y), \quad i = 1,2 \tag{3.12}$$

Where, w_i is the output that represents the firing strength of each rule.

Layer 3: Every node in this layer is fixed or non-adaptive and the circle node is labelled as N. Each node is a calculation of the ratio between the i-th rules firing strength and the sum of all rules' firing strengths. This result is known as the normalized firing strength.

$$O_{3i} = \overline{w}_i = \frac{w_i}{\sum_i w_i} \tag{3.13}$$

Layer 4: Every node in this layer is an adaptive node to an output, with a node function defined as

$$O_{4i} = \overline{w}_i f_i = \overline{w}_i(p_i x + q_i x + r_i) \tag{3.14}$$

Where $\overline{w}_i$ is the normalized firing strength from the previous layer (third layer) and $(p_i x + q_i x + r_i)$ a parameter in the node. The parameters in this layer are referredto as consequent parameters.
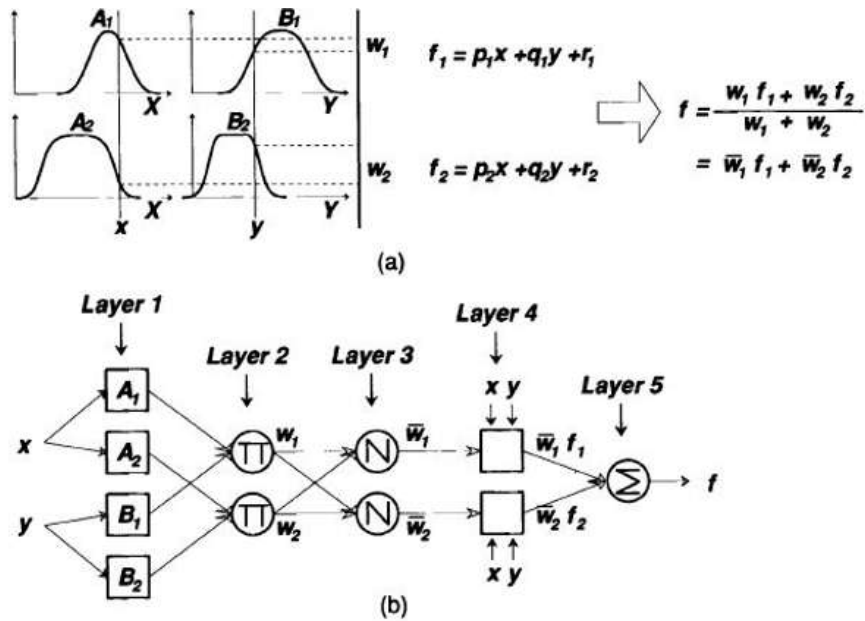
Figure 3.16 (a) Sugeno FIS "If-Then" and Fuzzy Logic Mechanism. (b) ANFIS Architecture (Suparta and Alhasa 2013)

Layer 5: The single node in this layer is a fixed or non-adaptive node that computes the overall output as the summation of all incoming signals from the previous node. In this layer, a circle node is labelled as Σ.

$$O_{4i} = \sum_i \overline{w}_i f_i = \frac{\sum_i w_i f_i}{\sum_i w_i} \tag{3.15}$$

3.10 CONTACT STRESS ANALYSIS

When the radial load is transferred between two races of rotating bearing assembly, contact stress is developed at the point of contact. These contact stresses concentrates along the length of bearing due to irregular surface and lead to friction and wear of the material. The study of contact stress was published by Heinrich Hertz and is still basis for computing contact stresses. In this study, the composites material developed is analyzed to estimate contact stresses using analytical method and the results are validated by Finite Element Method (FEM). Complex geometries can be divided in to series of many smaller shapes/elements which represents series of simultaneous

66

partial differential equations. These equations are solved numerically to get closed form solution.

3.10.1 Analytical solution for parallel cylinders (Scarcella 2008)

Theory of elasticity is used to find contact stress between rollers with assumption that the strain is linear and small. It is because of the fact that the bearings are designed for number of revolutions without failure. The geometry of the rollers is assumed to be same along its length. To model the interface infinite, stress, pressure, and deformation is assumed to be constant and defined in terms of unit per length of roller.

When the load is applied on two bodies in contact with each other, the elastic deformation will occur at the interface and line of contact will transform into area of contact having width. This strain leads to development of stresses in the material. For simplicity in calculation the area in contact is confined to a rectangular area by assuming smooth surface contact and no discontinuities. Figure 3.17 shows two cylinders (no load condition) in contact with each other such that their axes are parallel to each other. The axes of these two cylinders are perpendicular to the plane of the paper and are denoted by 'Y' axis.

As described by Jeffrey A. Scarcella (2008) in his report of 'Contact Stress Concentration due to Surface Irregularity in cylindrical Rolling Element Bearings and considering above assumptions the surface profile of each cylinder may be represented as

$$Z_i = A_i x^2 + B_i y^2 + C_i xy + D_i x^3 ....\text{where i= 1, 2 for each cylinder} \quad (3.16)$$

The unloaded separation distance between the two points at the same x-coordinate on the two cylinders may be defined as

$$h = Z_1 - Z_2 \quad (3.17)$$
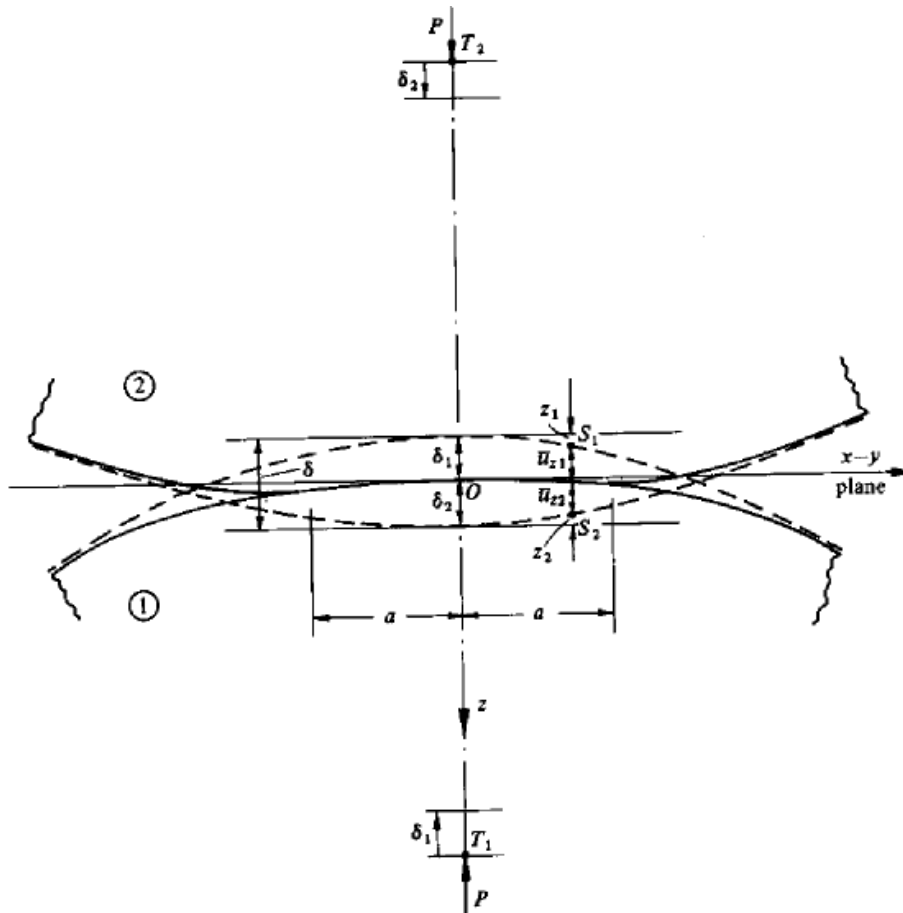
Figure 3.17 Two Parallel Cylinders in Contact with Each Other. (Scarcella 2008)

Johnson K L (1985) shows that Z_1 and Z_2 can be expressed in terms of the radii of curvature of the solid in the principal axes. R'_i is the local radius of curvature of the surface about an axis normal to x and z for cylinder i, and R''_i is the local radius about an axis normal to y and z.

$$Z_1 = \frac{1}{2\,R'_1}x_1^2 + \frac{1}{2\,R'_1}y_1^2 \qquad\qquad (3.18\ a)$$

$$Z_2 = -\frac{1}{2\,R'_2}x_2^2 - \frac{1}{2\,R'_2}y_2^2 \qquad\qquad (3.18\ b)$$

Of course, for two cylinders that have parallel axes along y, the surfaces are linear along y, which is effectively an infinite radius, i.e. $R'' = \infty$. This eliminates variation in z due to y-position and leaves simplified expressions for z.

$$Z_1 = \frac{1}{2R'_1}x_1^2 \qquad\qquad (3.19\ a)$$

68

$$Z_2 = \frac{1}{2R_2'} x_2^2 \tag{3.19 b}$$

Recalling that, $h = Z_1 - Z_2$, if the x_1 and x_2 axes are aligned, or if one radius is infinite, a value R' can be defined that combines the R'$_1$ and R'$_2$ quantities into a single effective radius of curvature for interface between the two cylinders. Solving for R' in terms of the two cylinders' radii gives an expression for effective radius.

$$R' = \left(\frac{1}{R_1} + \frac{1}{R_2}\right)^{-1} \text{such that} \tag{3.20}$$

$$h = \frac{1}{2\,R'} x^2 = \frac{1}{2}\left(\frac{1}{R_1} + \frac{1}{R_2}\right) x^2 \tag{3.21}$$

Given this relation for the separation between surface contours in the un-deformed and unloaded state, the next step is to apply a normal compressive load and find the resulting deformation in both solids.

Under a load P (in this case, P is per unit of cylinder length), each cylinder will translate an amount δ_i, measured as the distance that the bulk solid body moves towards theorigin of the coordinate system defined above (Figure 3.17). As the two bodies cannot occupy the same space, both will deform locally by amounts $\bar{u}_{zi}$. The interface is notnecessarily symmetric and, in this general case, the materials of the two cylinders maydiffer, so $\bar{u}_{zi}$ does not necessarily equal δ_i. The sum of the cylinders translations can be equated to the total combined deformation of both bodies plus any initial separation in the un-deformed state.

$$\bar{u}_{z1} + \bar{u}_{z2} + h = \delta_1 + \delta_2 \tag{3.22}$$

Introducing a displacement sum $\delta = \delta_1 + \delta_2$ and substituting the generic expression $h = A\, x^2 + B\, y^2$ for h, we find the displacements in terms of location on the body.

$$\bar{u}_{z1} + \bar{u}_{z2} + h = \delta - Ax^2 + By^2 \tag{3.23}$$

As earlier, the y term falls out when limited to the 2D cylindrical case, and we can combine equations 3.21 and 3.23 to give:

$$\bar{u}_{z1} + \bar{u}_{z2} + h = \delta - \left(\frac{1}{2\,R'}\right)x^2 \qquad (3.24)$$

It is necessary to note that this equation holds true within the area of contact under the normal load. Outside the contact area, the displacements will be lower than at contacting points, or:

$$\bar{u}_{z1} + \bar{u}_{z2} + h < \delta - \left(\frac{1}{2\,R'}\right)x^2 \qquad (3.25)$$

Equation 3.25 can be differentiated with respect to x to give the displacement gradient at the contact, or the slope of the body surface when deformed under load. The equation is thus simplified as constants are eliminated.

$$\frac{\partial \bar{u}_{z1}}{\partial x} + \frac{\partial \bar{u}_{z2}}{\partial x} = -\left(\frac{1}{R'}\right)x \qquad (3.26)$$

From Johnson, the general expression for the displacement gradient in z, derived from elasticity and the half-space model, is given as:

$$\frac{\partial \bar{u}_z}{\partial x} = -\frac{2\,(1-v^2)}{\pi E} \int_{-b}^{a} \frac{p(s)}{x-s}\,ds + \frac{(1-2v)(1+v)}{E}q(x) \qquad (3.27)$$

Where, p (s) and q (x) are the normal and tangential surface tractions respectively. We are assuming the case of no tangential forces, so q(x)=0. The effective elastic modulus E* will be defined as follows.

$$E^* = \left(\frac{1-v_1^2}{E_1} + \frac{1-v_2^2}{E_2}\right)^{-1} \qquad (3.28)$$

If materials 1 and 2 are the same, E* simplifies to the plane strain elastic modulus of the material. Combining equations 3.26, 3.27, and 3.28 gives the following.

$$\int_{-a}^{a} \frac{p(s)}{x-s}\,ds = \frac{\pi E^*}{2R'}x \qquad (3.29)$$

The solution to 3.29, as described in Johnson (1985) shows the following distribution of pressure over the contact surface:

$$p(x) = \frac{2p}{\pi a^2}\left(a^2 - x^2\right)^{1/2} \qquad (3.30)$$

70

$$\text{Where } a = 2\sqrt{\frac{P\,R'}{\pi\,E^*}} \tag{3.31}$$

The maximum contact pressure can be found by differentiating $p(x)$, and, as would be expected, the max pressure occurs at the center of the interface such that $x=0$.

$$P_{max} = \frac{2P}{\pi a} \quad \text{or} \tag{3.32}$$

$$P_{max} = \left(\frac{PE^*}{\pi R'}\right)^{1/2} \tag{3.33}$$

Extension of equations 3.10, 3.11, and 3.12 to a contact region of a finite width, as shown in Johnson, gives the following expressions for the stress at the contact area:

$$\sigma_x = -\frac{2z}{\pi}\int_{-a}^{a}\frac{p(s)(x-s)^2}{((x-s)^2+z^2)^2}ds \tag{3.34}$$

$$\sigma_z = -\frac{2z^3}{\pi}\int_{-a}^{a}\frac{p(s)}{((x-s)^2+z^2)^2}ds \tag{3.35}$$

$$\tau_{xz} = -\frac{2z^2}{\pi}\int_{-a}^{a}\frac{p(s)(x-s)}{((x-s)^2+z^2)^2}ds \tag{3.36}$$

Substituting equation 3.30 for $p(x)$ and the expression for P_{max} gives the following stress relations. For simplicity of the calculations, we will consider the stress variation across the contact surface and along the line (plane) $x=0$.

Contact stress at the surface:

$$\sigma_x = p(x), -a \le x \le a \tag{3.37}$$

$$\sigma_z = p(x), -a \le x \le a \tag{3.38}$$

Stress within the material above the point of initial (unloaded) contact:

$$\sigma_x = -\frac{P_{max}}{a}\left((a^2 + 2z^2)(a^2 + z^2)^{-\frac{1}{2}} - 2z\right) \tag{3.39}$$

$$\sigma_z = -P_{max}\cdot a(a^2 + z^2)^{-\frac{1}{2}} \tag{3.40}$$

$$\tau_1 = P_{max}\cdot a(z - z^2(a^2 + z^2)^{-\frac{1}{2}}) \tag{3.41}$$

Differentiating the principal shear stress expression with respect to *z* gives the location of the maximum shear stress along the z-axis:

$$\tau_{1max} = \tau_1(0.78a) = 0.30P_{max} \tag{3.42}$$

Above analytical solutions by Scarcella (2008) and Johnson (1985) are used to estimate the contact stresses in cylinders considering physical properties of F20/G5/B15, F20/G10/B10and F20/G15/B5 composites. The same are validated by carrying finite element analysis using FEA tool.

CHAPTER 4

RESULTS AND DISCUSSION: MECHANICAL CHARACTERIZATION

This chapter describes the measured values of mechanical and physical properties of glass fiber reinforced epoxy composites filled with graphite and sintered bronze. The results of mechanical characterization are in line with the results of the previous work carried by researchers. The effect of glass fiber reinforcement and the filler incorporation on various properties of epoxy matrix composites have been discussed.

4.1 TENSILEPROPERTIES OF COMPOSITES

The samples for tensile tests are prepared according to the ASTM D-3039 and tensile tests are carried out with maintaining the speed of a crosshead 2 mm/min. The tensile test samples are made of thickness 3 mm and the area of cross-section is rectangular. These test samples carry tabs at the ends to hold firmly in the jaws of UTM. Five tests are conducted for each composition and the average results are tabulated as shown in Table 4.1.

Figure 4.1 shows the variation in tensile properties of the composites with varying volume percentage of glass fiber, graphite and bronze filler. Remarkable enhancement in tensile strength of 20 vol% of glass fiber composites is observed, as compared to 10

Table 4.1 Tensile Characteristics of Composites

Specimen	Maxi Force in (N)	Tensile Modulus (GPa)	Tensile strength (MPa)	Elongation (%)
10F/10G/20B	1070	4.764	44.76	0.98
10F/15G/15B	888	4.464	39.84	0.75
10F/20G/10B	1290	3.72	41.28	1.51
15F/5G/15B	1540	4.176	63.72	1.76
15F/10G/10B	1680	5.088	53.52	1.5
15F/15G/5B	1330	5.256	71.16	1.27
20F/5G/15B	2050	5.172	69.24	2.16
20F/10G/10B	1540	5.268	56.04	2
20F/15G/5B	958	4.644	37.08	1.46

vol% and 15 vol%. Similar observations are reported by various researchers. It is observed that tensile strength depends on the percentage of reinforcing E-glass fiber than the fillers graphite and bronze. Inclusion of graphite and bronze nullifies their effect on tensile behavior of the composites because graphite has low strength and bronze has high strength. The decreased tensile strength for compositions 15F/10G/10B and 20F/15G/5B may be due to improper fabrication of test specimens or due to presence of voids at the interface between the fibers, fillers and the matrix. And the weak interfacial adhesion does not transfer the tensile stresses to fibers and composites undergo failure before its maximum strength.

The change in tensile modulus of the composites with varying volume percentage of glass fiber, graphite and bronze filler is presented in Figure 4.2. It can be seen that the tensile modulus increase significantly with 20 vol% of glass fiber reinforcement irrespective of the percentage of graphite and bronze. Many published work reported that the increased fiber content in the composites leads to increase in tensile strength and decrease in tensile strain. Hence even though the tensile strength decreases with addition of graphite, the tensile modulus of the composites is bound to increase and it is observed in this investigation. As the graphite content for composites with glass fiber 10 vol% and 20 vol% is increased, the tensile modulus show decrease trend. The increased tensile property of composite was attributed to the increased volume percentage of E-glass fiber and increased bronze and/or decreased volume percentage of graphite. It can also be noted that the decrease in graphite filler has a positive effect on tensile properties. It might be due to the mechanical properties of the bronze and/ or graphite filler.

4.2 FLEXURALSTRENGTH OF COMPOSITES

Flexural strength is the ability of the material to withstand bending failure when subjected to bending load. To make use of composite material for machine element, the flexural properties are needed to be improved. The flexural tests are carried to measure the flexural strength and flexural modulus of composites as per ASTM D790 and the tests are carried at the cross head speed of 1mm/min. The tests are carried out on five specimens and average results obtained are tabulated as shown in Table 4.2.
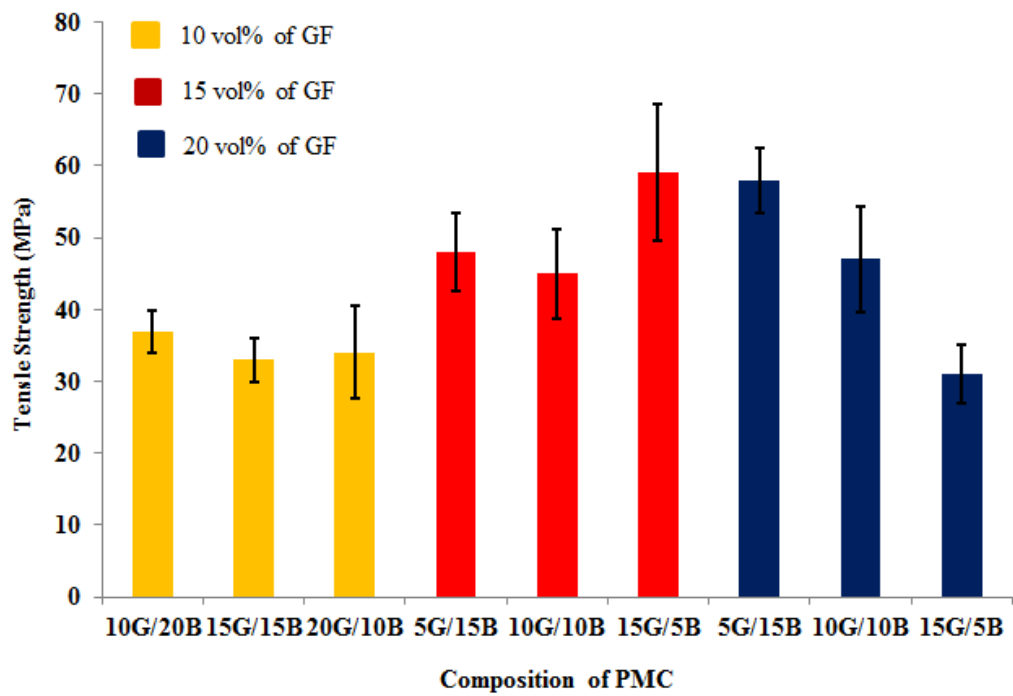
74

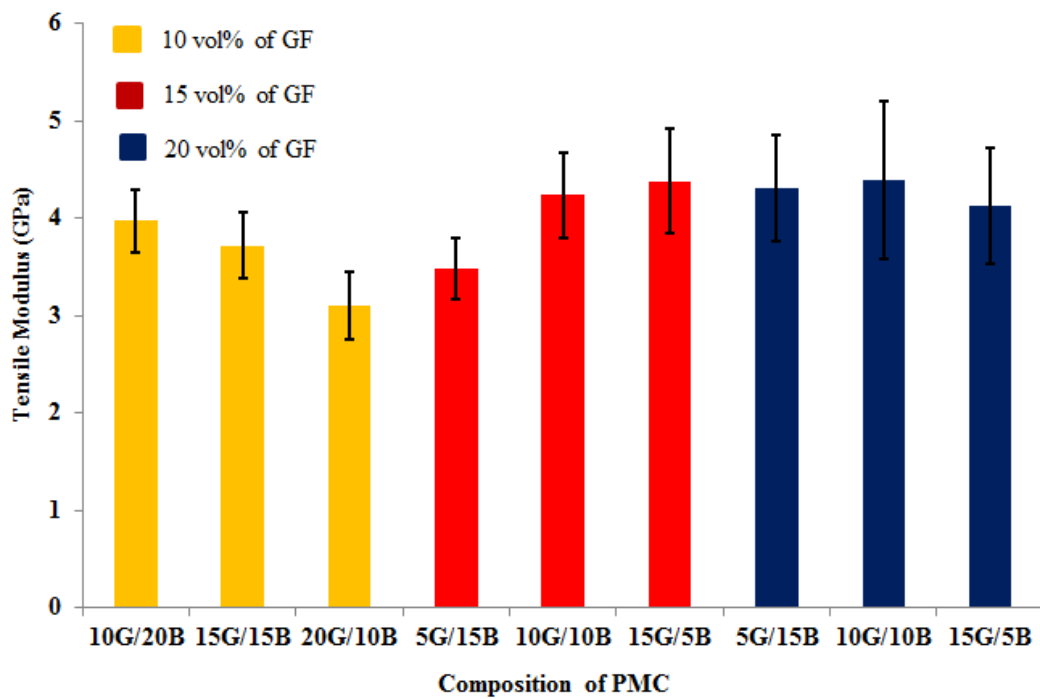**Figure 4.1 Tensile Strength of Different Composites**

Figure 4.2 Tensile Modulus of Composites

75

The change in flexural strength of the composites with varying volume percentage of glass fiber, graphite and bronze filler is presented in Figure 4.3. An increase in flexural strength is recorded for 15 vol% and 20 vol% of fiber reinforcement and highest strength is observed in case of composites 20F/10G/10B. It is clear from the Figure 4.3 that the flexural strength is influenced by the glass fiber reinforcement irrespective of the volume percentage of fillers. This is attributed to the increased volume percentage of E-glass fiber and the interfacial bond between the fiber and matrix. It is also observed that decreased volume percentage of bronze helped in enhanced flexural modulus. The incompatibility of the bronze filler might be the reason for reduced flexural strength. Sintered bronze behaves like a brittle material in the composite as compared to graphite. The lower values of flexural strength may be because of the voids and improper mixing or dispersion of the fibers and fillers.

Glass fiber reinforcement and graphite filler improved ability of material to resist bending of the composites. The change in flexural modulus of the composites with varying volume percentage of glass fiber, graphite and bronze filler is presented in Figure 4.4. The results show remarkable improvement in flexural modulus with increase in reinforcing glass fiber from 10 vol% to 20 vol%. These results are in line with the previous study carried by various researchers. The addition of graphite and bronze shows marginal effect on the flexural modulus. But addition of graphite as compared to bronze showed positive effect on flexural modulus.

Table 4.2 Flexural Strength of Composites

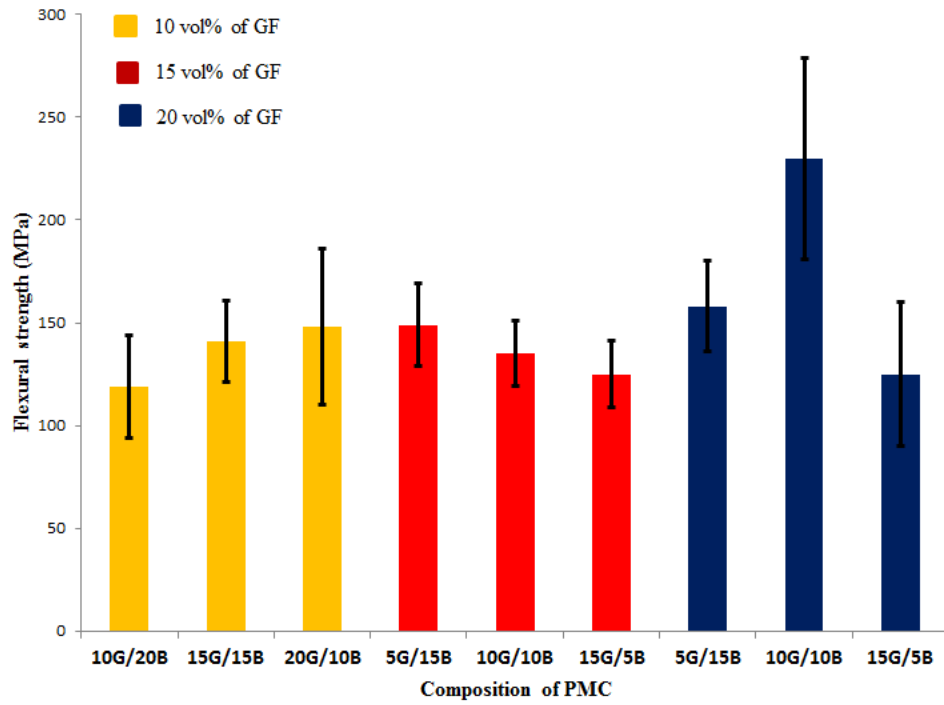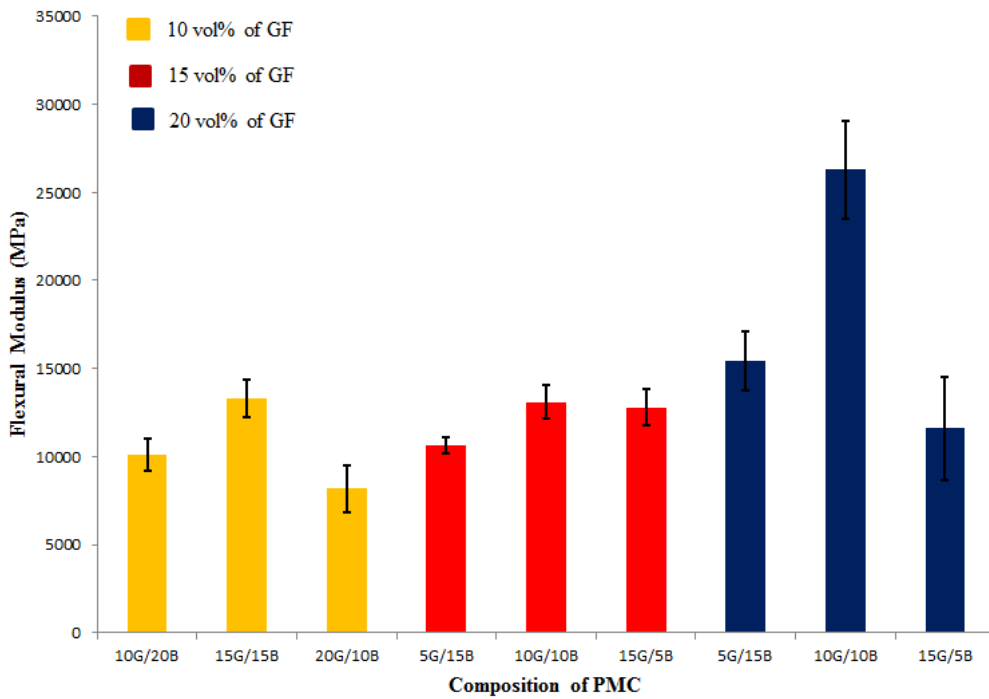| Specimen	Maxi Force in (N)	Flexural Modulus (GPa)	Maxi Stress (MPa)
10F/10G/20B	175	10.10	119
10F/15G/15B	188	13.30	141
10F/20G/10B	232	8.17	148
15F/5G/15B	233	10.60	149
15F/10G/10B	212	13.10	135
15F/15G/5B	195	12.80	125
20F/5G/15B	195	15.40	158
20F/10G/10B	347	26.30	230
20F/15G/5B	145	11.60	125

Figure 4.3 Flexural Strength of Composites

Figure 4.4 Flexural Modulus of Composites

4.3 IMPACT STRENGTH OF COMPOSITES

The impact strength of the material is the ability to absorb the energy when shock or impact load is applied and dissipate the energy. Impact test is carried on AIT-300EN (Fasne test equipment Pvt., Ltd.) to measure materials resistance to impact from a swinging pendulum as per ASTM D256. The test is carried on Notch free test specimens and average values of 5 specimens are noted for each composition and reported in Table 4.3. The measured impact energy for various composites is presented in the Figure 4.5. It is observed from the Figure that the impact energies of glass fiber reinforced composites increase with increase in graphite filler content from 5 vol% to 15 vol%.

Table 4.3 Impact Energy of Composites

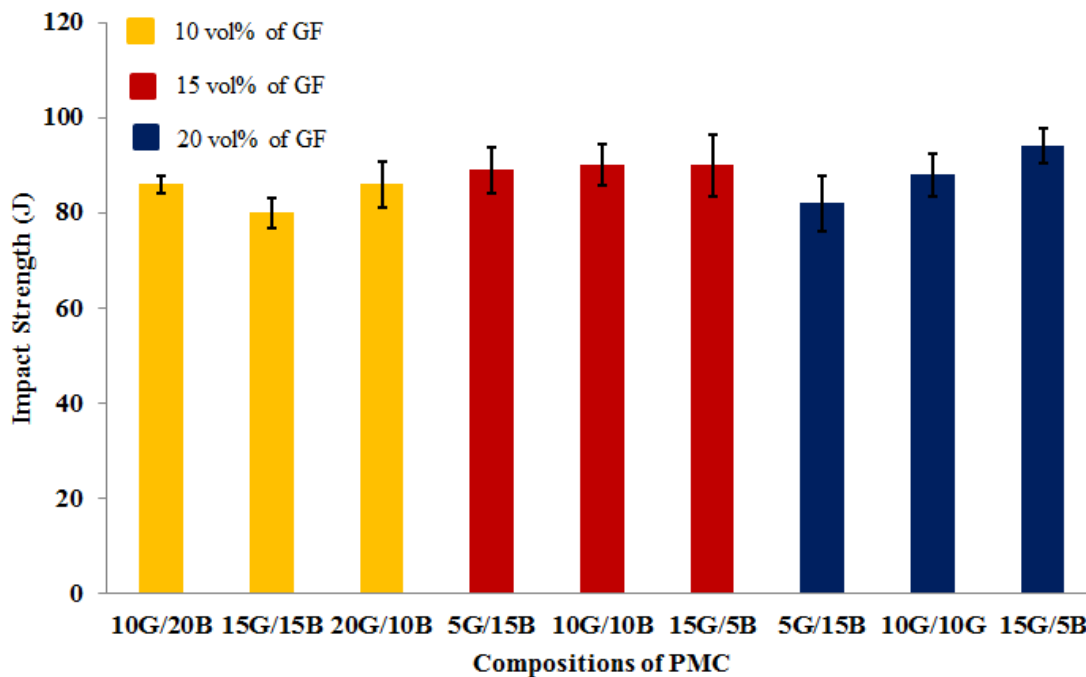| Composition	10F/ 10G/ 20B	10F/ 15G/ 15B	10F/ 20G/ 10B	15F/ 5G/1 5B	15F/ 10G/ 10B	15F/ 15G/ 5B	20F/ 5G/ 15B	20F/ 10G /10B	20F/ 15G/ 5B
Impact Energy (J)	86	84	86	89	90	90	89	91	94
Std. Dev.	4.38	2.45	4.69	4.69	4.77	4.77	3.41	3.29	3.29

Figure 4.5 Impact Energy of Composites

78

It is also found that, increase in E-glass fiber from 10 vol% to 20 vol%, showed significant increase in impact energy absorbed. This is attributed to the use of chopped glass fibers. The investigation shows enhancement in impact strength with increase of glass fiber and graphite content in the composites.

4.4 HARDNESS OF COMPOSITES

Hardness is the property of the material to resist scratch or indentation. Rockwell hardness test is carried to measure the hardness of the composite as per ASTM D-785. A ¼" indenter ball is pressed against polished composite surface for 10 s under a load of 100 Kg. The M scale is selected which indicate type of material to be tested i.e. composite material. The average results obtained for five different locations are taken for each composition and is shown in Table 4.4.

Table 4.4 Rockwell Hardness of Composites

Composition	10F/ 10G/ 20B	10F/ 15G/ 15B	10F/ 20G/ 10B	15F/ 5G/1 5B	15F/ 10G/ 10B	15F/ 15G/ 5B	20F/ 5G/ 15B	20F/ 10G/ 10B	20F/ 15G/ 5B
Hardness (HRB)	M71	M70	M76	M82	M82	M84	M80	M78	M74
Std. Dev.	1.90	3.03	4.69	4.69	4.34	6.45	5.69	4.43	3.63

Figure 4.6 presents the measured hardness values of the glass fiber reinforced and graphite and bronze filled epoxy composites. It is clear from the Figure that the use of glass fiber and graphite filler greatly increases the hardness of composites. This is attributed to the recipe of chopped fiber and graphite in the epoxy matrix. The hardness value is desirable in the composites to exhibit the wear resistance and abrasion resistance properties for tribological applications.

4.5 THEORETICAL AND MEASURED DENSITY OF COMPOSITES

Density is the vital material property which governs selection of material in case of weight sensitive applications. Hence, polymer composites are replacing the conventional materials because of their low density. Density of the polymer composites depends on the volume percent of the matrix, fibers and fillers. It is

observed that the values of theoretical and measured density differ because of formation of voids. The formation of void reduces the mechanical property of composites. The information of the void percent is necessary to judge the soundness of the composites. The theoretical density of the epoxy matrix composites in this study is estimated using rule of hybrid mixture (RoHM) as per equation 4.1 and presented in Table 4.5 and the comparison between theoretical, experimental and void fraction is presented in Table 4.6.

$$\rho_{th} = \rho_m V_m + \rho_f V_f + \rho_g V_g + \rho_b V_b \tag{4.1}$$

Where, ρ is the density and V is volume fraction and the suffix m, f, g and b refers to the matrix material, glass fiber, graphite and bronze fillers respectively. The experimental density is calculated using the Archimedes Principle (Patil and Prasad 2015).
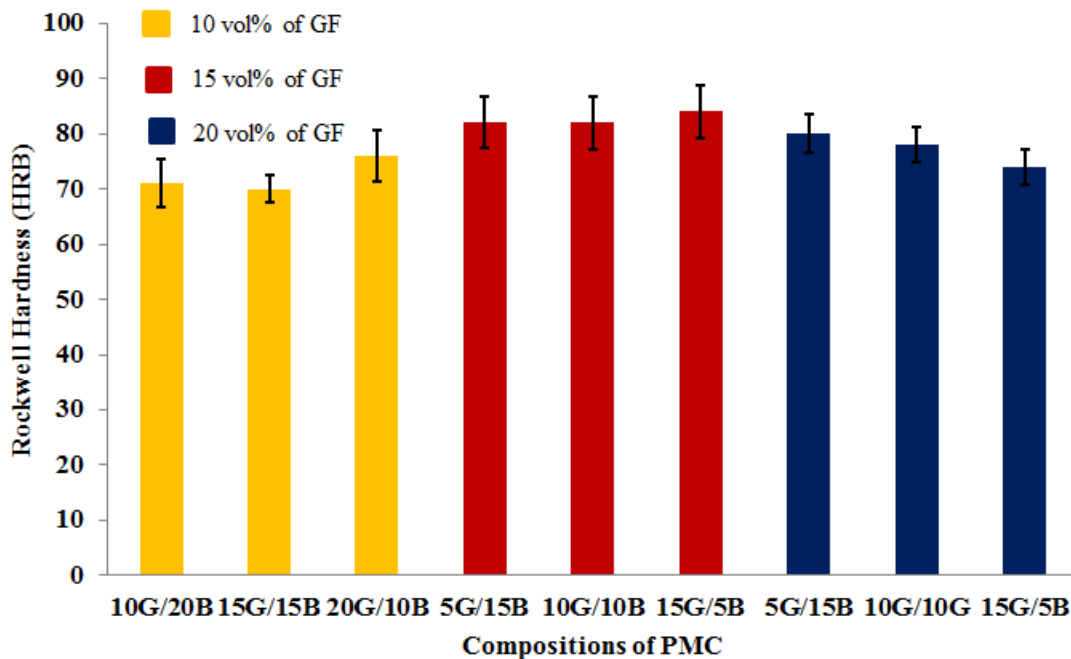

Figure 4.6 Hardness Values of the Composites

Table 4.5 Theoretical Density of Composites

Composites	ρ_m	V_m	ρ_g	V_g	ρ_b	V_b	ρ_f	V_f	ρ_{th}(g/cc)
10F/10G/20B	1.1383	0.72	2.23	0.12	6.4	0.24	2.62	0.12	2.94
10F/15G/15B	1.1383	0.72	2.23	0.18	6.4	0.18	2.62	0.12	2.69
10F/20G/10B	1.1383	0.72	2.23	0.24	6.4	0.12	2.62	0.12	2.44
15F/5G/15B	1.1383	0.78	2.23	0.06	6.4	0.18	2.62	0.18	2.65
15F/10G/10B	1.1383	0.78	2.23	0.12	6.4	0.12	2.62	0.18	2.40
15F/15G/5B	1.1383	0.78	2.23	0.18	6.4	0.06	2.62	0.18	2.14
20F/5G/15B	1.1383	0.72	2.23	0.06	6.4	0.18	2.62	0.24	2.73
20F/10G/10B	1.1383	0.72	2.23	0.12	6.4	0.12	2.62	0.24	2.48
20F/15G/5B	1.1383	0.72	2.23	0.18	6.4	0.06	2.62	0.24	2.23

The change in theoretical and measured density of the various composites is presented in Figure 4.7 and 4.8. It is observed that the addition of sintered bronze filler increase the density of composites because sintered bronze has density of 6.4 g/cc. Density is experimentally calculated by Archimedes Principle using equation 4.2 and the void fraction by the equation 4.3.

$$\rho_{solid} = \rho_{liquid} \left(\frac{m_1}{m_1 - m_2} \right) \tag{4.2}$$

$$Void\ fraction = \frac{(Theoretical\ density - Measured\ density)}{Theoretical\ density} \tag{4.3}$$

The comparison between theoretical density, measured density and void fraction is shown in Table 4.6. Figure 4.8 shows the change in measured density for various composites. It can be observed from the Figure 4.9 that the percentage void fraction drastically increased for composites with 10 vol% to 20 vol% of glass fiber addition. This is attributed to the increased volume percentage of glass fiber and graphite. Chopped glass fiber has tendency of forming lumps when reinforced in epoxy matrix.
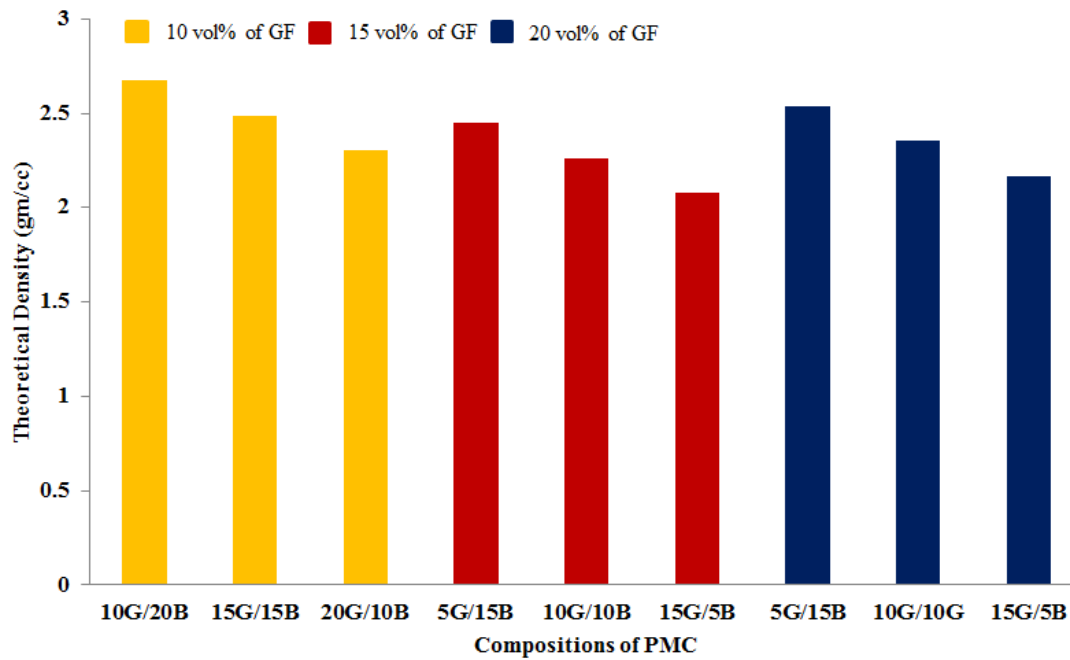
Figure 4.7 Theoretical Density of Composites using RoHM

Table 4.6 Theoretical Density, Measured Density and Void Fraction

Composites	Theoretical density	Measured density	Volume fraction of void (%)
10F/10G/20B	2.94	2.83	3.71
10F/15G/15B	2.69	2.60	3.39
10F/20G/10B	2.44	2.36	3.32
15F/5G/15B	2.65	2.56	3.33
15F/10G/10B	2.40	2.33	2.80
15F/15G/5B	2.14	2.08	2.84
20F/5G/15B	2.73	2.61	4.43
20F/10G/10B	2.48	2.35	5.27
20F/15G/5B	2.23	2.13	4.52

The void and porosity cannot be eliminated completely because of the various factors like the resin viscosity at room temperature, amount of air entrapped and geometrical factors (Campbell). Figure 4.9 shows the change in void fraction for various composites. It is observed that addition of graphite filler increase the void fraction in all composites except 10G/10B composite with 20 vol% of glass fiber content. It can

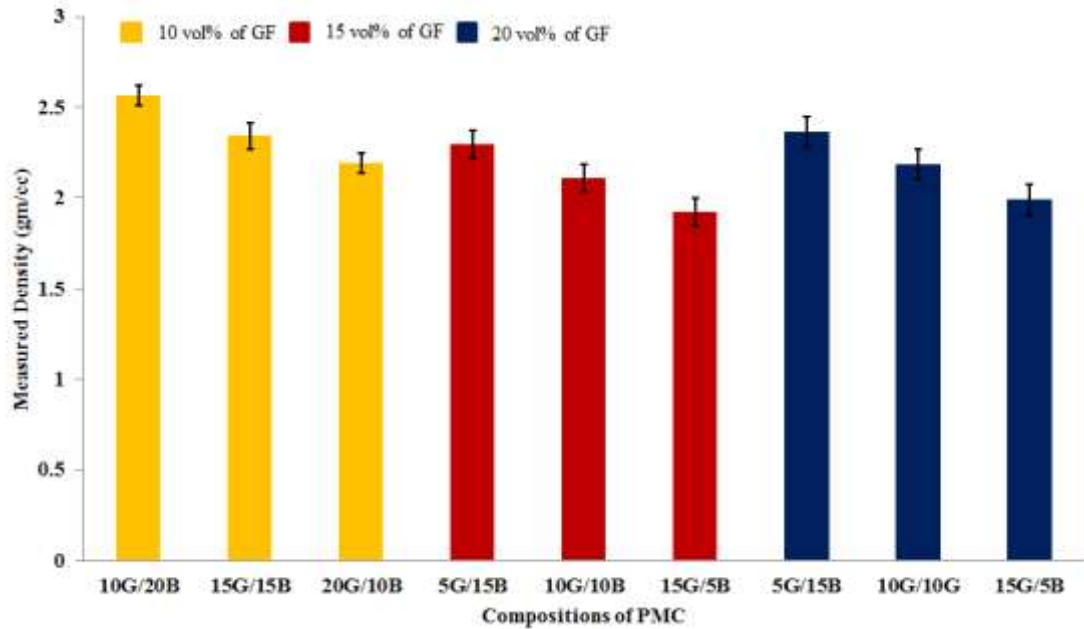also be observed from this Figure that addition of 20 vol% of glass fiber increase void fraction noticeably.

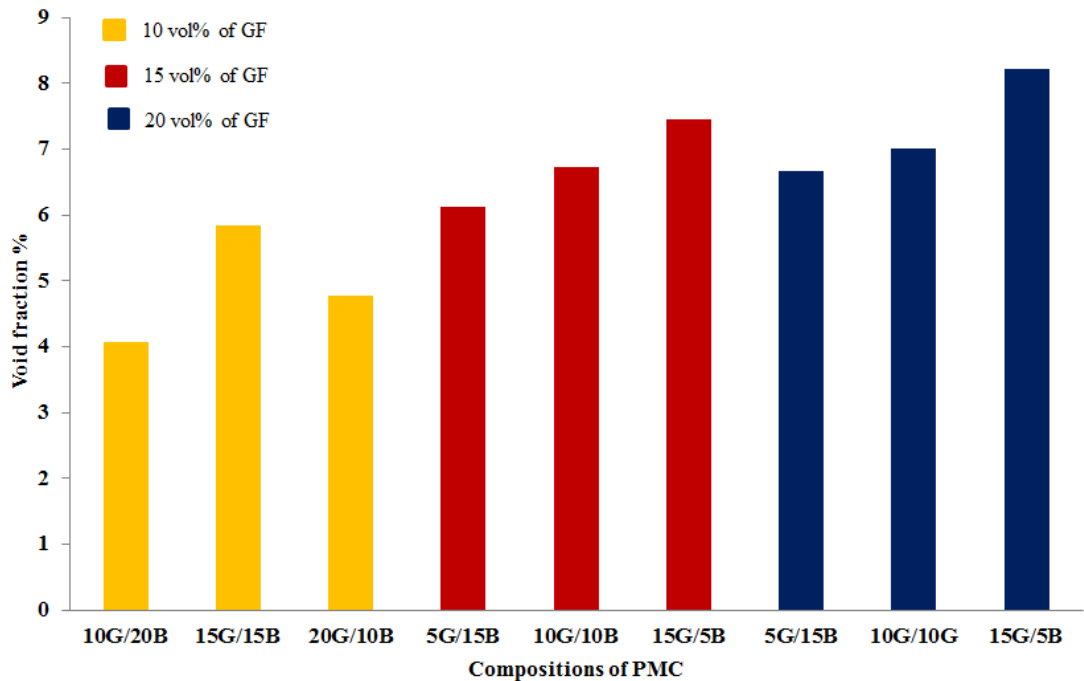**Figure 4.8 Measured Density of Composites using Archimedes Principle**

Figure 4.9 Void Volume Fraction % of Composites

4.6 METALLURGICAL MICROSCOPIC IMAGE ANALYSIS

The metallurgical electron micrograph analysis is carried to study the dispersion of graphite and bronze fillers and orientation of glass fiber reinforcement. The specimens are prepared using different emery papers having grades 400 to 1200 before micrographs are taken with a metallurgical electron microscope. In this analysis, it is found that graphite and sintered bronze particles are uniformly distributed and E-glass fibers are randomly distributed as shown in Figure 4.10 (Patil and Prasad 2015). The micrographs of the PMC as shown in Figure 4.10 (a, b & c) is reinforced with 10 vol% of glass fiber. The Figure 4.10 (a) indicates the major portion is occupied by the sintered bronze and E-glass fiber. The theoretical density of the composites with 20 vol% of sintered bronze showed higher values and this composition showed the lower void fraction. Figure 4.10 (b) shows evenly distributed graphite and bronze fillers. It can also be seen the randomly oriented glass fibers in the composite. It consists of 15 vol% of graphite and bronze. The void fraction for this composition is more than the previous composition. Figure 4.10 (c) show micrograph of 20 vol% of graphite and 10 vol% of bronze. It is clear from the micrograph that the graphite is seen evenly distributed across the surface. The void fraction for this composite is lower compared to the composite filled with 15 vol% of graphite.

The micrographs of composites reinforced with 15 vol% are shown in Figure 4.10 (d, e & f). Figure 4.10 (d) shows the composite filled with 15 vol% of sintered bronze and 5 vol% of graphite. The effect of increased glass fiber reinforcement is reflected in increased void fraction as shown in figure 4.9. The reinforced glass fibers of the composites are seen to be coated with the sintered bronze and graphite particles in figure 4.10 (e to h). These graphite and sintered bronze coated glass fibers showed enhanced performance of the composites in tribological analysis. The worn out debris of the pin of 'pin on disc wear test' setup provided lubricating layer between two rotating element. This lubricating film helped in reducing the friction. The reduction in friction further helped in reducing wear of the composite pin.
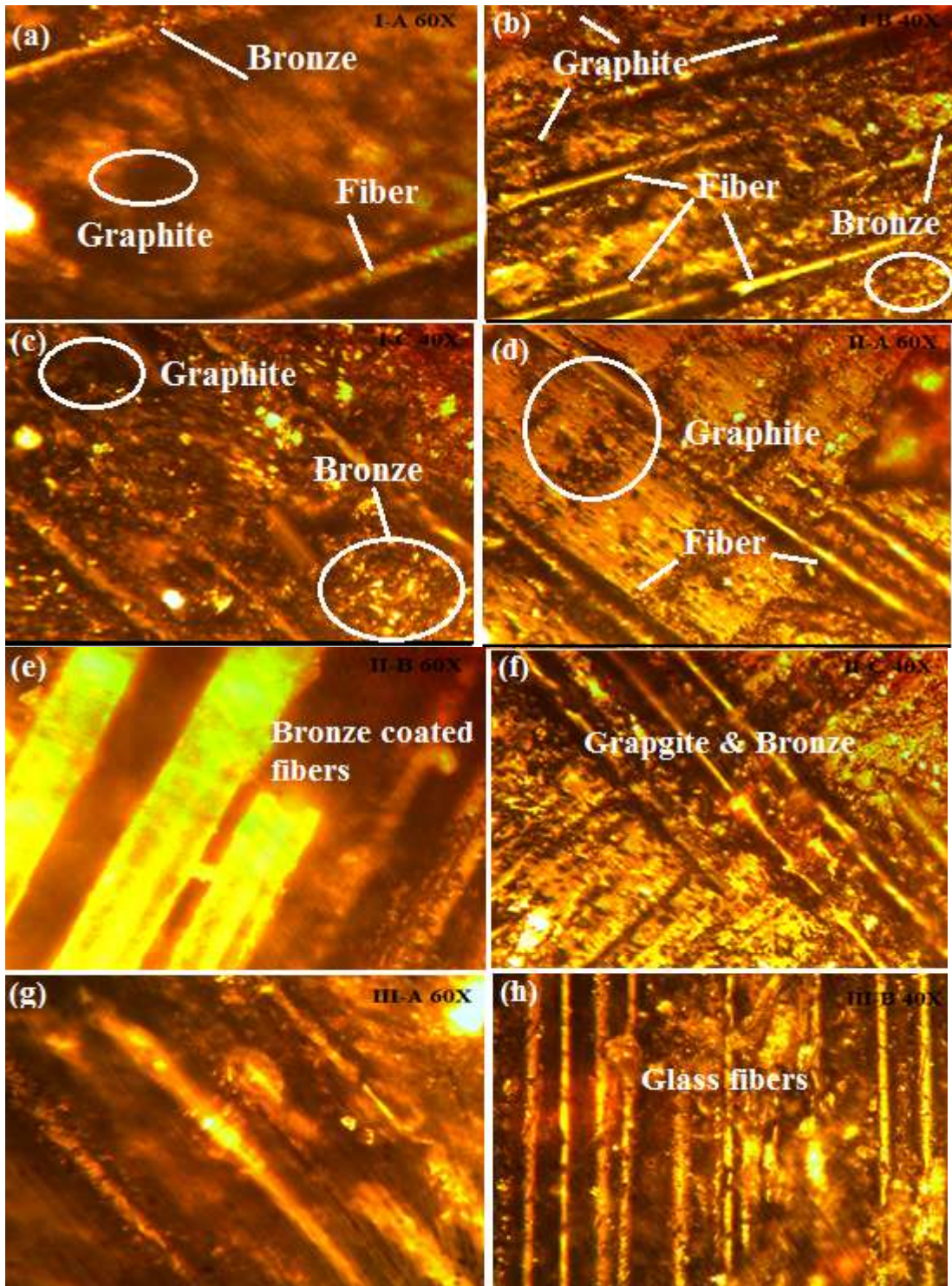
Figure 4.10 Optical Microscope Images of Composites (a) 10F/10G/20B (b) 10F/15G/15B (c) 10F/20G/10B (d) 15F/5G/15B (e) 15F/10G/10B (f) 15F/15G/5B (g) 20F/5G/15B (h) 20F/10G/10B

CHAPTER 5

RESULTS AND DISCUSSION: TRIBOLOGICAL CHARACTERIZATION

This chapter deals with dry sliding wear characteristics of glass fiber reinforced epoxy composites. The pin on disc wear test is carried out as per Taguchi experimental design (L_{27} orthogonal array) as shown in Table 3.10 and the analysis of the results is obtained using MINITAB 18, the data analysis software made for Taguchi experimental design. The experimental results of dry sliding wear test are analysed using Taguchi DOE and the most significant factor governing the wear is identified. At the end the micro-structural analysis of the pin surface are described using SEM micrographs.

5.1. WEAR CHARACTERISTICS ANALYSIS

The results of dry sliding wear experiments performed as per predetermined Taguchi design on graphite and sintered bronze filled and glass fiber reinforced epoxy composites are presented in Table 5.1. This table gives the experimental specific wear rate and friction coefficient along with signal-to-noise ratio for individual test run. The results of specific wear rate presented here are average of three test trials preformed. The overall mean of the S/N ratios for the wear and coefficient of friction is found to be -42.7877 db and 12.9841db respectively. It is seen from the Table 5.1 that for similar test conditions, the composites containing 20 vol% of glass fiber and 15 vol% of sinter bronze exhibit lower specific wear rates as compared to other composites. Figure 5.1 and 5.5 illustrates the effect of the four control factors on wear and coefficient of friction respectively.

Analysis of the results leads to the conclusion that factor combination of A3 (Sliding distance: 6000 m), B3 (Filler content: 15 vol%), C1 (Sliding velocity: 210 cm/s) and D3 (Normal load: 40 N) gives minimum wear and B1 (Filler content: 5 vol%), C3 (Sliding velocity: 320 cm/s), A2 (Sliding distance: 4000 m) and D2 (Normal load: 30 N) gives minimum coefficient of friction. The interaction graphs for wear and coefficient of friction are shown in Figures 5.2 to 5.4 and in Figure 5.6 to 5.8

respectively. As far as minimization of wear is concerned, factors A, B and C have significant effect whereas factor D has least effect. The S/N ratio response is given in Table 5.2 and 5.3, which indicates that among all the control factors, filler content is most significant factor followed by sliding distance and sliding velocity while the normal load has the least or almost no significance on wear of the reinforced composite.

Table 5.1 Output Results of L$_{27}$ Orthogonal Array

Sr. No	SD (m)	FC (Vol%)	SV (cm/s)	NL (N)	Wear (µm)	S/N Ratio (db)	Friction coefficient	S/N Ratio (db)
1	2000	5	210	20	178	-45.0084	0.224	12.995
2	2000	5	260	30	194	-45.756	0.235	12.578
3	2000	5	320	40	167	-44.4543	0.241	12.359
4	2000	10	210	30	147	-43.3463	0.216	13.310
5	2000	10	260	40	134	-42.5421	0.221	13.112
6	2000	10	320	20	140	-42.9226	0.223	13.033
7	2000	15	210	40	109	-40.7485	0.189	14.470
8	2000	15	260	20	123	-41.7981	0.213	13.432
9	2000	15	320	30	125	-41.9382	0.211	13.514
10	4000	5	210	30	195	-45.8007	0.249	12.076
11	4000	5	260	40	166	-44.4022	0.249	12.076
12	4000	5	320	20	179	-45.0571	0.256	11.835
13	4000	10	210	40	140	-42.9226	0.232	12.690
14	4000	10	260	20	145	-43.2274	0.242	12.323
15	4000	10	320	30	160	-44.0824	0.245	12.216
16	4000	15	210	20	102	-40.172	0.204	13.807
17	4000	15	260	30	126	-42.0074	0.219	13.191
18	4000	15	320	40	121	-41.6557	0.227	12.879
19	6000	5	210	40	132	-42.4115	0.22	13.151
20	6000	5	260	20	143	-43.1067	0.274	11.244
21	6000	5	320	30	165	-44.3497	0.291	10.722
22	6000	10	210	20	117	-41.3637	0.215	13.351
23	6000	10	260	30	132	-42.4115	0.218	13.230
24	6000	10	320	40	123	-41.7981	0.21	13.555
25	6000	15	210	30	110	-40.8279	0.184	14.703
26	6000	15	260	40	102	-40.172	0.201	13.936
27	6000	15	320	20	112	-40.9844	0.197	14.110

The most significant factor influencing the friction coefficient is filler content followed by sliding velocity and sliding distance. Figure 5.2 show the interaction between B and C has greater effect on wear. Interaction between A and C also has second highest significant effect on the output performance as shown in Figure5.3. The factors A and B shown in Figure 5.4 have negligible effect on wear of the composites. It is also seen that the factor D has least effect on the wear. Factors A and B interaction has negligible effect on the output performance. As factor D has negligible effect so for further study, it can be neglected. Analysis of Variance (ANAVO) is carried out to identify the most significant factor and least significant interaction.

Figure 5.6 show the interaction between B and C. It is observed from the figure that this interaction has significant effect on friction coefficient.

Figure 5.8 shows the interaction between A and B. This interaction has the second highest significant effect on the output performance.

Figure 5.7 shows the factors A and C. It is observed from the figure that these factors do not have significant effect on specific wear rate. This analysis also show that the factor D do not have significant effect on the coefficient of friction. Hence, factor D can be neglected for further study.

Table 5.2 Response Table of Sliding Wear (Smaller is better S/N ratio)

Level	SD (A)	V% (B)	SV (C)	NL (D)
1	-43.17	-44.48	-42.51	-42.63
2	-43.26	-42.72	-42.82	-42.39
3	-41.94	-41.14	-43.03	-42.35
Delta	1.42	3.44	1.34	0.12
Rank	2	1	3	4

Table 5.3 Response Table of Friction Coefficient (Smaller is better S/N ratio)

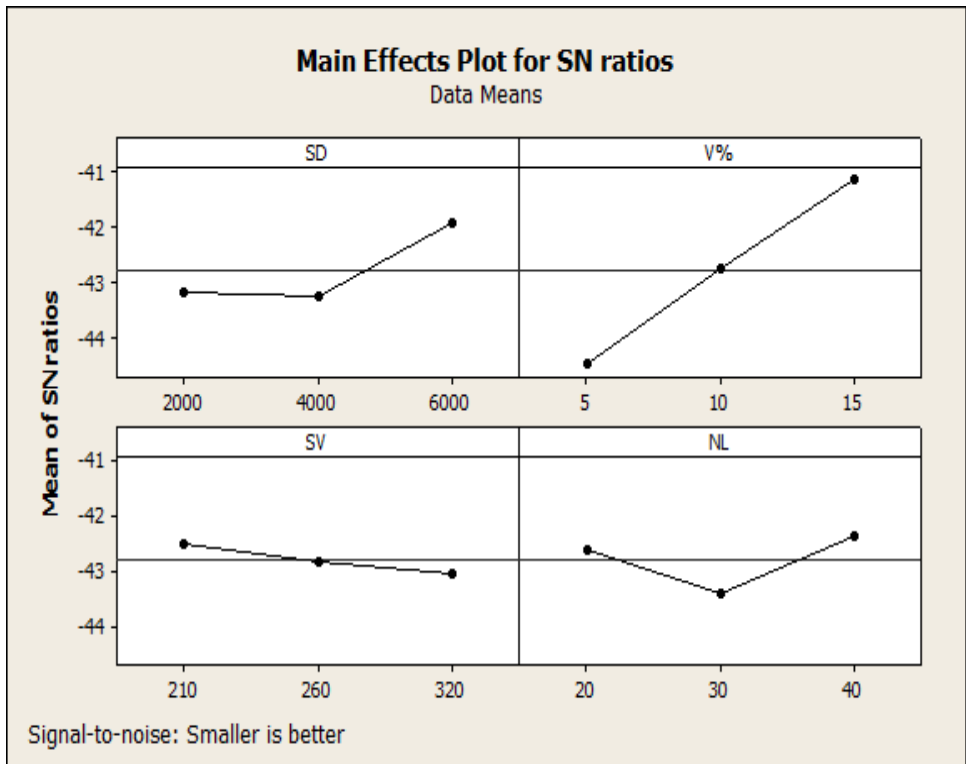| Level	SD (A)	V% (B)	SV (C)	NL (D)
1	13.21	12.12	13.40	12.90
2	12.57	12.98	12.79	12.84
3	13.11	13.78	12.69	13.14
Delta	0.63	1.67	0.70	0.30
Rank	2	1	3	4

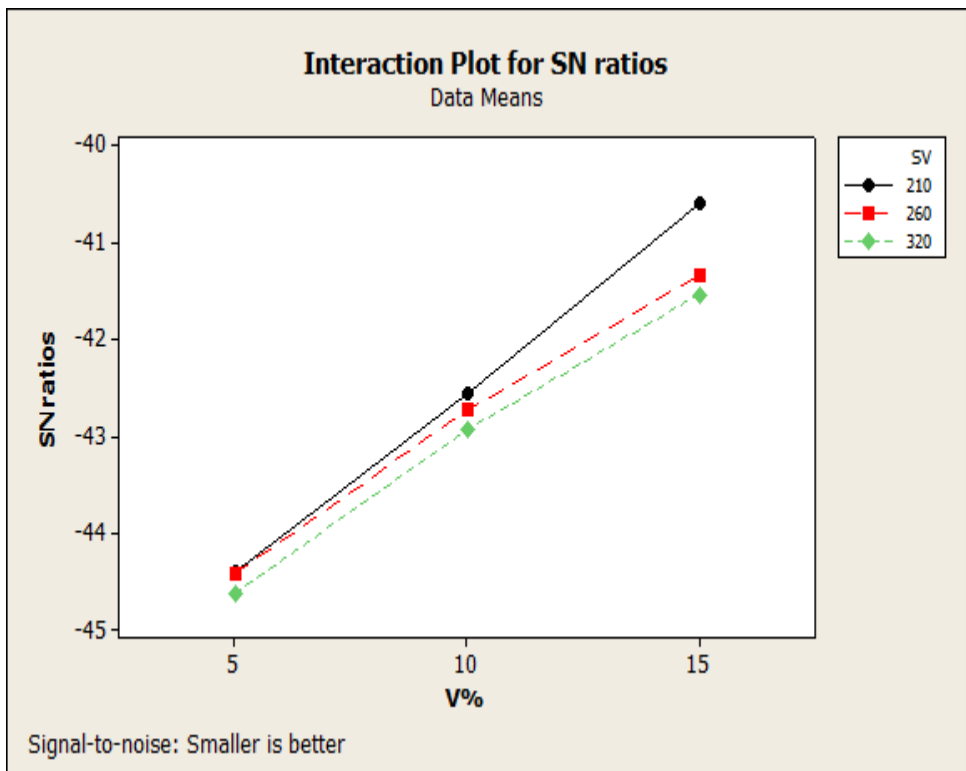**Figure 5.1 Effects of Control Factors on Wear**

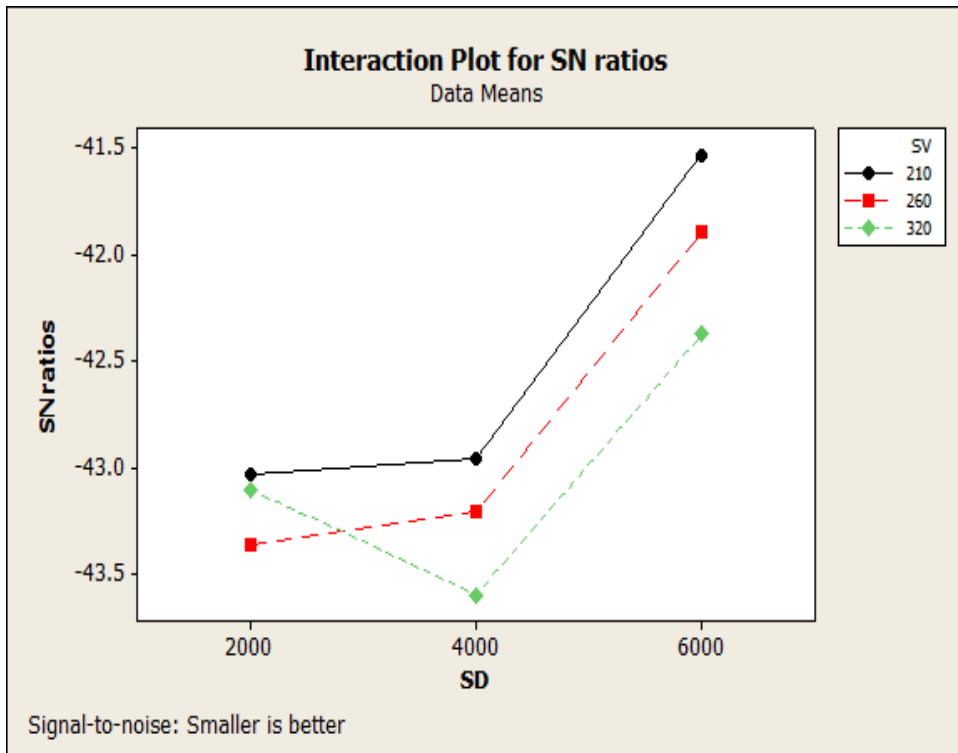**Figure 5.2 Interaction plot of B x C for Wear.**

89

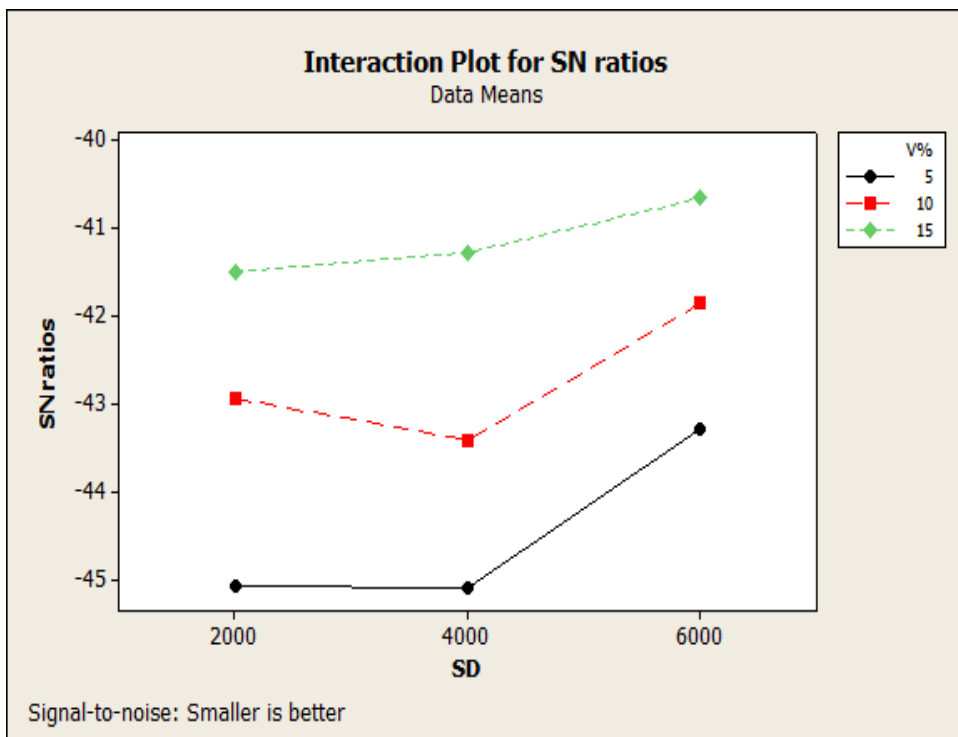**Figure 5.3 Interaction plot of A x C for Wear.**

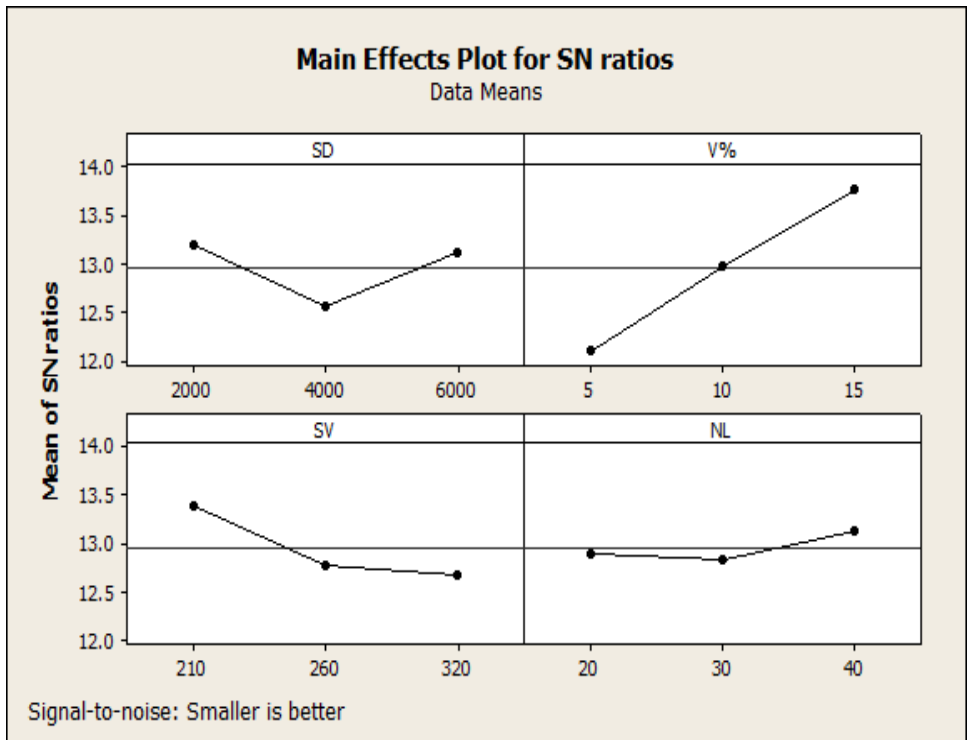**Figure 5.4 Interaction plot of A x B for Wear.**

Figure 5.5 Effects of Control Factors on Coefficient of Friction
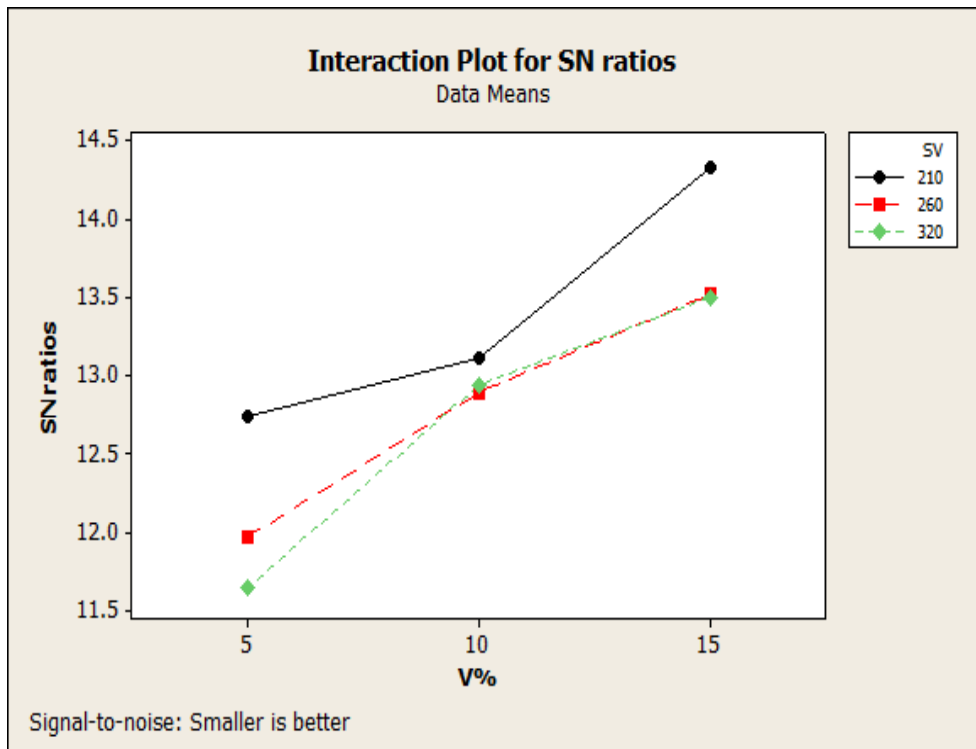

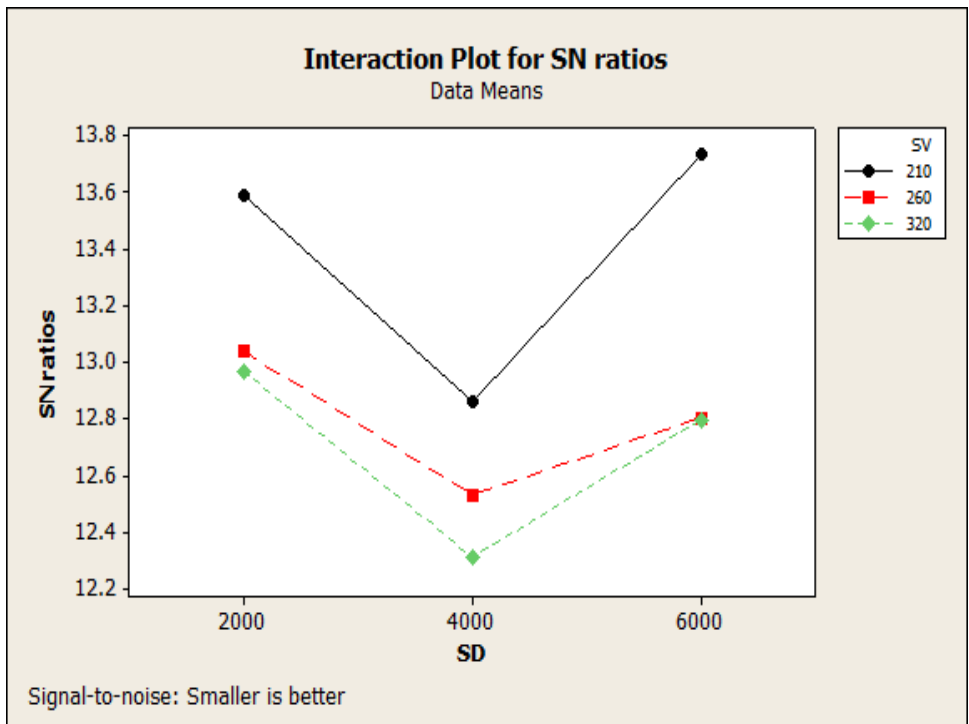**Figure 5.6 Interaction plot of B x C for Coefficient of Friction**

Figure 5.7 Interaction plot of A x C for Coefficient of Friction
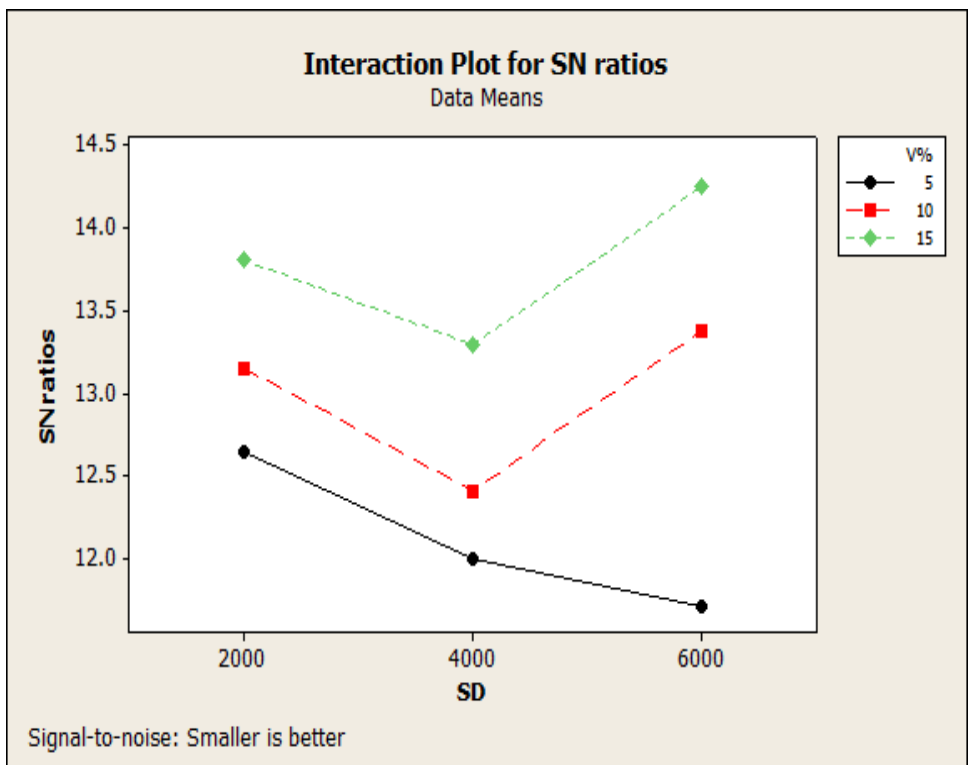

Figure 5.8 Interaction plot of A x B for Coefficient of Friction

92

5.2 ANALYSIS OF VARIANCE (ANOVA)

Analysis of variance is necessary to identify the influence of various factors like sliding distance (A), filler content (B), sliding velocity (C) and normal load (D) on the output performance. The analysis of variance (ANOVA) table identify the order of significant factors. Table 5.4 and 5.5 shows the results of the ANOVA for the wear and coefficient of friction. This analysis is undertaken for a level of confidence of significance of 5 %. From Table 5.4, it can observe that the sliding distance (p = 0.000), fiber content (p= 0.000), sliding velocity (p=0.057) and normal load (0.002) have great influence on specific wear rate. However, the interaction between sliding distance and filler content (p=0.112) and sliding velocity and sliding distance (p=0.317) show significance of contribution on the specific wear rate and the remaining interaction i.e. filler content and sliding velocity (p=0.417) presents less significance of contribution on specific wear rate.

Table 5.4 Analysis of Variance for Specific Wear Rate

Source	DF	Seq SS	Adj SS	Adj MS	F	P
(A) SD	2	9.8255	9.8255	4.9127	38.93	0.000
(B) V%	2	50.1786	50.1786	25.0893	198.82	0.000
(C) SV	2	1.2151	1.2151	0.6076	4.81	0.057
(D) NL	2	5.2725	5.2725	2.6362	20.89	0.002
SD*V%	4	1.5099	1.5099	0.3775	2.99	0.112
SD*SV	4	0.6515	0.6515	0.1629	1.29	0.371
V%*SV	4	0.5808	0.5808	0.1452	1.15	0.417
R.Error	6	0.7571	0.7571	0.1262		
Total	26	69.9910				

Table 5.5 Analysis of Variance for Coefficient of Friction

Source	DF	Seq SS	Adj SS	Adj MS	F	P
(A) SD	2	2.1254	2.1254	1.06271	5.85	0.039
(B) V%	2	12.5170	12.5170	6.25852	34.48	0.001
(C) SV	2	2.6059	2.6059	1.30293	7.18	0.026
(D) NL	2	0.4432	0.4432	0.22160	1.22	0.359
SD*V%	4	2.1782	2.1782	0.54456	3.00	0.111
SD*SV	4	0.2965	0.2965	0.07414	0.41	0.797
V%*SV	4	0.7368	0.7368	0.18419	1.01	0.469
R.Error	6	1.0891	1.0891	0.18151		
Total	26	21.9921				

*DF: degree of freedom; Seq.SS: sequential sum of squares; AdjSS: extra sum of squares; Adj MS: extra mean squares; p: level of significance

From Table 5.5, it is observed that the sliding distance (p = 0.039), fiber content (p= 0.001) and sliding velocity (p=0.026) have great influence on coefficient of friction and the factor like normal load has least effect (0.359) on coefficient of friction. However, the interaction between sliding distance and filler content (p=0. 111) and sliding velocity (p=0.469) show significant contribution on the coefficient of friction and the remaining interaction i.e sliding velocity and sliding distance (p=0.797) shows the negligible effect on wear rate.

5.3 EFFECT OF SLIDING DISTANCE AND SLIDING VELOCITY ON WEAR.

The changes in specific wear rate and coefficient of friction of glass fiber reinforced, sintered bronze and graphite filled epoxy composites are shown in Figures 5.9 to 5.12. It is observed that the specific wear rate of the composites decrease with increase in sliding velocity from 210 cm/s to 320 cm/s as shown in Figure 5.9.It is noted that increase in sliding velocity is not responsible for wear of the composites rather it minimizes the specific wear rate. But in the previous study (Basavrajappa et al) it is revealed that sliding distance has the highest influence on specific wear rate of composites. This difference is attributed to presence of sintered bronze as filler along with graphite.

Extensive research is carried out to study wear behaviour of polymer composites in past years. The wear trend presented is of the mixed nature. In few research articles the specific wear rate is decreasing and in some it is reported as increasing with increase of sliding velocity. It may depend on the nature of fillers and the reinforcing element used. One of the major reasons for initial high wear rate may be the separation of fiber and fillers. The higher thermal conductivity of the amorphous graphite and sintered bronze fillers plays very important role in decreased specific wear rate of the polymer composites. Figure 5.10 shows the effect of increase in sliding distance on the specific wear rate of the composites. It can be observed from the Figure that the specific wear rate indicates steep drop initially and later on it is almost steady converging to a single point.
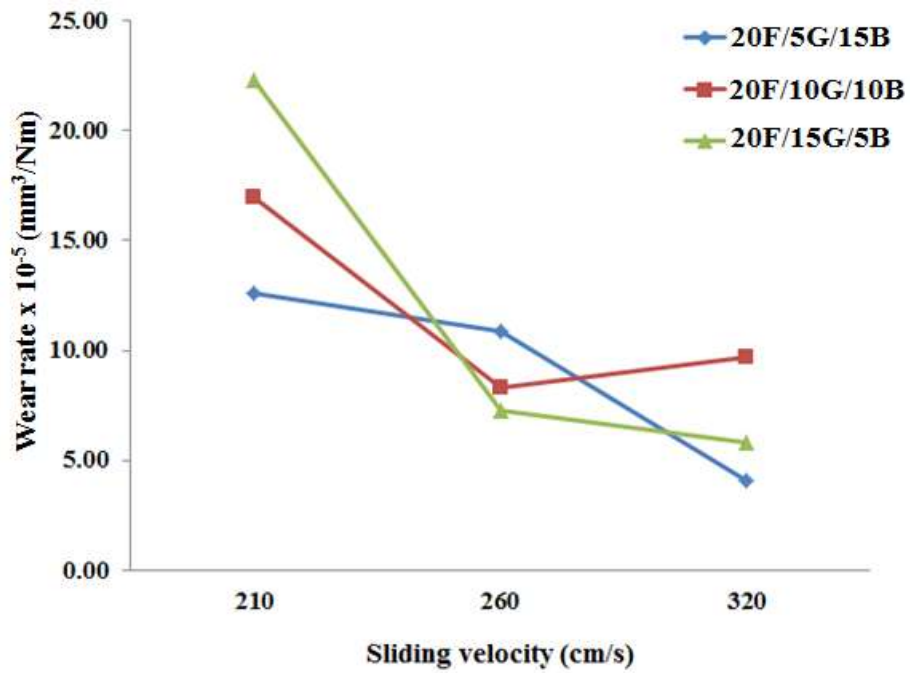
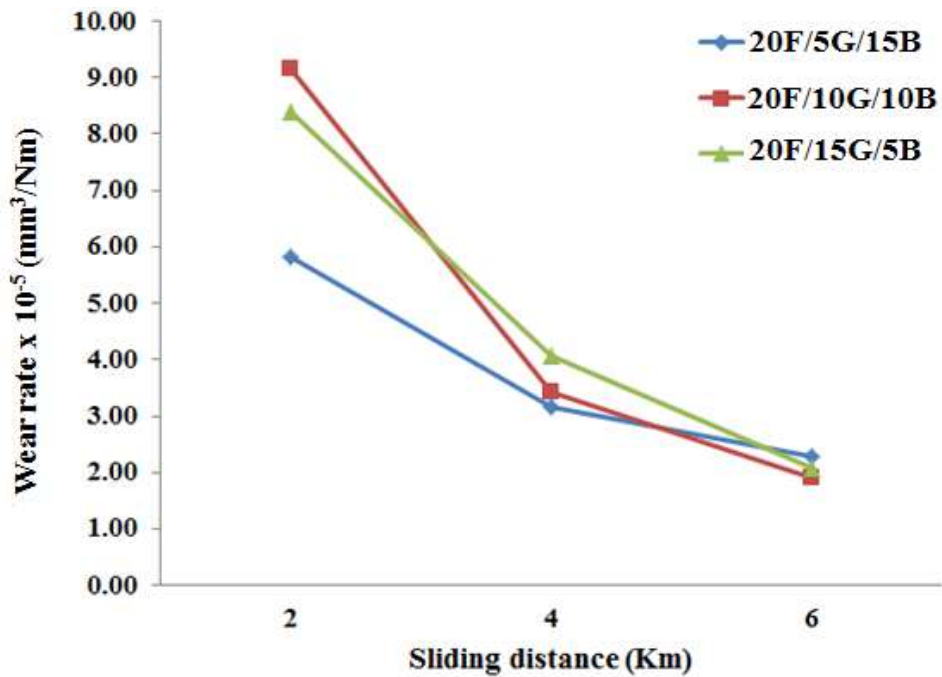**Figure 5.9 Graph of Sliding Velocity Vs Specific Wear Rate.**

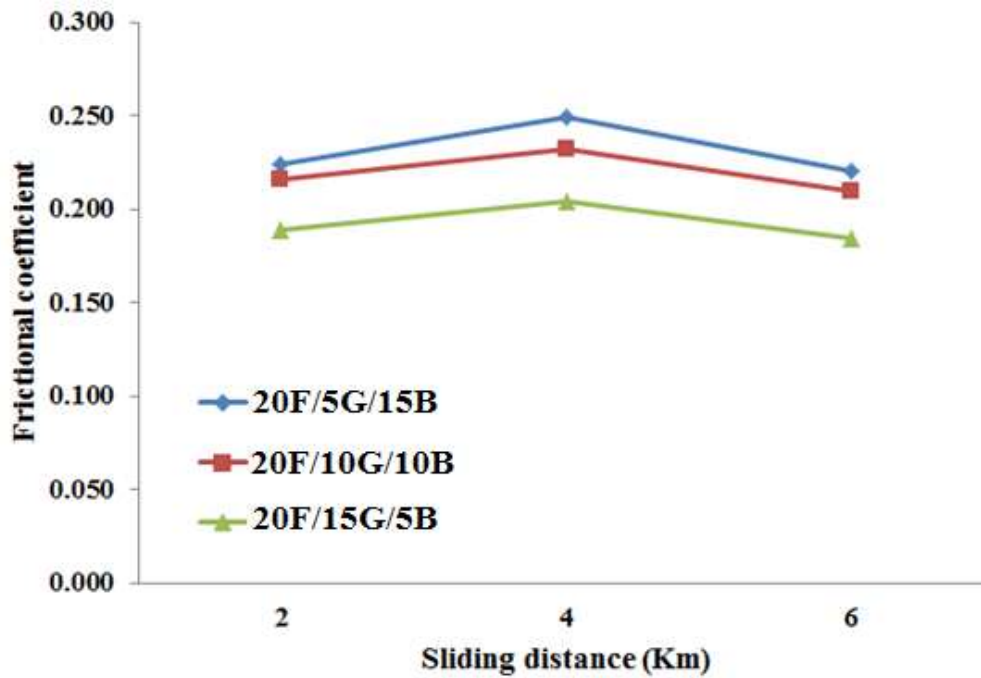**Figure 5.10 Graph of Sliding distance Vs Specific Wear Rate.**

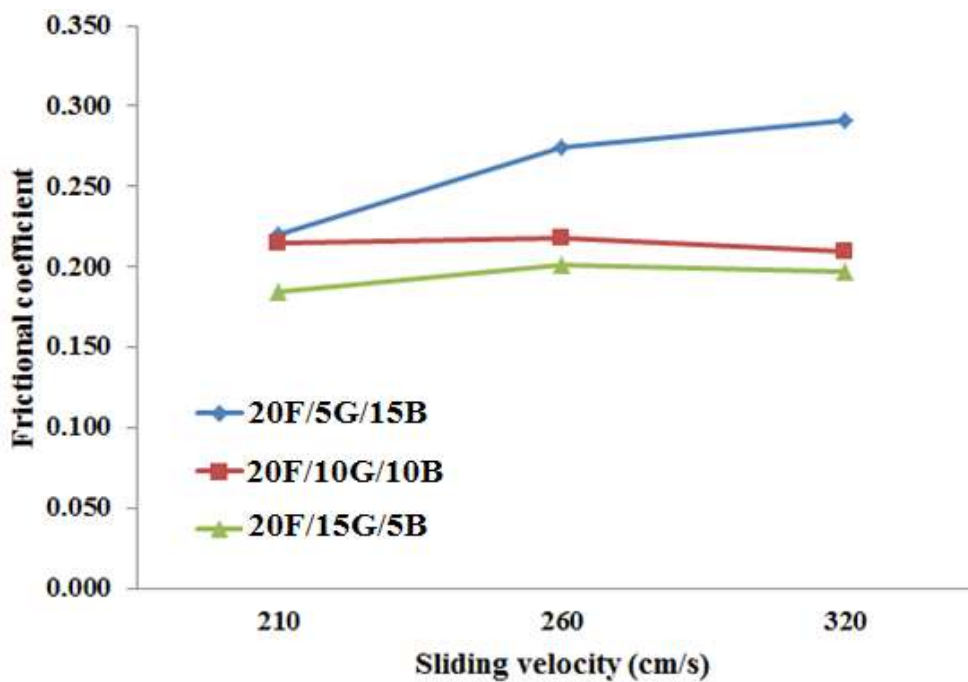**Figure 5.11 Graph of Sliding Distance Vs Coefficient of Friction.**

Figure 5.12 Graph of Sliding Velocity Vs Coefficient of Friction.

This is because of the combined effect of sintered bronze filler and solid lubricant Graphite. The sintered bronze particles in the epoxy forms physical interaction with

96

the counter surface and graphite acts as a solid lubricant thus safeguards the matrix material. . It happens only because of development of lubricating film on the counter surface. As the sliding speed and sliding distance increase the epoxy resin becomes soft due to friction and heat. Thus the bronze and graphite particles in the vicinity of the resin get separated. Some of these particles are transferred on to the counter surface as well as test specimen to form lubricating film. This lubricating film acts as insulator and protects further damage to composites. Specific wear rate largely depends upon the thickness of the lubricating film formed. More the thickness of the lubricating film, lower will be the specific wear rate. The amount of bronze and graphite particles in a lubricating film decides the rate of wear. The effect of change in sliding velocity and sliding distance on coefficient of friction of composites is illustrated in Figure 5.11 and 5.12. It can be seen that addition of graphite not only reduce specific wear rate but it also decrease the coefficient of friction. It can also be seen that the addition of sintered bronze to fiber reinforced epoxy composites resulted in improvement in the tribological properties. The addition of bronze with graphite exhibited properties of solid lubricants. As the sliding distance exceeds 4 Km, the lubricating film developed plays important role in enhancing the Tribological performance to a great extent. It may be because of the consolidation of its mechanical properties. The combined properties of the bronze, graphite, glass fiber and epoxy matrix are the most favourable in enhancing the wear resistance and coefficient of friction of the composites due to their combined effects.

5.4 SEM ANALYSIS OF PIN WORN SURFACE

To find out the wear mechanism in composites, scanning electron microscopy (SEM) is common practice. The micrographs of worn pin surfaces of composites 20F/5G/15B, 20F/10G/10B and 20F/15G/5B are illustrated in Figure 5.13 to 5.15. Enough literature is available indicating the effect of unfilled over filled composites. In this study only filled composites are investigated to study friction and wear behaviour of the composites.
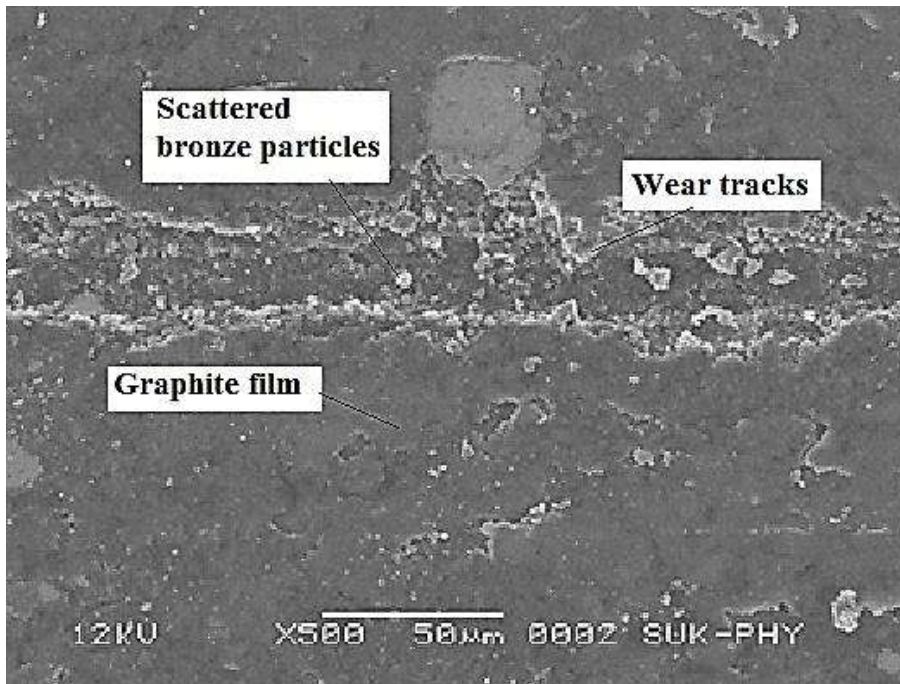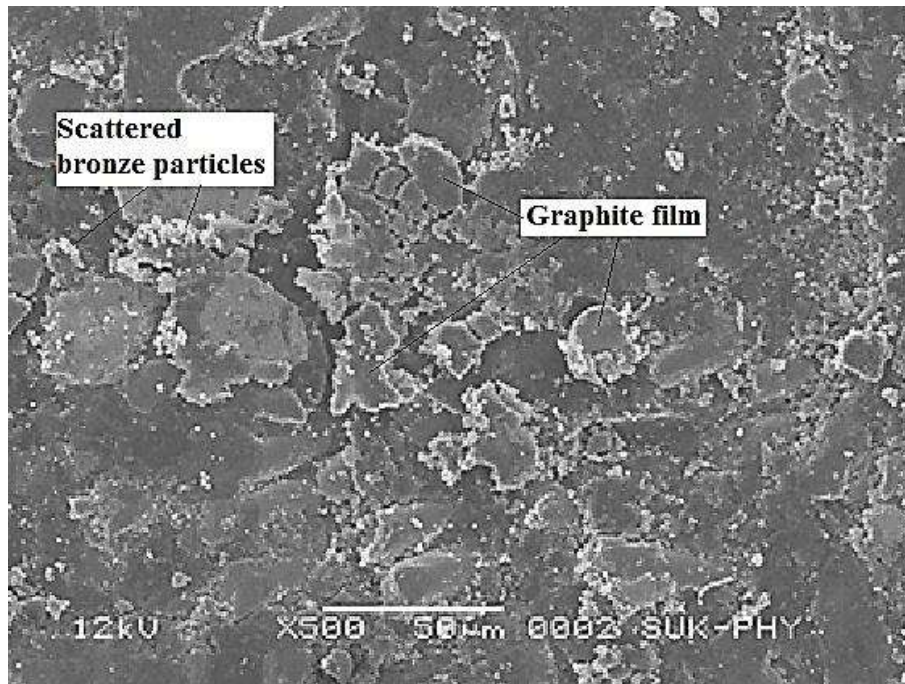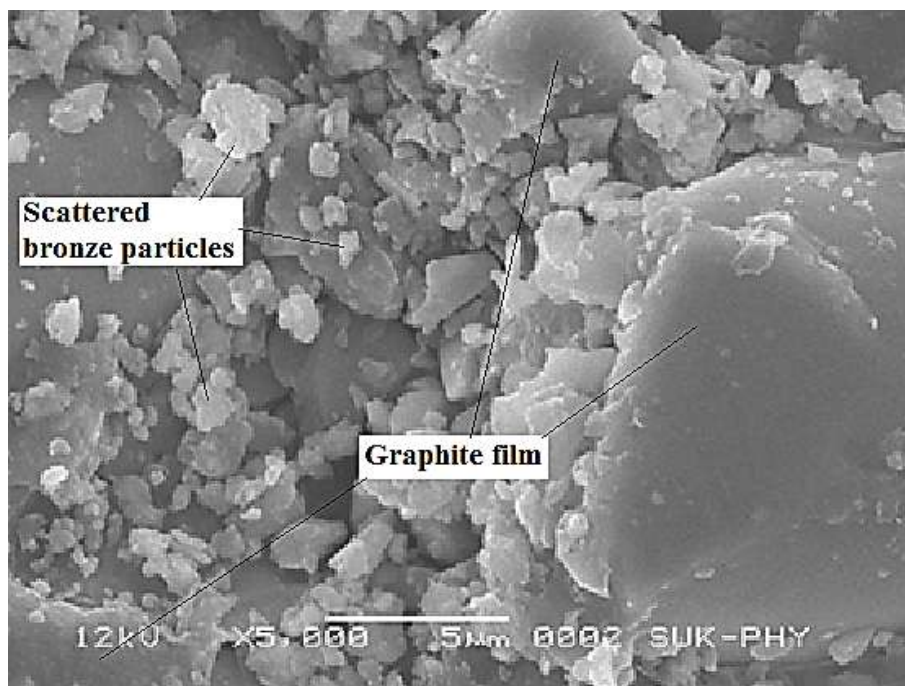
(a)
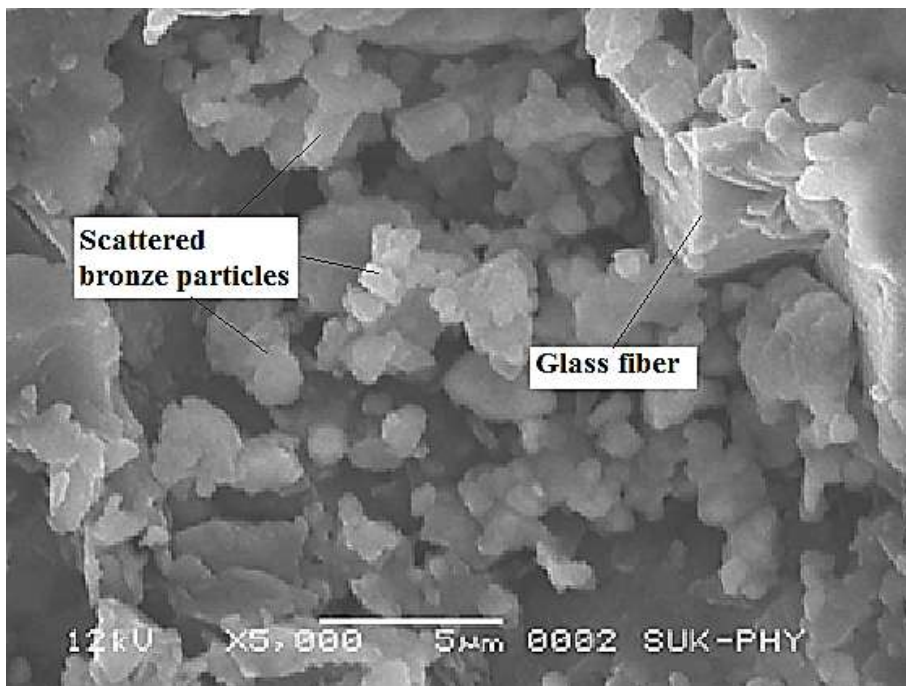
(b)

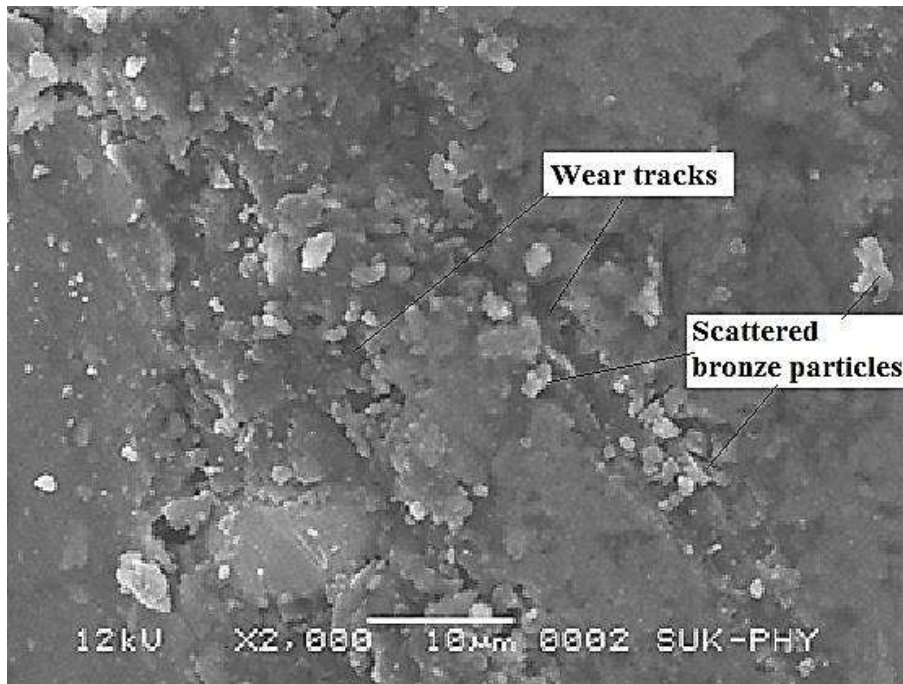**Figure 5.13 (a-b) SEM Micrographs of Pin Surface of Composites**
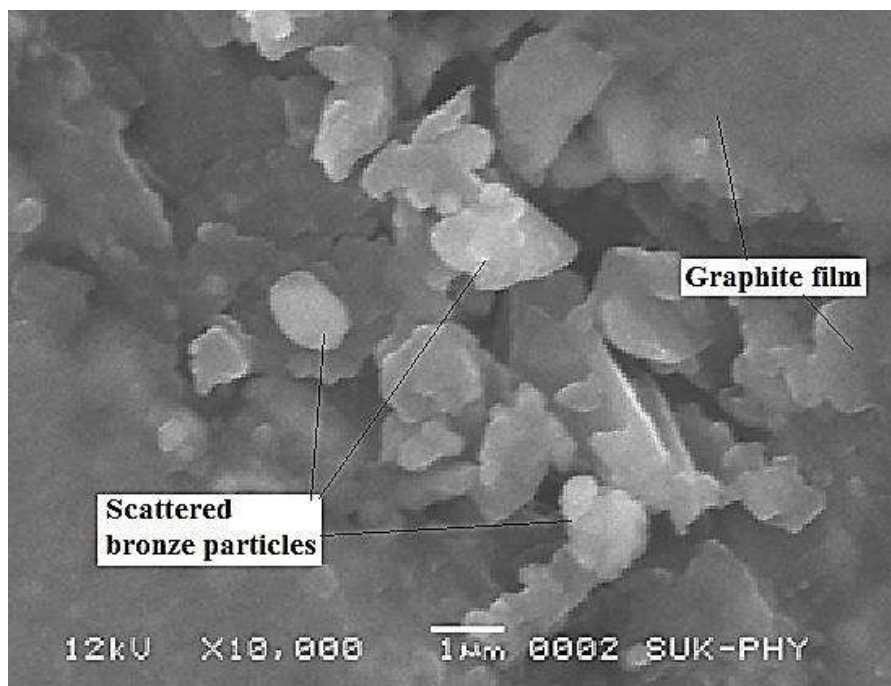
20F/5G/15B

(a)

(b)

Figure 5.14 (a-b) SEM Micrographs of Pin Surface of Composites

20F/10G/10B

(a)

(b)

Figure 5.15 (a-b) SEM Micrographs of Pin Surface of Composites

20F/15G/5B

(Basavarajappa and Ellangovan 2012) showed the ploughing action on the surface of the unfilled composite over filled composites through SEM micrographs. The morphology of worn pin surface of graphite and sintered bronze filled glass fiber epoxy composites is analysed by means of SEM micrographs.

Figure 5.13 (a-b) shows the SEM of worn pin surface of composites 15F/5G/15B. Figure 5.13 (a) indicates the lubricating film comprising of graphite and scattered bronze particles. The wear tracks are also observed on the worn pin surface. Figure 5.13 (b) shows the glass fiber pull out of the matrix material. The thin lubricating film developed on the pin surface might have helped in reducing friction and wear of the composites. At higher loads, velocity and sliding distance the entrapped bronze particles get clogged together and lead to wear scars marked on the pin surface.

It is also evident from the Figure 5.14 (a), that the sintered bronze particles are seen well bonded with matrix and fibers. These bronze particles enhanced the thermal conductivity of the composites and improved the coefficient of friction even at high speed and loads (Patil and Prasad 2015). The matrix undergo plastic deformation and micro cracking at low sliding velocity but at higher sliding velocity the lubricating film undergo sever damage in the form of cracks leading to large scale fracture of the lubricating film as shown in Figure 5.14 (b). Apart from sliding velocity, normal load and sliding distance also influence the wear mechanism. Figure 5.15 (a) shows the numbers of wear cracks formed on the lubricating film of the worn pin surface. These small cracks, at higher speed and longer sliding distances propagate but do not lead to increased specific wear rate. (Gai Zhao et al) observed that the crushed particles provide additional protection of polymer matrix from sever wear. This is attributed to the cracks developed itself. These cracks might be carrying separated graphite and bronze particles in it and moreover also act as heat dissipating edges. These cracks carrying sintered bronze particles and lubricating film is shown in Figure 5.14 (a). The increased volume percentage of sintered bronze material resulted in the less bonding between the filler and matrix material. The wettability of filler is must to produce a good bonding between the filler and matrix material to prevent its separation from matrix (Patil and Prasad 2015). It is observed that for higher normal load, sliding velocities and distances the lubricating film become smoother and

101

carried the graphite and sintered bronze particles in its cracks. This phenomenon of self-lubricating film might have led to reduced specific wear rate and friction coefficient. The tribological characteristic of the developed composites mainly depends on the bonding between fillers and fibers, formation of lubricating film on pin worn surface by filler materials and voids of the composites.

5.5 SEM ANALYSIS OF WORN PIN DEBRIS

The SEM analysis of worn pin debris is carried out to identify the composition of debris. The worn pin debris is collected from the counter surface and micrographs of the same are shown in Figure 5.16 to 5.18. The micrographs clearly help to identify the fillers, fibers and matrix material. All the micrographs shown in Figure 5.14 to 5.17 illustrate the damaged glass fibers. The bronze fillers can be seen sticking to the surface of glass fiber. The graphite filler is seen with the matrix material epoxy. It is also clear from the micrographs that the percent of glass fibers separated from the pin is less as compared to the fillers and the matrix material. It is reflected in the mechanical characterization where the maximum tensile properties of composites consists of 15 vol% glass fiber are resulted. The strength of composites resists the debonding of the fibers from the matrix material.

The micrographs of debris of the composite containing 15 vol% of bronze and 5 vol% of graphite seems to be coarse whereas for 5 vol% of bronze and 15 vol% of graphite it is finer. So these fine particles of graphite help in forming thin lubricating film on the pin surface and some of the particles may migrate to the counter surface to add lubricating effect.

The sintered bronze particles can be seen in the debris of all composites. These bronze particles act as heat transfer medium and dissipate the heat generated to the fibers and to surroundings. Thus limits excess heat generation at the time of dry sliding.
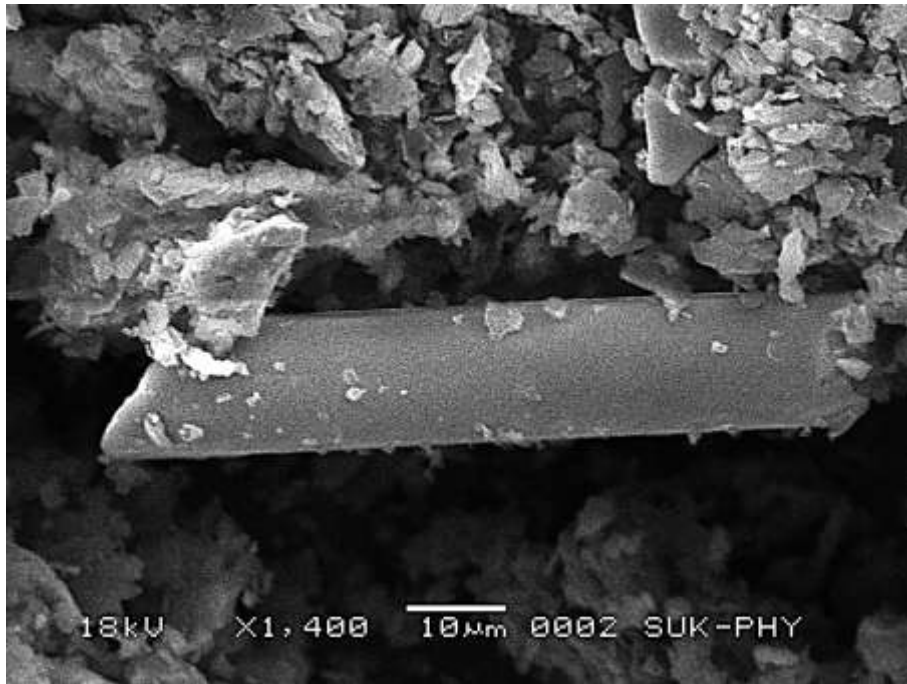
(a)

(b)

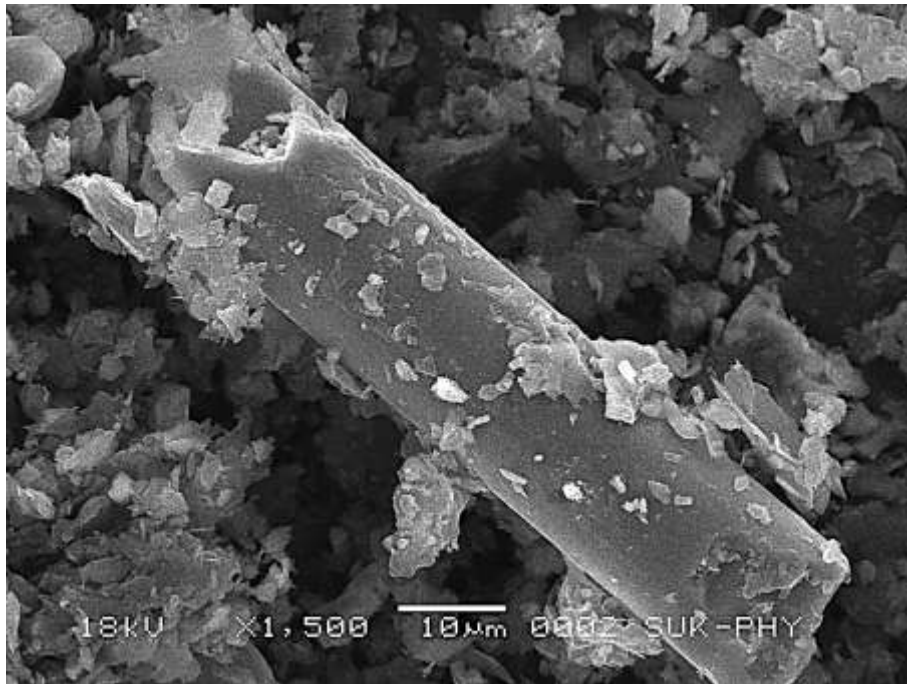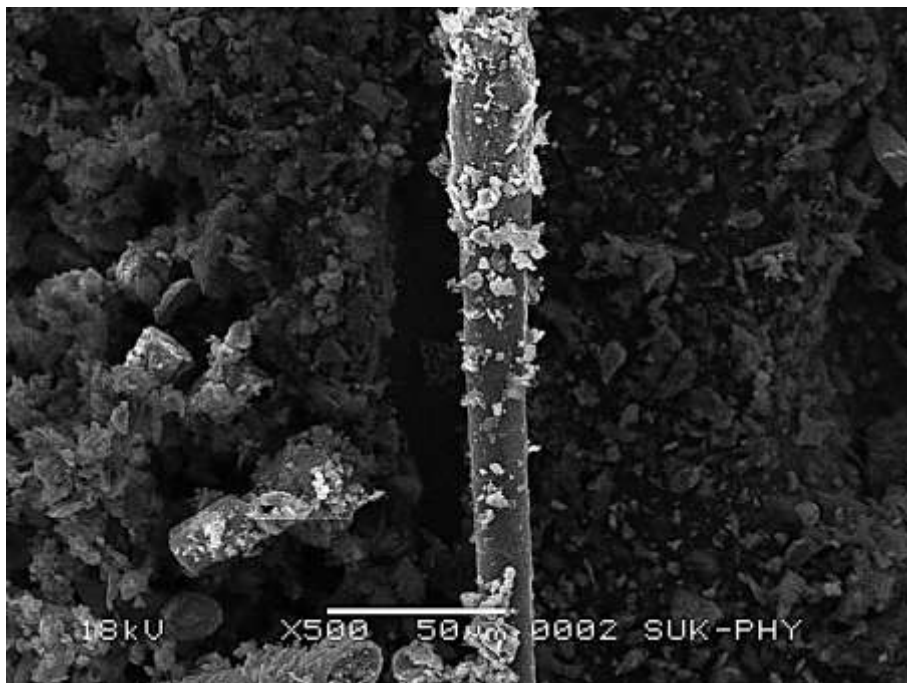**Figure 5.16 (a-b) SEM micrographs of Pin Debris of Composites**

20F/5G/15B

(a)

(b)

Figure 5.17 (a-b) SEM micrographs of Pin Debris of Composites

20F/10G/10B

(a)

(b)

Figure 5.18 (a-b) SEM micrographs of Pin Debris of Composites

20F/15G/5B

5.6 ANFIS SIMULINK MODEL

Adaptive Neuro Fuzzy Inference System (ANFIS) Simulink model is developed to predict the specific wear rate of three composites, 15F/5G/15B, 15F/10G/10B and 15F/15G/5B, as shown in Figure 5.19. Fuzzy logic toolbox is used to develop the ANFIS model with five inputs (mass loss, density, sliding velocity, time and normal load applied) and output of the model is prediction of specific wear rate. Figure 5.20 shows the ANFIS architecture which is developed after loading the input data in the workspace after training the input data. The number of the runs considered for the training is 1 to 71 and for testing it is 72 to 81.

5.6.1 Experimental and ANFIS results

The predicted results of ANFIS Simulink model and experimental results are shown in Table 5.6. The predicted specific wear rates are about 99% same as compared to the experimental results.

Figure 5.21 shows the experimental and Simulink model results of specific wear rate for the runs 71 to 81. It is evident from the graph that the experimental results and predicted results differ by negligible amount. The ANFIS prediction results are shown with red line and experimental results with blue line. The difference between experimental value and predicted value is very small i.e. negligible.
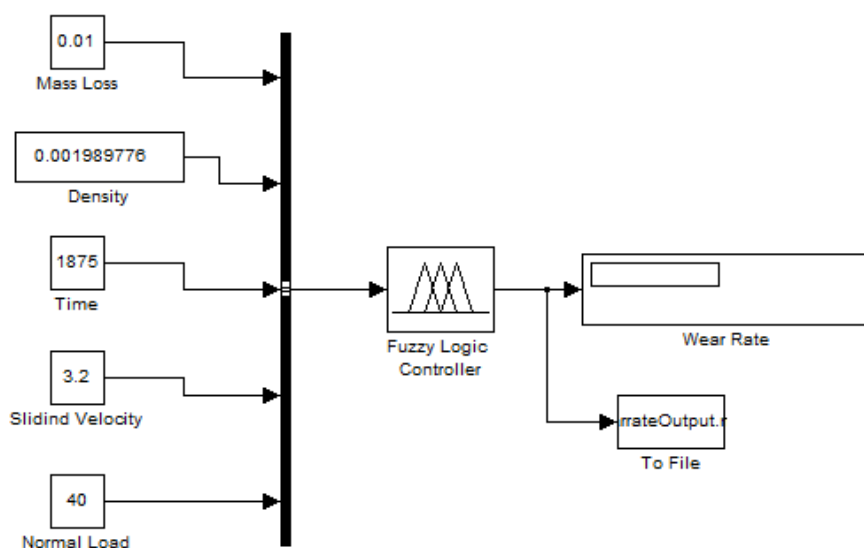

Figure 5.19 ANFIS Simulation Model

Table 5.6 Comparison of experimental and ANFIS Simulink results

Experimental Specific wear rate (10^{-5})	15.68	4.6	4.07	7.04	3.28	2.28	4.57	3.04	1.90	7.53	3.07	2.09
Simulink results (10^{-5})	15.64	4.6	4.08	7.07	3.29	2.26	4.65	3.04	1.86	7.53	2.91	2.15
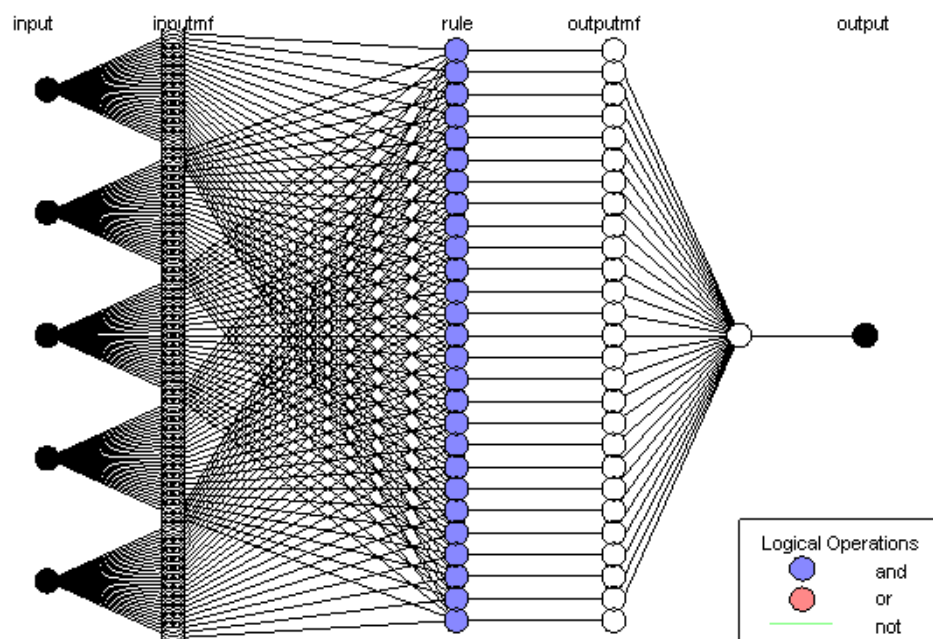
Figure 5.20 ANFIS Architecture of Specific Wear Rate Prediction

The maximum error reported is 1.5 x 10-7 mm^3/Nm. This error does not affect the specific wear rate and friction coefficient of the composites. Figure 5.22 show the comparison between experimental results and ANFIS Simulink model results during the data set testing. The comparison graph shows a high correlation between the model outputs and real results.

Figure 5.21 Experimental and Simulink Model Results of Specific Wear Rate

Figure 5.22 Comparison of Experimental Wear Rate Vs Simulation Result

The quality of the prediction is normally decided by computing the root mean square error (RSME) between the predicted values and measured empirical data. The smaller

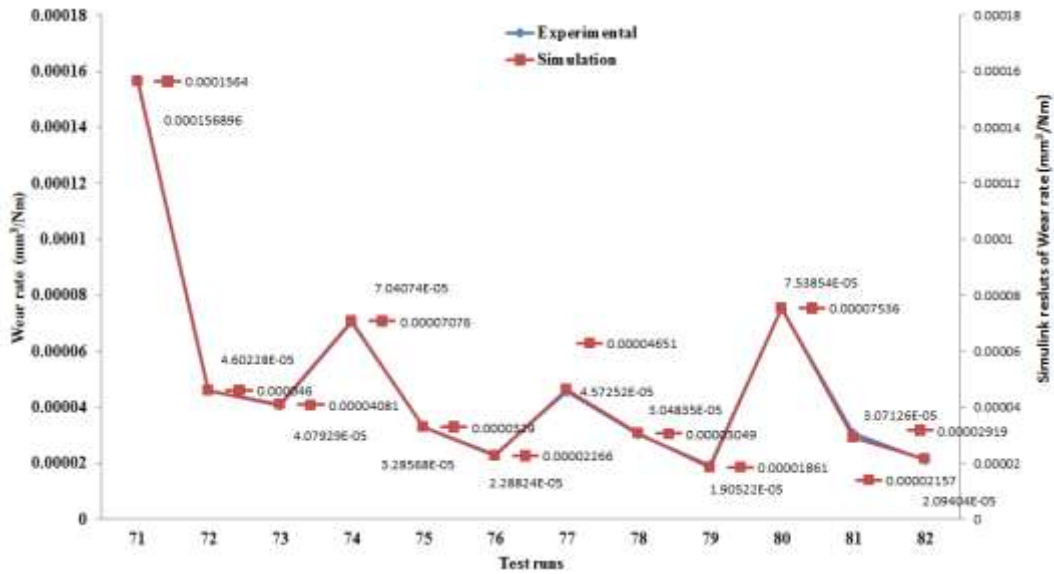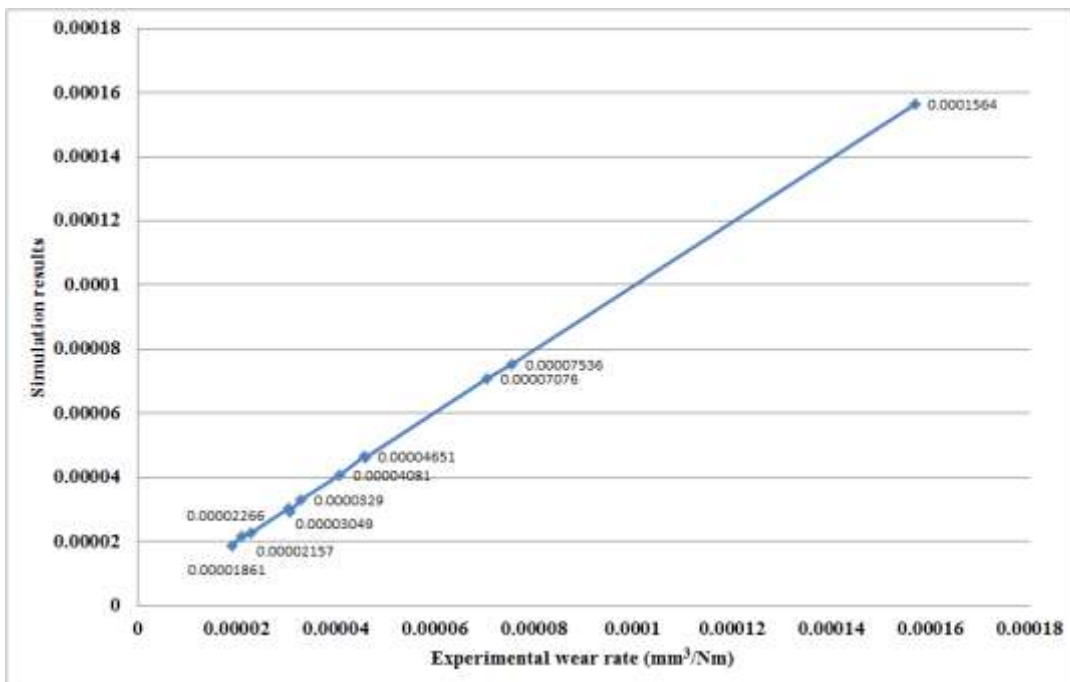the RSME value of the test data set, the higher the prediction quality. The RMSE value is computed by equation 5.1, and the computed value of RMSE is 5.73 x 10^{-7}.

$$RMSE = \sqrt{\frac{\sum_{i=1}^{N}(Experimental\ value - simulation\ value)^2}{N}}$$ (5.1)

5.7 THERMOGRAVIMETRIC ANALYSIS

The results of thermogravimetric analysis are shown in Figure 5.23. The TGA graph is analysed and the initial decomposition temperature (IDT) for the 5 % weight loss and the temperature corresponding to maximum rate of weight loss (T_{max}) are measured. These are tabulated in Table 5.7 and the thermal stability of the composites is determined. Comparing the three TGA curves, composite 'C' showed maximum 29 % weight loss at 566 ^{0}C while composite 'A' showed maximum 55% weight loss at 701 ^{0}C. Initial decomposition temperature for Composites 'C' is recorded as 281 ^{0}C and for 'A' it is 276 ^{0}C.
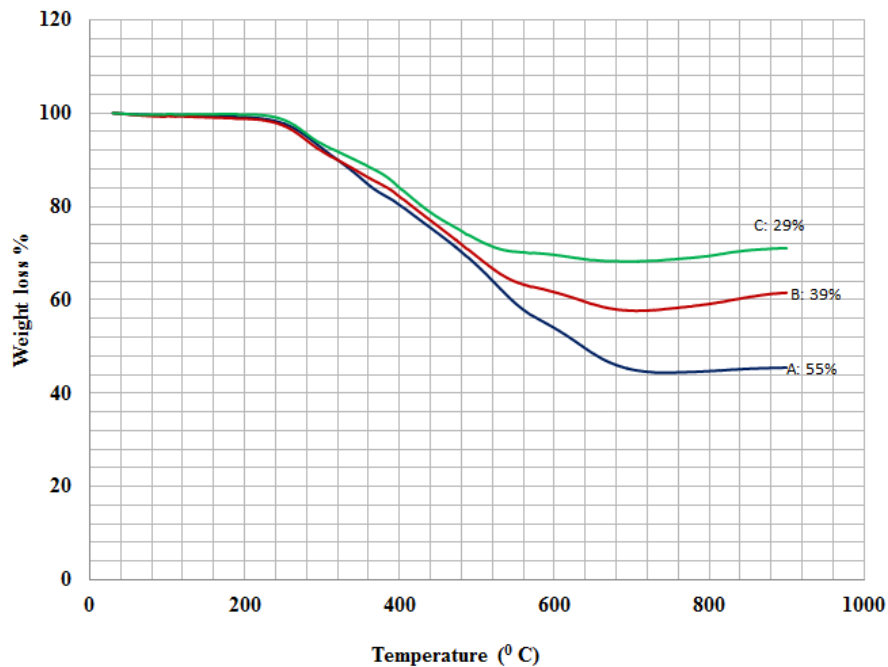

Figure 5.23 Thermogravimetric Analysis (A) 20F/5G/15B Composite (B) 20F/10G/10B Composite (C) 20F/15G/5B Composite

It is very much clear from Figure 2.23 that the all the three samples loses about 2.5% of its mass at about 240 ^{0}C. This effect is due to the loss of moisture and is

109

well known for polyamides. Between 300 ^{0}C to 850 ^{0}C all the samples decompose completely. The three samples consist of reinforcing glass fiber and two fillers viz. graphite and sintered bronze. For sample 'A' the residue is about 45% and this is assigned to glass fiber (20 vol%) and sintered bronze (15 vol%) content. The residue is about 60% and 70% for the samples 'B' and 'C' respectively. This is attributed to the glass fiber (20 vol%) and sintered bronze (10 vol% & 5 vol%) respectively.

Table 5.7 Initial Decomposition Temperature (IDT) and Temperature at Maximum Rate of Weight Loss (T$_{max}$)

Specimen	IDT (^{0}C)	T$_{max}$(^{0}C) @ % weight loss
20F/5G/15B	276	701 @ 55% loss
20F/10G/10B	269	546 @ 35% loss
20F/15G/5B	281	566 @ 30% loss

5.8 XRD ANALYSIS

The X-ray Diffraction (XRD) analysis is carried out to characterize the wear debris accumulated due to wear of composites. Figure 5.24 demonstrates the XRD results of 20F/5G/15B, 20F/10G/10B and 20F/15G/5B composites debris. Figure 5.24 clearly shows the presence of constituent materials sintered bronze; graphite.

Figure 5.24 (a) shows the diffraction pattern of fiber reinforced, bronze and graphite filled epoxy composite, 20F/5G/15B. The XRD curve show several distinct diffraction peaks at $2\theta=26.2^0$, 43.4^0, 51^0 and 74^0. These diffraction peaks represents the diffraction planes of the graphite (chemical formula C) and sintered bronze (chemical formula is CuSn).

Figure 5.24 (b) is the XRD curve of 20F/10G/10B composite which show the several distinct diffraction peaks at $2\theta = 26.2^0$, 43.4^0, 49.5^0 and 73^0. Figure 5.24 (c) is the XRD curve of 20F/15G/5B composite which show the distinct diffraction peaks at $2\theta = 26.1^0$, 43.2^0, 50^0 and 74^0. These diffraction peaks correspond to the fillers graphite (C) and sintered bronze (CuSn). $2\theta = 26.2^0$ and 26.1^0 correspond to the graphite filler.

$2\theta = 43.4^{0}$ corresponds to copper and $2\theta = 51^{0}$ corresponds to tin present in the worn pin debris.
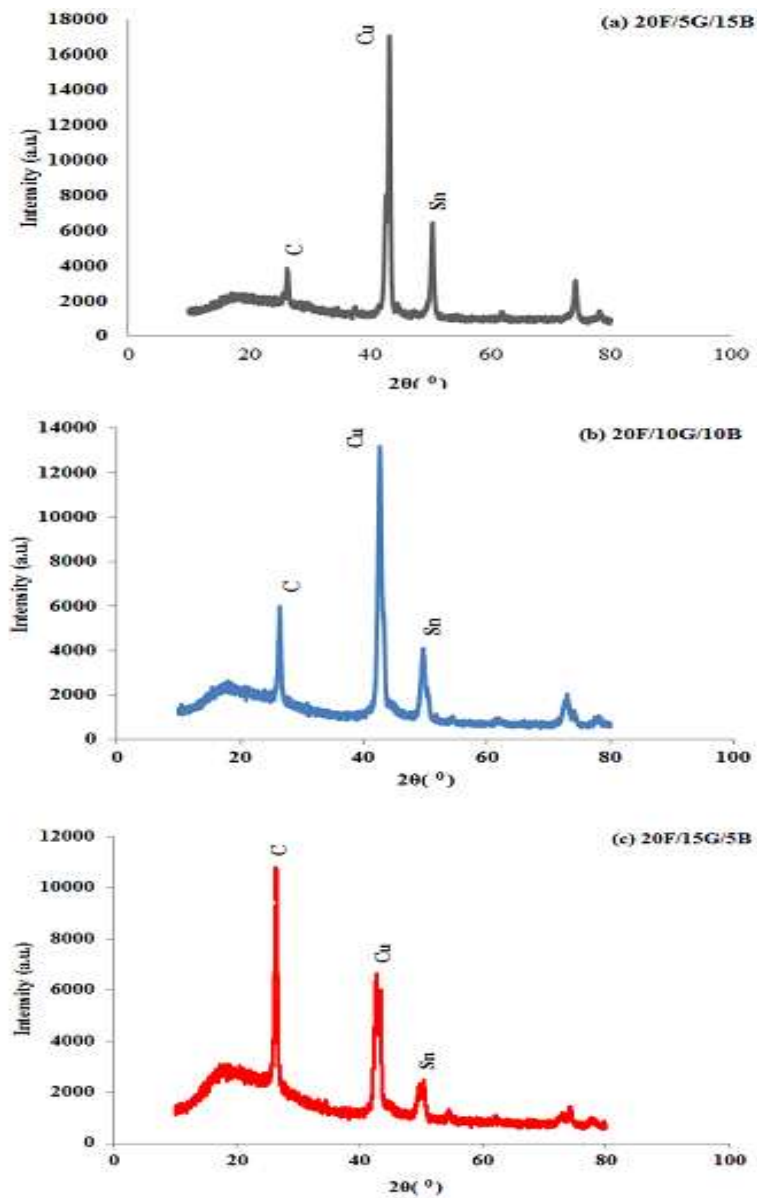

Figure 5.24 X-ray Diffraction analyses of debris with composite (a) 20F/5G/15B (b) 20F/10G/10B (c) 20F/15G/5B composites.

CHAPTER 6

RESULTS AND DISCUSSION: CONTACT STRESS ANALYSIS

In this chapter the analytical solution for contact stress analysis of composite materials is discussed and the results are validated using ANSYS workbench software. The aim of this analysis is to compare the contact stress induced in the cylinders made of the composite material characterized in this study and validate the analytical results. This analysis is an attempt to check feasibility of the developed tribo-composite material in real time practical application.

6.1 ANALYTICAL ESTIMATION OF CONTACT PRESSURE

The contact pressure is calculated using the equation3.33. The derivation of contact pressure is discussed in chapter 3. This relationship between contact pressure and the input variables load, effective modulus and radius elaborates the analytical estimation. This is calculated for the composite material (20F/5G/15B, 20F/10G/10B and 20F/15G/5B).

6.1.1 Contact Pressure of Composite 20F/5G/15B

Composite 20F/5G/15B has following mechanical properties. These properties are characterized in this study.

Elastic Modulus (E)   = 5.172 x 10^9 N/mm2

Poisson's ratio (v)   = 0.366

Normal load (P)   = 100 N per mm of width

                        = 2000 N (Considering width = 20 mm)

Bearing roller radius (R_1)   = 10 mm

Bearing race radius (R_2)   = ∞ (considering flat surface)

The effective radius of curvature for interface between two cylinders is calculated using equation 3.20,

Effective radius = $R' = \left(\frac{1}{R_1} + \frac{1}{R_2}\right)^{-1} = 10$ mm

The effective elastic modulus is calculated using equation 3.28,

Effective elastic modulus = $E^* = \left(\frac{1-v_1^2}{E_1} + \frac{1-v_2^2}{E_2}\right)^{-1}$

$$= 2986.56 \text{ MPa}$$

The half width of contact (a) is calculated using equation 3.31,

The half width of contact = $a = 2\sqrt{\frac{P\,R'}{\pi\,E^*}}$

$$= 0.6529 \text{ mm}$$

This value 'a' is half width of contact between cylinder and flat surface when load is applied on the cylinder. To estimate maximum contact pressure, whole width of contact in deformed state is required at the area of contact of cylinder and flat surface,

Whole width of contact   = 2 x a

$$= 1.305 \text{ mm}.$$

The maximum contact pressure is calculated using equation 3.33,

Maximum contact pressure = $P_{max} = \left(\frac{P E^*}{\pi R'}\right)^{1/2}$

$$= 97.50 \text{ MPa}.$$

The contact pressure of other composite materials F20/G10/B10 and F20/G15/B5 is estimated by the same procedure as above,

6.1.2 Contact pressure of Composite 20F/10G/10B

Composite 20F/10G/10B has following mechanical properties. These properties are characterized in this study.

Elastic Modulus (E)   = 5.26 x 10^9 N/mm2

Poisson's ratio (v)   = 0.3612

Normal load (P)   = 100 N per mm of width

                = 2000 N (Considering width = 20 mm)

Bearing roller radius (R_1)   = 10 mm

Bearing race radius (R_2)   = ∞ (considering flat surface)

The maximum contact pressure is calculated using equation 3.33,

Maximum contact pressure= $P_{max} = \left(\frac{PE^*}{\pi R'}\right)^{1/2}$

                = 138.93 MPa.

6.1.3 Contact pressure of Composite 20F/15G/5B

Composite 20F/15G/5B has following mechanical properties. These properties are characterized in this study.

Elastic Modulus (E)   = 4.644 x 10^9 N/mm2

Poisson's ratio (v)   = 0.3558

Normal load (P)   = 100 N per mm of width

                = 2000 N (Considering width = 20 mm)

Bearing roller radius (R_1)   = 10 mm

Bearing race radius (R_2)   = ∞ (considering flat surface)

The maximum contact pressure is calculated using equation 3.33,

$$\text{Maximum contact pressure} = P_{max} = \left(\frac{PE^*}{\pi R'}\right)^{1/2}$$

$$= 91.98 \text{ MPa.}$$

6.2 FINITE ELEMENT MODEL

Finite Element (FE) model of the plane strain is created in the ANSYS WORKBENCH. The material properties of roller and race (flat surface) are same as used in section 6.1. Plane strain module is used for modelling of the roller and flat surface. The plain strain module is based on plane stress assumption. The plane strain implies no strain in depth direction and it is limited to only thin section. It is assumed that all the applied loads act in the X or Y direction and the displacements are function of X and Y location only. The strain in Z direction is zero ($\varepsilon_{zz} = \varepsilon_{xz} = \varepsilon_{yz} = 0$). As the load is applied in XY plane, there is no deformation in Z direction so no stress in Z direction (Scarcella, 2008).

Figure 6.1 (a) illustrate the meshed 2D cylinder and flat surface model, whereas Figure 6.1 (b) shows enlarged region of the contact area. Fine meshing at the contact zone is created to predict the accurate result for the contact pressure and to get the right contact nature between the contact of bearing and surface.

(a)   (b)
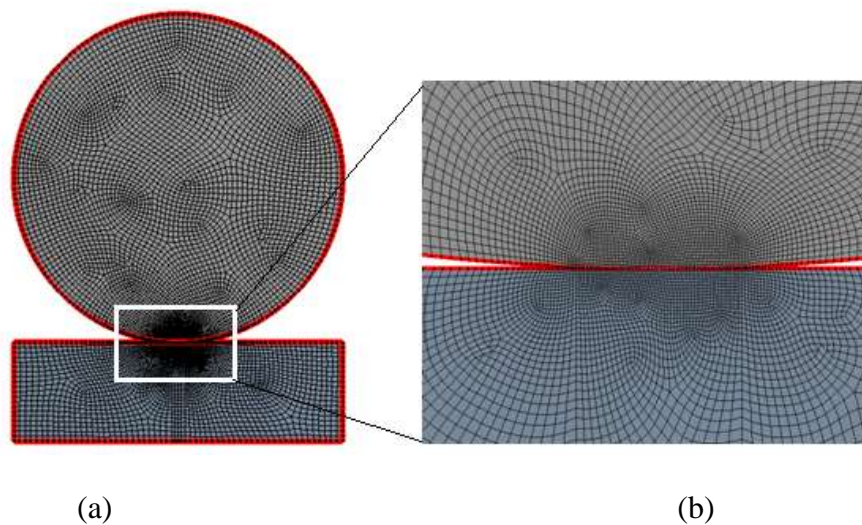
Figure 6.1 (a) Meshed 2D Model of Cylinder and Flat Plate (b) Enlarged Region of Contact Area.
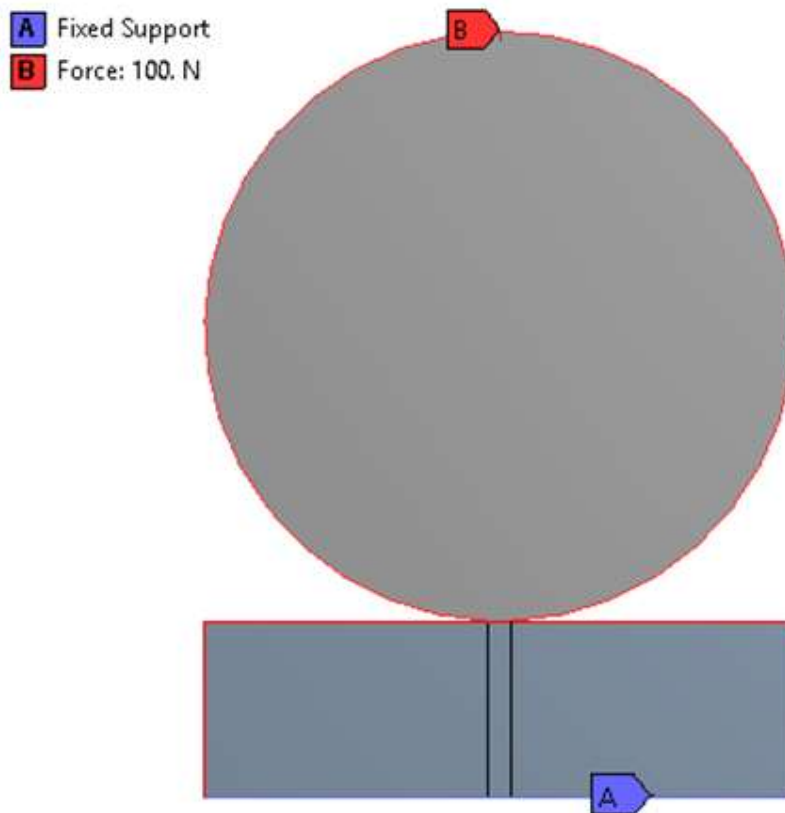
Figure 6.2 Boundary Conditions Applied to the Cylinder and Flat Surface

Meshing the module is done with minimum mesh size of 0.03 mm. The number of nodes and elements created during meshing are 39208 and 12866 respectively. The boundary conditions applied to the model are shown in the Figure 6.2. The load of 100 N is applied to the roller per unit length of the roller. The lower surface of the bearing surface is considered to have fixed boundary condition to simulate the outer surface of the bearing fixed in fixture so that it will not move. The test run is performed and results are obtained for the stresses, deformation, and normal stresses and contact pressures.

6.3 FEM RESULTS

The contact pressure distribution on the deformed model of 20F/5G/15B composite is shown in Figure 6.3. The contact pressure of the magnitude 106.99 MPa is observed at the center of contact. The theoretical contact pressure calculated is 97.5 MPa. The

difference between theoretical and FE contact pressure is about 10%. The maximum contact pressure of the magnitude 250 MPa is observed near the ends of the contact. It may be due to high stress concentration regions created at mesh transition.

Von-Mises stress plot shows maximum stress limit of 295 MPa but it can clearly be observed from the plot that stress value is very local and is only present at the end point at of the contact. This reflects the stress concentration and singularity and is neglected. Hence the maximum stress observed at the contact zone and nearby area is of the range of 65 to 98 MPa as shown in Figure 6.4.

Figure 6.5 show the total deformation near the interface between cylinder and flat surface model. The maximum deformation of the model is 0.03 mm and the deformation at the interface is between 3.3 to 13.4 micro-meters.

Figure 6.6 to 6.8 shows FEA results of composite 20F/10G/10B. Figure 6.6 show pressure distribution at the contact of cylinder and flat surface. The pressure distribution in the vicinity of contact is between 119 to 159 MPa, which is very much close to the theoretical value. It can be seen from some custom settings that pressure at the major contact region is nearly 142 MPa.

Figure 6.3 Contact Pressure Variation Between Elastic Cylinder and Flat Surface of 20F/5G/15B Composite.

Figure 6.4 Von-Mises Stress Variation Between Elastic Cylinder and Flat Surface of 20F/5G/15B Composite.

Figure 6.5 Total Deformation Variation Between Elastic Cylinder and Flat Surface of 20F/5G/15B Composite.
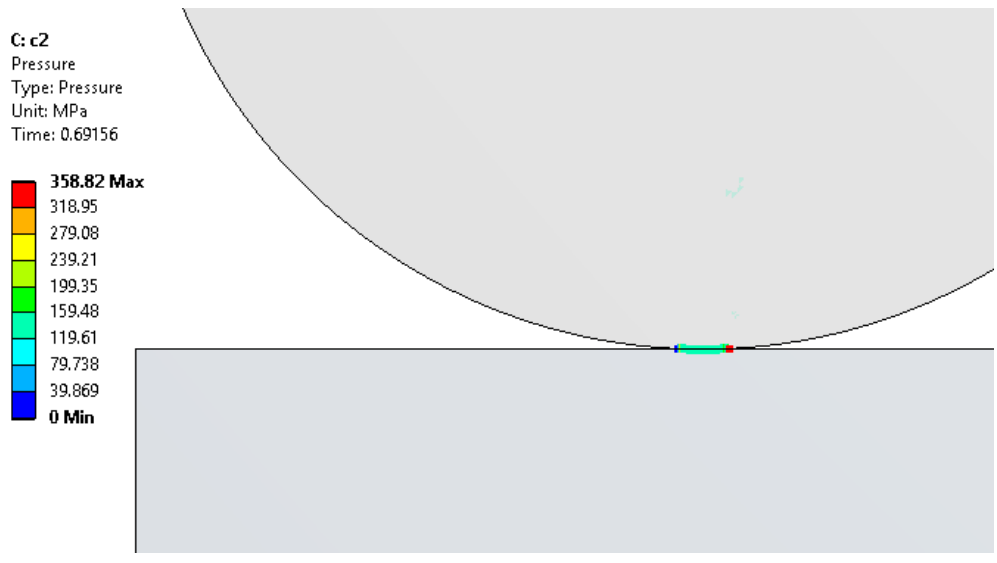
Figure 6.6 Contact Pressure Variation Between Elastic Cylinder and Flat Surface of 20F/10G/10B Composite.

Figure 6.7 Von-Mises Stress Variation Between Elastic Cylinder and Flat Surface of 20F/10G/10B Composite.

Figure 6.7 show Von-Mises stress distribution and the maximum value of stress is around 55 to 66 MPa. The total deformation is shown in Figure 6.8. The maximum

deformation observed in the vicinity of contact is in the range of 0.0026 mm to 0.013 mm.

Figure 6.9 to 6.11 shows FEA results of composite 20F/15G/5B. The maximum contact pressure of the model is 84.09 MPa. The FEA value of contact pressure is lower than the analytical value. The maximum theoretical contact pressure of the 20F/15G/5B composite is 91.98 MPa. Hence the FEA results are in good agreement with the theoretical one. The maximum Von-Mises stress of 39.55 MPa is observed for this composite and is shown in Figure 6.10. These values of Von-Mises stresses are low as compared to other composites. The total deformation of the model is in the range of 0.0028 mm to 0.026 mm. The comparative summary of these results is given in   Table 6.1

Table 6.1 Comparative Summary of Analytical and FEA Results

Material	Contact Pressure (MPa)		Deformation (mm)		Von-Mises stress (MPa)
	Analytical	FEA	Analytical	FEA	
20F/5G/15B	97.5	106.99	0.65	0.03	98
20F/10G/10B	138.93	142	0.22	0.024	66
20F/15G/5B	91.98	84.09	0.69	0.026	39.55
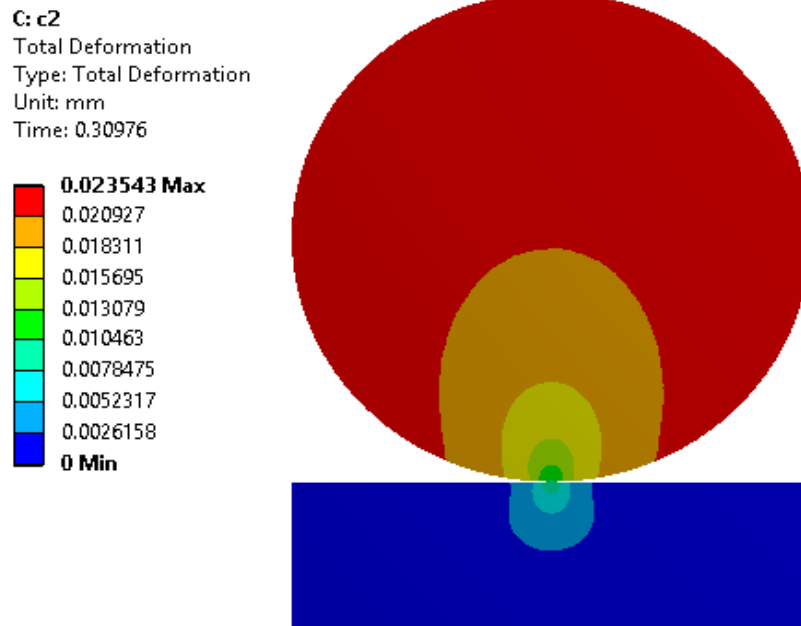
**Figure 6.8 Total Deformation Variation Between Elastic Cylinder and Flat
Surface Of 20F/10G/10B Composite.**

**Figure 6.9 Contact Pressure Variation Between Elastic Cylinder and Flat
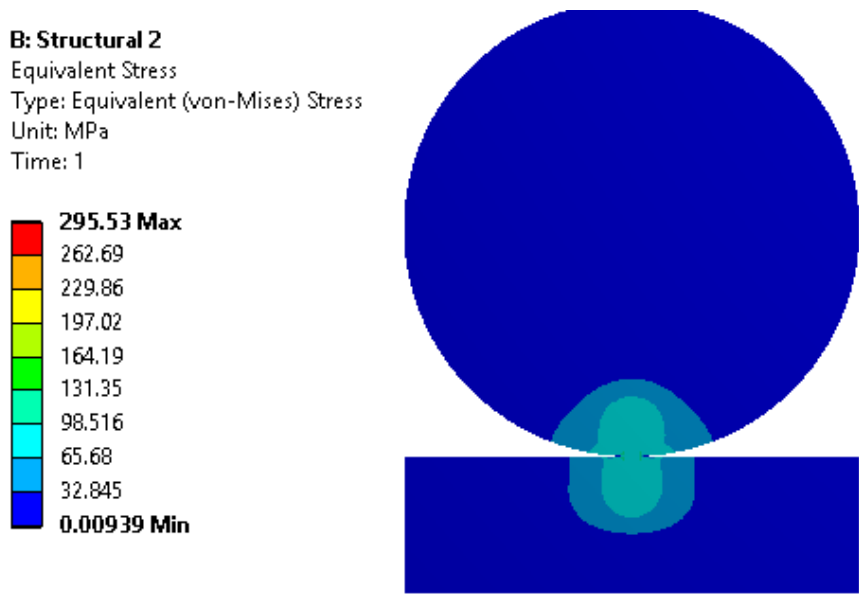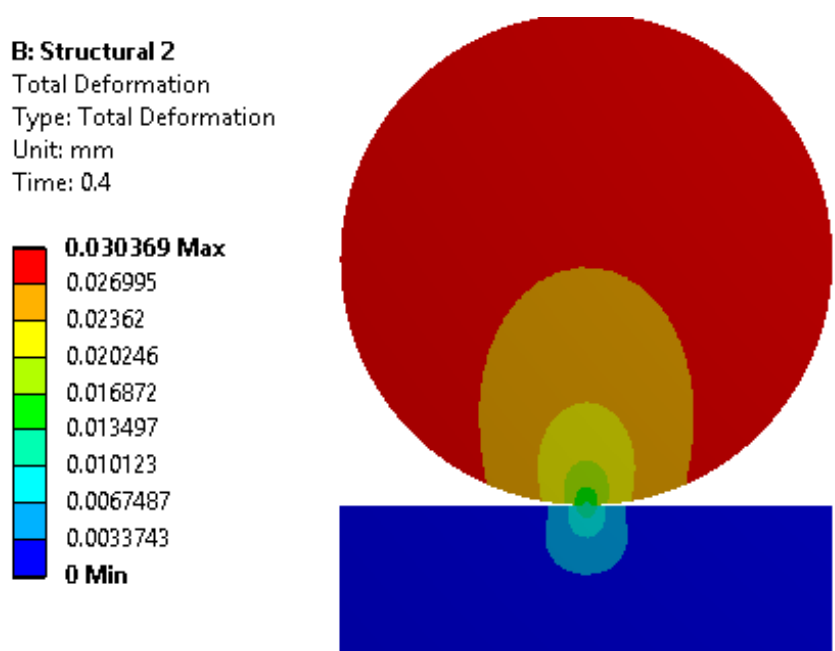Surface of 20F/15F/5B Composite.**

Figure 6.10 Von-Mises stress variation between elastic cylinder and flat surface of 20F/15G/5B composite.

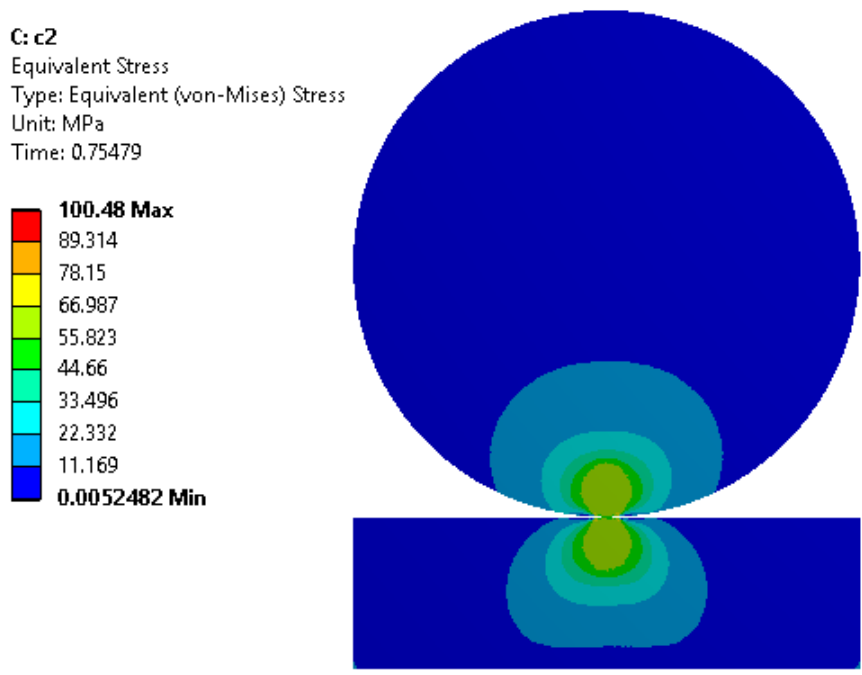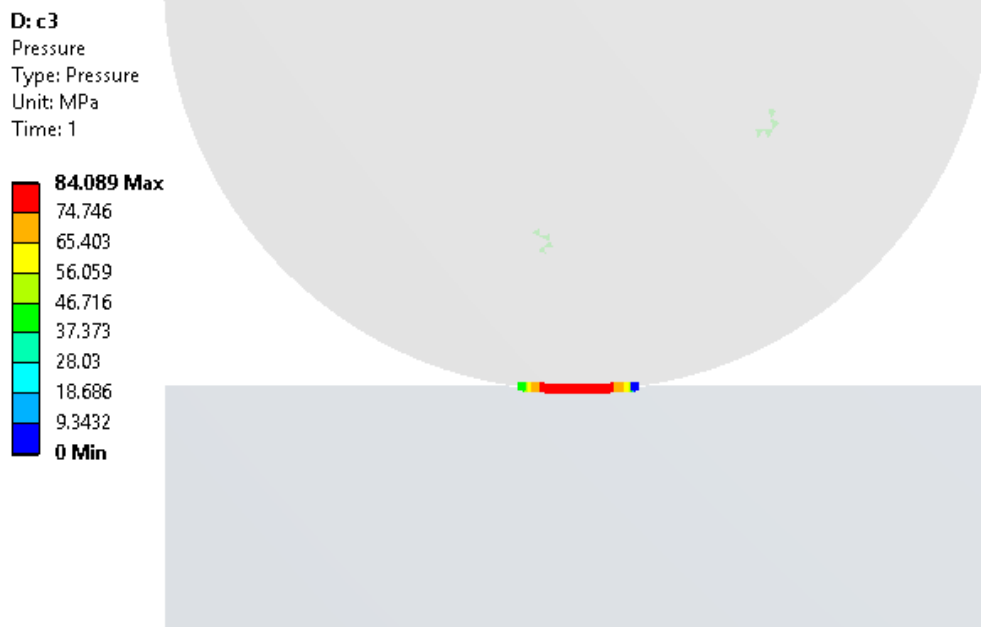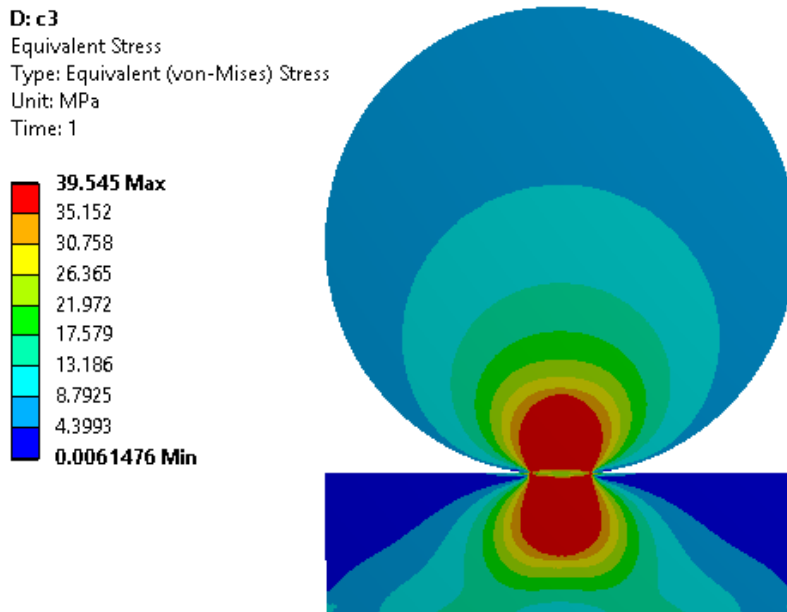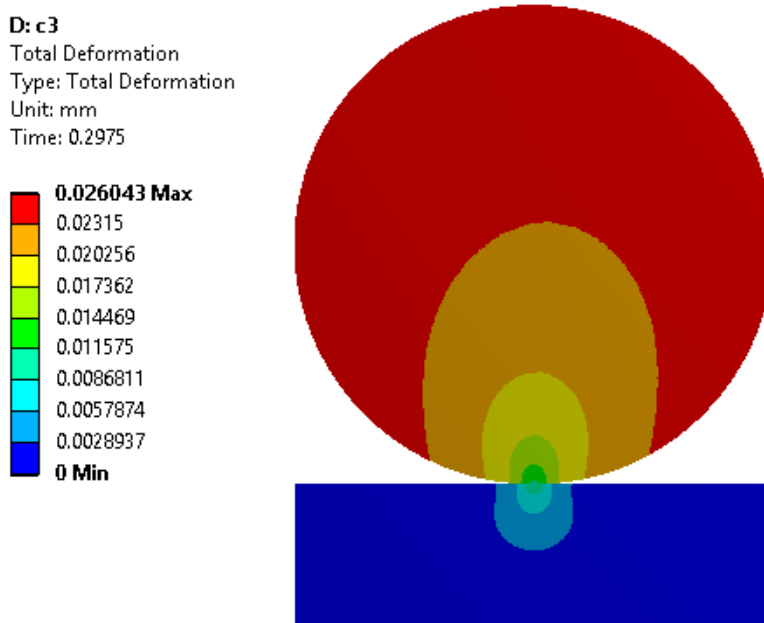**Figure 6.11 Total Deformation Variation Between Elastic Cylinder and Flat Surface of 20F/15G/5B Composite.**

CHAPTER 7

SUMMARY AND CONCLUSION

7.1 SUMMARY

Characterization of Glass fiber reinforced epoxy matrix composites with graphite and sintered bronze filler is carried out in this work. Most of the studies were focused on tribological characterization with little attention towards mechanical characterization. In the first part of this work, the focus is on characterization of mechanical properties. Two different fillers graphite and sintered bronze with varying volume percentage (5 vol%, 10 vol% and 15 vol%) has been used to study their effect with glass fiber (10 vol%, 15 vol% and 20 vol%) reinforced epoxy resin.

Remarkable improvement is observed in each mechanical property of graphite, bronze filled and glass fiber reinforced epoxy composites. The increasing and or decreasing volume percentage of graphite and bronze filler have shown positive effect on one or the other mechanical property. The reinforcement glass fiber and the fillers showed interaction between matrix-fiber and matrix-fillers through the experimental results of tensile, flexural, density, hardness and impact tests.

The increase volume percent of glass fiber reinforcement enhanced the tensile and, flexural strength whereas addition of bronze and graphite showed improved impact strength and hardness of the composites.

In the second part of the study friction and wear performance of the composites is carried out using DOE by Taguchi Orthogonal Array L_{27}. The tests are carried out by considering four controlling factors viz. sliding distance, Filler content, sliding velocities and normal load each at 3 levels. Design of Experiments by Taguchi orthogonal array helps to optimize the control factor. The results showed that the filler content and sliding distance is the most significant factor affecting specific wear rate of the composites. The factors like normal load and sliding velocity has least effect.

 The sliding distance as compared to sliding velocity is more sensitive in case of specific wear rate of the composite. The friction coefficient of the composites showed

reduced trend with addition of graphite filler. This confirms that the addition of this graphite with e-glass fiber is beneficial in reducing the wear of neat epoxy.

An artificial intelligent Simulink model (ANFIS) is developed to predict the specific wear rate. The results of this model is confirming to almost 99% to the experimental values.

To study the behaviour of the developed composites for practical application, analytical and FEA is carried out. The finite element model results are very much close to the analytical results. It is also observed that the contact pressure under the load for the tribo-composites is lower than steel.

7.2 CONCLUSIONS

The results of the Mechanical Characterization are concluded as below:

1. The increased reinforcement of E-glass fiber from 10 vol% to 20 vol% showed two fold increases in tensile strength irrespective of volume percentage of fillers.

2. Addition of glass fiber from 10-20 vol% resulted in threefold improvement in flexural modulus.

3. Addition of glass fiber from 10-20 vol% resulted in 80% increase in flexural modulus.

4. Addition of glass fiber from 10-20 vol% resulted in twofold increase in void volume fraction.

5. The flexural modulus of composites with 20 vol% of fiber showed 3 fold improvements over composite with 10 vol% of fiber.

6. Addition of graphite from 5 to 15 vol% resulted in reduced tensile strength by 50%.

7. Addition of graphite from 5 to 15 vol% resulted in enhanced flexural strength by 30-40%.

8. Increased volume percentage of sintered bronze helped in improving the density of the composite and also it helped in improving hardness of the composite.

9. The tensile strength of composite G15/B5 with 15 vol% of fiber showed maximum tensile strength of 71.16 MPa.

10. Tensile modulus of composite G10/B10 with 15 vol% of fiber showed maximum tensile modulus of 5.26 GPa.

11. Increased volume percentage of sintered bronze helped in improving the density of all the compositions.

12. It was observed that decreased vol% of bronze tends to lower the hardness of the composite with 20 vol% of glass fiber.

The pin on disc wear test of fiber reinforced graphite and sintered bronze filled epoxy composites was carried at different sliding velocity, normal load and sliding distance. The sliding wear resistance of neat epoxy is appreciably enhanced by incorporation of e-glass fiber of 20 vol%. The specific wear rate of the composite also decreases with addition of graphite filler from 5 vol% to 15 vol%. The addition of maximum 15 vol% of graphite showed maximum wear resistance.

The results of wear test are summarized as below:

1. An Increase in sliding velocity, normal load and sliding distance showed reduced specific wear rate and friction coefficient. Composition 20F/5G/15B has better wear resistance against sliding velocity compared to 20F/10G/10B and 20F/15G/5B whereas composition 20F/15G/5B has better wear resistance against normal load and sliding distance. Composition 20F/15G/5B showed better coefficient of friction against sliding distance.

2. The addition of fillers in fiber reinforced epoxy composites has positive effect on wear resistance and tribological property. Composite with 5 vol% of sintered bronze showed better friction and wear performance compared to 10 vol% and 15 vol%.

3. Inclusion of both soft graphite and hard sintered bronze fillers in epoxy matrix along with e-glass fiber enhanced the self-lubricating and load carrying capacity of the matrix thus helped in enhancing tribological properties of the epoxy.

4. Analysis of wear mechanism was carried by SEM micrographs which indicated the micro cracks, formation of lubricating film, loosening of fillers and peeling of the matrix.

5. The cracks developed in the layer helped in dissipating the heat generated

6. TGA showed the thermal stability of the composites to a maximum temperature range of 546^0C to 701^0C for weight loss of 35% to 55% respectively.

7. The calculated analytical contact pressure is in close agreement with finite element model results.

8. ANFIS simulator predicted specific wear rate close to 99% compared to experimental results.

9. The analytical and FEA results of contact pressure and deflection for developed composite are very much same.

7.3 RESEARCH CONTRIBUTION

The aim of this research work is to develop an antifriction polymer material to reduce friction. Glass fiber reinforced epoxy matrix composite filled with sintered bronze and graphite is developed. The pressure die moulding setup is designed and developed at my institute to fabricate the test specimens for Mechanical characterization and Tribological characterization. DOE by Taguchi is used to predict the influencing parameter on specific wear rate by OA L_{27} (13^3). ANFIS Simulink model is also developed to predict the specific wear rate for any PMC. The results of FEA of PMC bearing is compared with analytical results.

The contribution can be summarized as:

1. Developed new friction material which can be replacement for existing material.

2. Designed and developed the pressure die moulding setup to fabricate the test specimens to carry mechanical and tribological characterization.

3. The use of glass fiber, fillers sintered bronze and graphite enhanced the mechanical and tribological behaviour of epoxy matrix composite. The results are published in reputed international journal and presented in National conference.

4. FEA is carried to study the behaviour of the composite under loading. The contact pressure and deformation at the point of contact is obtained by analytical method and FEA.

126

7.3 FUTURE SCOPE

In this study characterization of the epoxy composite reinforced with glass fiber and filled with graphite and sintered bronze is carried out. The matrix, fiber and filler are the constituent element of the composites which is varied to optimize the properties. This study is not limited to characterization of the composite material. An attempt is made to study behavior of the composite using FEA model. This work can be further extended by following ways

1. The filler volume percent can be varied to optimize the filler content and use of solid lubricant can be analyzed.
2. Natural fiber can be used instead of glass fiber to take care of environment and cost of the fabrication.
3. Thermal analysis can be carried out to assess the thermal conductivity, coefficient of thermal expansion and heat transfer.
4. The experimental contact pressure can be computed by fabricating the cylinder and flat plate of the composite material.
5. Fatigue analysis of the composites can be area of interest.

APPENDICES

APPENDIX I

Test specimens

(a) Tensile test specimen

(b) Flexural test specimen
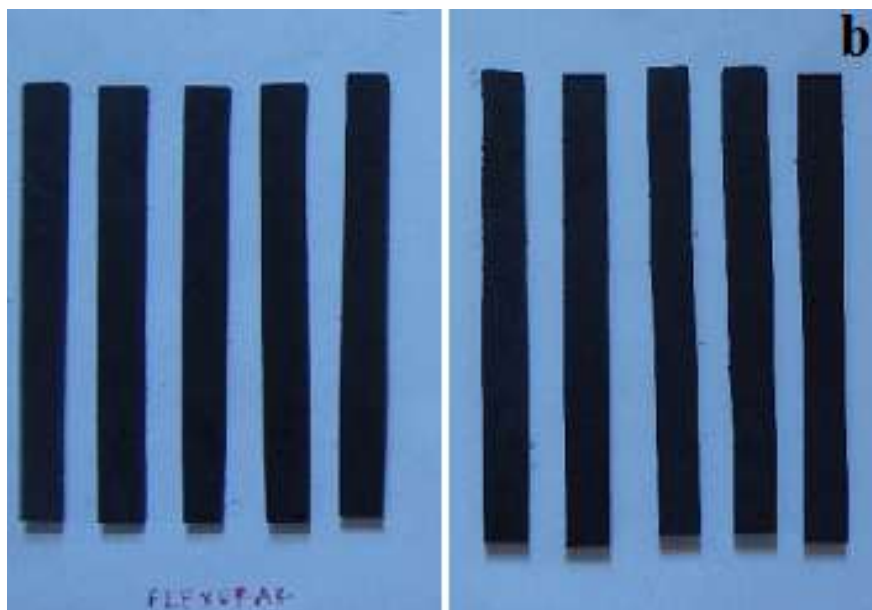
(c) Impact test specimen
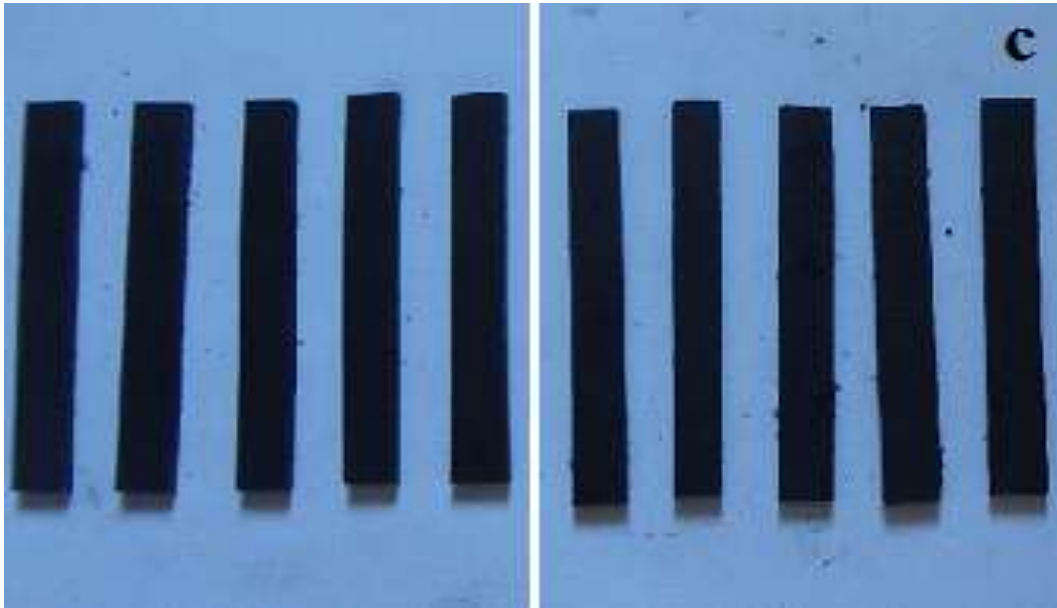
(d) Hardness tests test specimen

APPENDIX II

Tensile Test Specimen
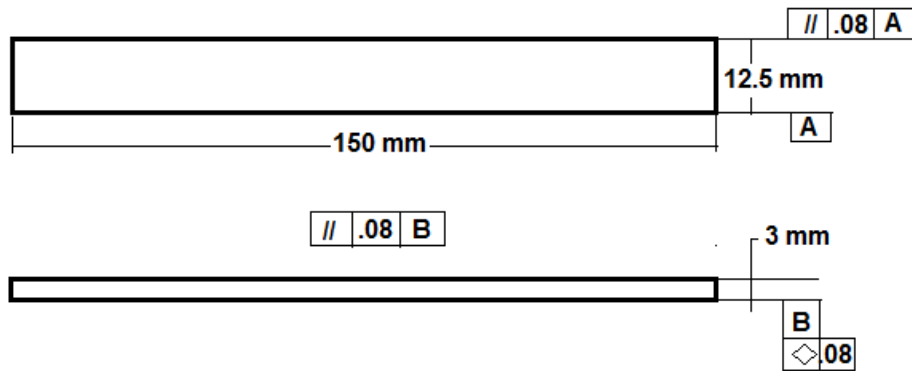
APPENDIX III

Universal Testing Machine (UTM) Setup at NITK

APPENDIX IV

Hydraulic Circuit Diagram of Pressure Die Moulding.
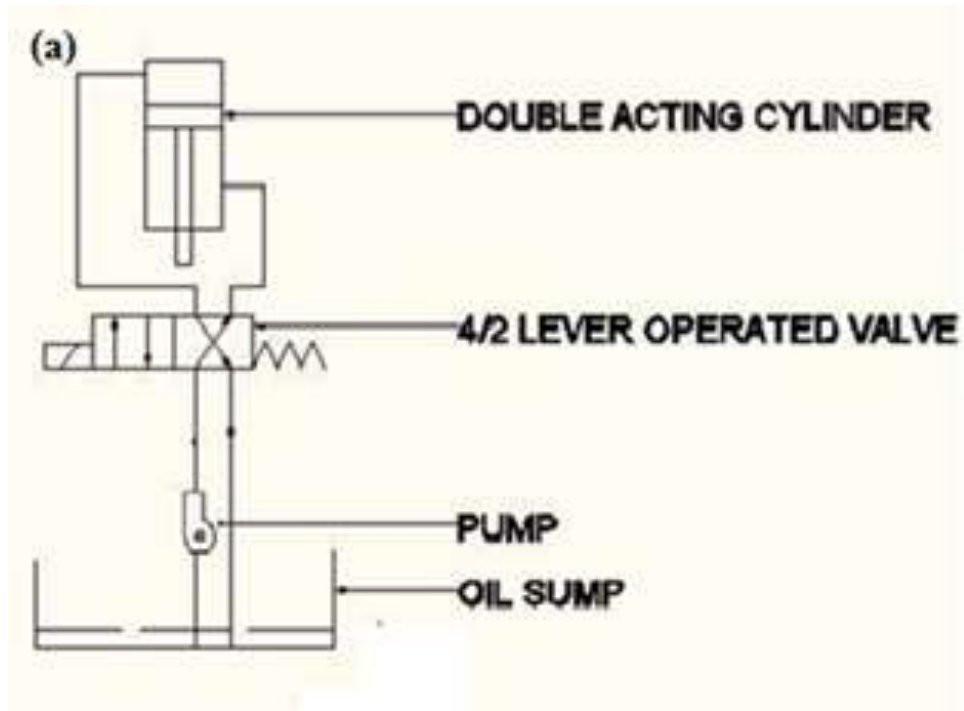
APPENDIX V

Pressure Die Moulding Setup developed at NKOCET

APPENDIX VI

SEM micrographs of Composites

(10 vol% of graphite and bronze)
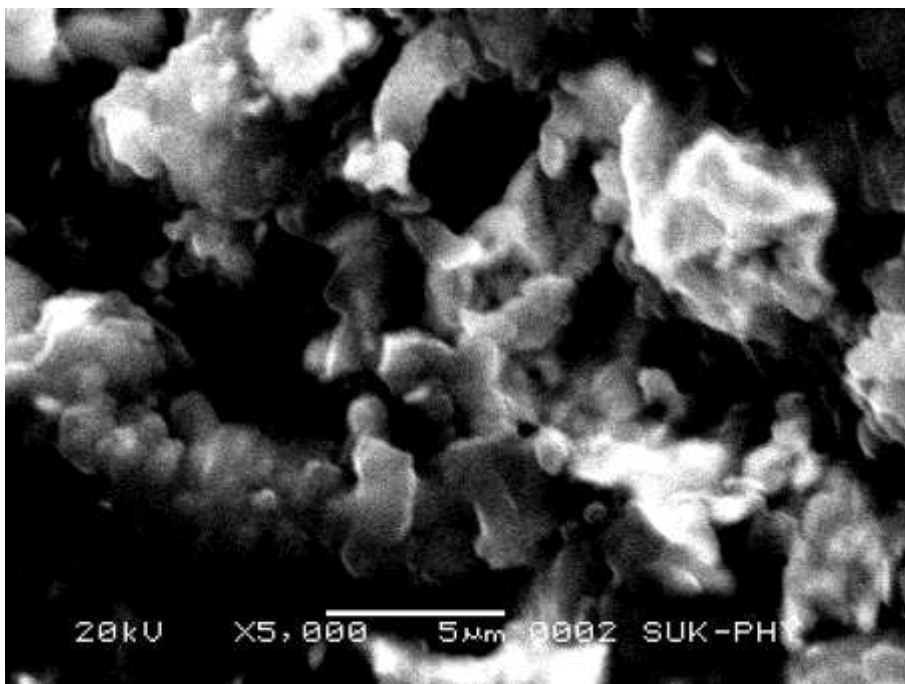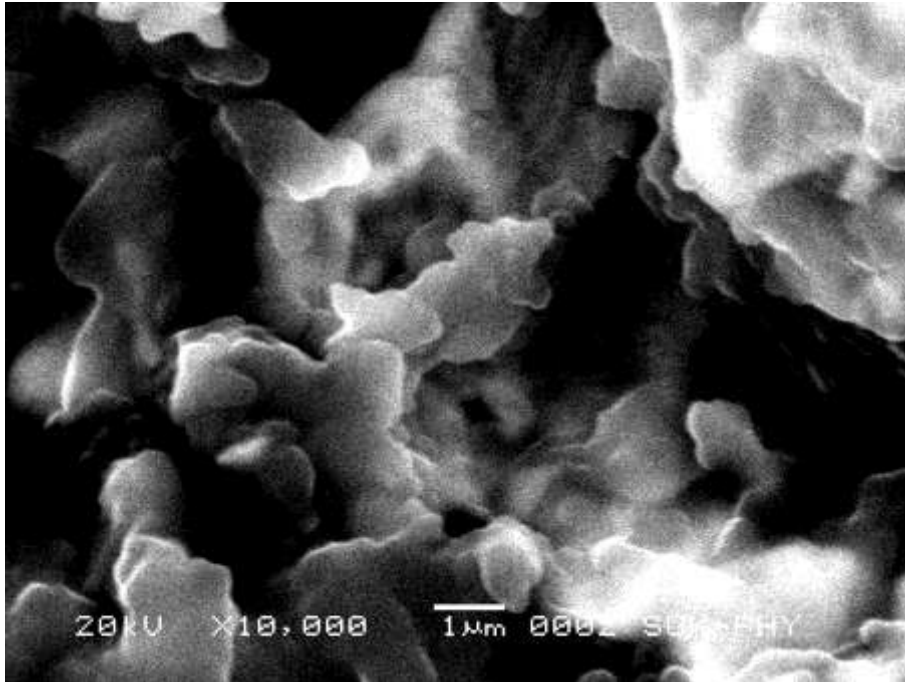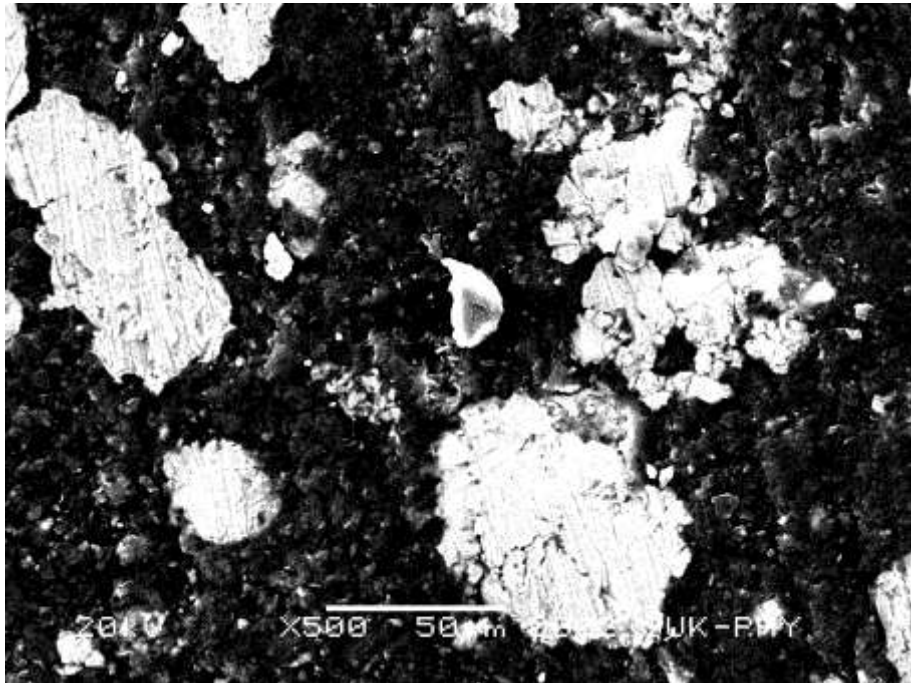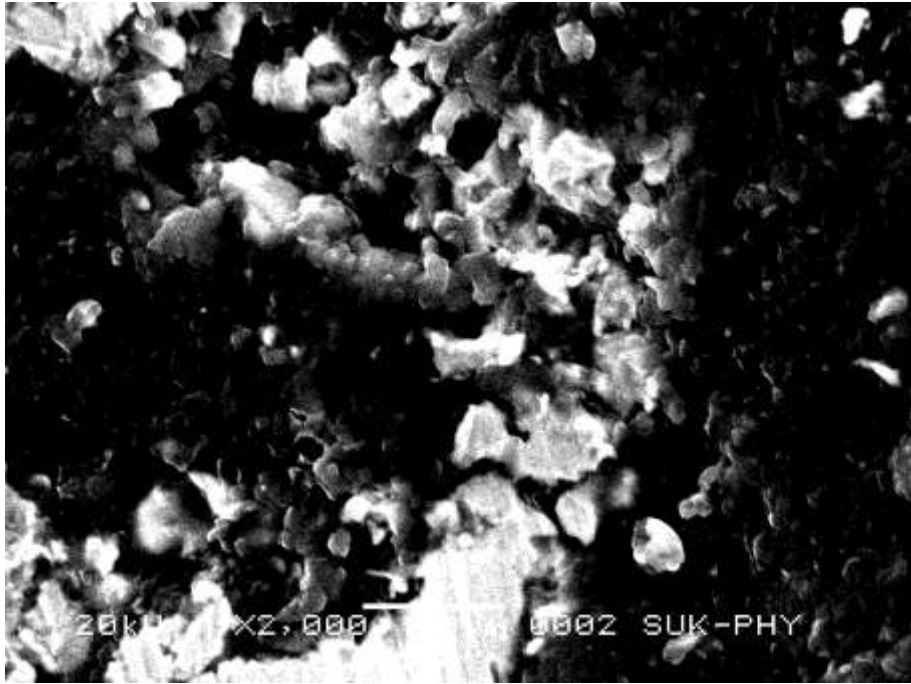
APPENDIX VII

Additional SEM micrographs of Composites

(20F/15G/5B)
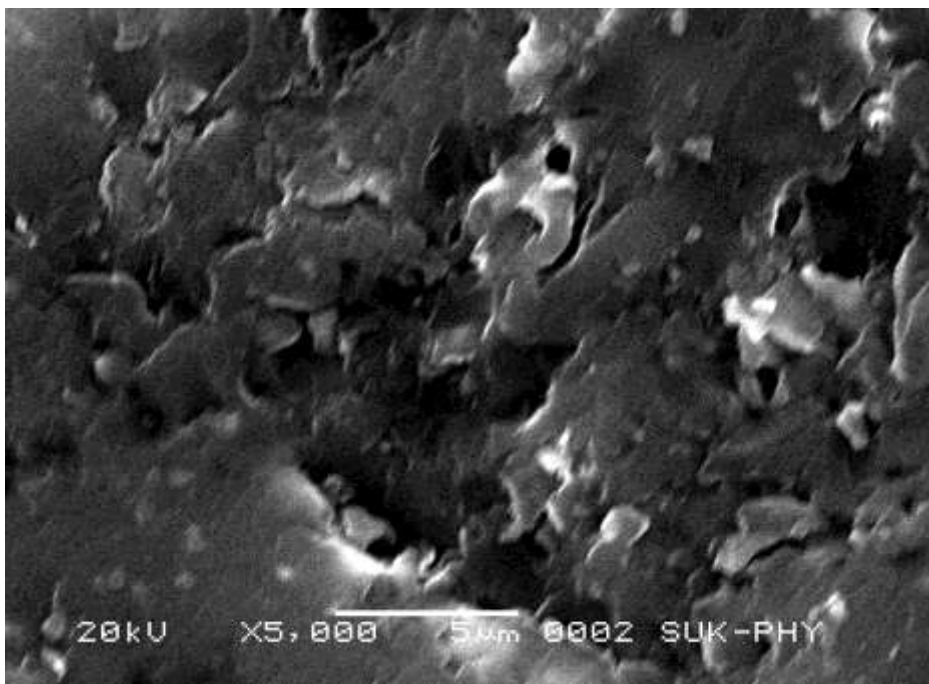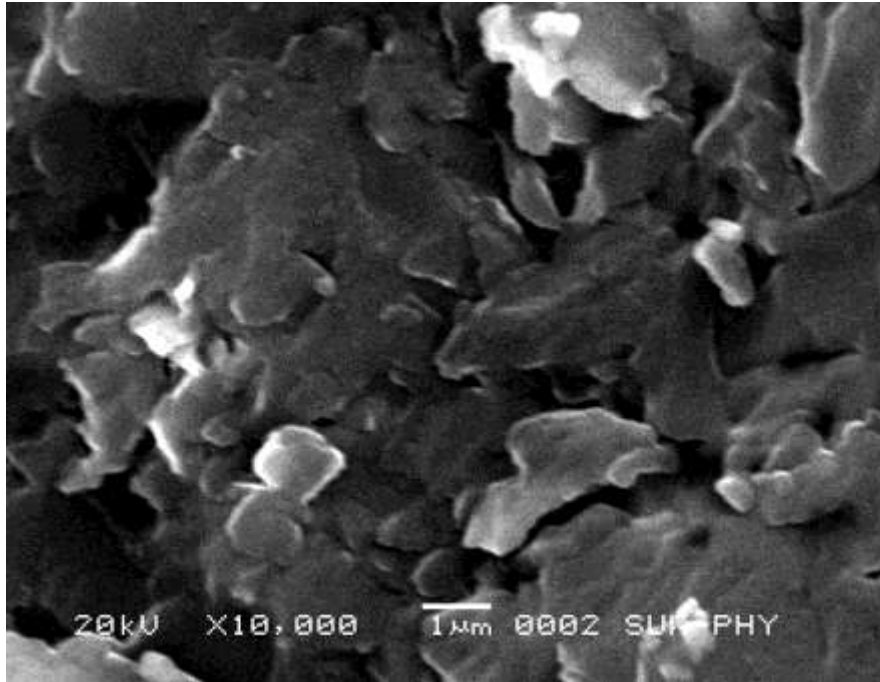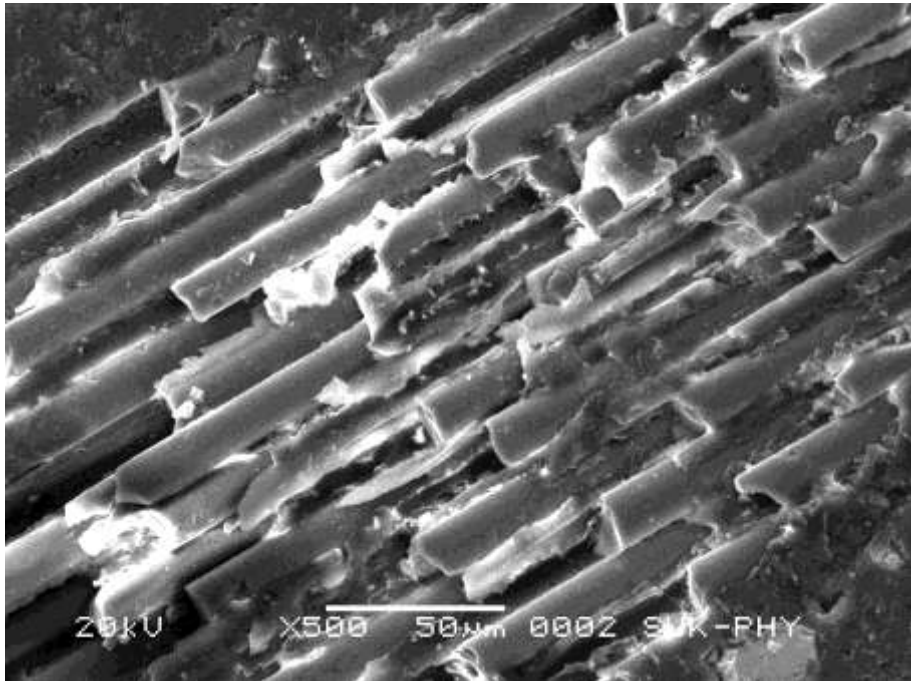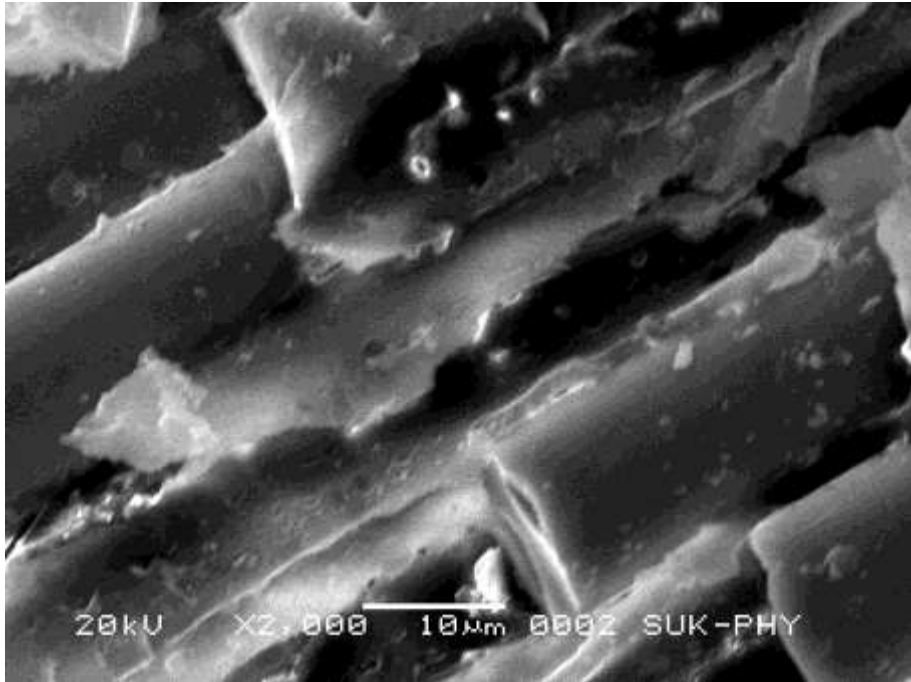
REFERENCES

Agrawal J. P. (1990). Composite Materials, DESIDOC, *Defence Scientific Information and Documentation Centre*, Publication, 6 to 13.

Agrawal Gaurav, Patnaik Amar and Sharma Rajesh Kumar. (2013). "Parametric optimization and three-body abrasive wear behavior of sic filled chopped glass fiber reinforced epoxy composites." *International Journal of Composite Materials*, 3(2), 32-38.

Anjum Naveed, Ajit Prasad S. L., and Suresha B. (2013). "Role of silicon dioxide filler on mechanical and dry sliding wear behaviour of glass-epoxy composites."*Ad vances in Tribology*, Volume 2013, Article ID 324952, 1-10.

Akinci A., Sen S. and Sen U. (2014). "Friction and wear behavior of zirconium oxide reinforced PMMA Composites." *Composites: Part B*, 56, 42–47.

Atuanya C.U., Aigbodion V.S. and Nwigbo S.C. (2014). "Experimental study of the thermal and wear properties of recycled polyethylene/breadfruit seed hull ash particulate composites." *Materials and Design*, 53, 65–73.

Alambeigi Farshid, Seyed Mohsen Khadem, Hamid Khorsand and Elnaz Mirza Seied Hasan. (2016). "A comparison of performance of artificial intelligence methods in prediction of dry sliding wear behavior." *Int J Adv Manuf Technol*, 84, 1981–1994.

Alimam H., Hinnawi M., Pradhan P. and Alkassar Y. (2016). "ANN & ANFIS models for prediction of abrasive wear of 3105 aluminium alloy with polyurethane coating." *Tribology in Industry*, Vol. 38, No. 2, 221-228.

Agrawal Sandeep, Singh K.K. and Sarkar P.K. (2016). "A comparative study of wear and friction characteristics of glass fibre reinforced epoxy resin, sliding under dry, oil-lubricated and inert gas environments." *Tribology International*, 96, 217–224.

Abenojar J., Tutor J., Ballesteros Y., Real J.C. and Martínez M.A. (2017). "Erosion-wear, mechanical and thermal properties of silica filled epoxy nanocomposites." *Composites Part B*, 120, 42-53.

Aziz Mohamed Hafizal Yazid A., Sahrim Ahmad, Jaafar Abdullah, M. Dahlan, Rozaidi Rasid, Megat Harun M. A, Mahathir Mohamad and M. Hamzah Harun. (2012). "Experimental optimization in polymer BLEND composite preparation based on mix level of taguchi robust design." *Journal of Nuclear and Related Technologies*, Volume 9, No. 1, 23-32.

Balley D. M. and Sayles B. S. (1991). "Effect of rouchness and sliding friction on contact stresses." *Journal of Tribology*, Vol, 113, 729-738.

Bourdon A., Rigal J. F. and Play D. (1999). "Static rolling bearing models in a CAD environment for the study of complex mechanisms: Part I—Rolling Bearing Model." *Journal of Tribology*, Vol. 121, 205-214.

Bryan Harris. (1999) Engineering Composite Materials, *The institute of Materials*, London, (pp. 6).

Bijwe J. and Indumathi J. (2004). "Influence of fibers and solid lubricants on low amplitude oscillating wear of polyetherimide composites." *Wear*, 257, 562–572.

Bondioli Federica, Valeria Cannillo, Elena Fabbri and Massimo Messori. (2006). "Preparation and characterization of epoxy resins filled with submicron spherical zirconia particles." *Polimery 51*, nr 11-12, 794-798.

Bhagyashekar M. S. and Rao R. M. V. G. K. (2007). "Effects of material and test parameters on the wear behavior of particulate filled composites part 1: SiC-Epoxy and Gr-Epoxy Composites." *Journal of Reinforced Plastics and Composites*, Vol. 26, No. 17.

Basavarajappa S., Arun K.V. and Paulo Davim J. (2009). "Effect of filler materials on dry sliding wear behavior of polymer matrix composites – A Taguchi

Approach." *Journal of Minerals & Materials Characterization & Engineering*, Vol. 8, No.5, 379-391.

Biswas Sandhyarani and Satapathy Alok. (2009). "Tribo-performance analysis of red mud filled glass-epoxy composites using Taguchi experimental design." *Materials and Design*. Volume 30, Issue 8, 2841-2853.

Boger Lars, Jan Sumfleth, Hannes Hedemann and Karl Schulte. (2010). "Improvement of fatigue life by incorporation of nanoparticles in glass fibre reinforced epoxy." *Composites: Part A*, 41, 1419–1424.

Basavarajappa S. and Ellangovan S. (2012). "Dry sliding wear characteristics of glass–epoxy composite filled with silicon carbide and graphite particles." *Wear*, 296, 491–496.

Benham A, Thyagarajan K and Sivapragash M. (2013). "Optimizing the material composition for a wind turbine blade using grey based Taguchi technique." *Life Science Journal*, 10(2), 1964-1969.

Brezeanu Ligia Cristina. (2013). "Contact stresses between two cylindrical bodies with parallel axes: Analysis By F.E.M." *Scientific Bulletin of the Petru Maior*, University of Tîrgu Mureş Vol. 10 (XXVII) no. 2, 9-14.

Bagci Mehmet and Imrek Huseyin. (2013). "Application of Taguchi method on optimization of testing parameters for erosion of glass fiber reinforced epoxy composite materials." *Materials and Design*, 46, 706–712.

Bhagat Subita and Verma Pardeep Kumar. (2013). "Effect of filler parameter on morphology of graphite filled epoxy composites." *International Journal of Scientific & Engineering Research*, Volume 4, Issue 4, 459-463.

Bakar Syamsiah Abu, Rosma Mohd Dom, Ajab Bai Akbarally, and Wan Hasamudin Wan Hassan. (2015). "Role of input selection prediction of physical properties of degradable composites using ANFIS." *International Journal of Materials, Mechanics and Manufacturing*, Vol. 3, No. 3, 213-217.

138

Brahmam D.Veera, Prakash M. Anil, Rao S.Srinivasa and Gopala Rao L.V.V. (2016). "Contact stress analysis of fly ash/ graphite particulate reinforced aluminium matrix hybrid composite spur gear." *International Journal of Innovative Research in Science*, Engineering and Technology, Vol. 5, Issue 4, 6395-6407.

Baptista R., Mendao A., Rodrigues F., Figueiredo-Pina C.G., Guedes M. and Marat-Mendes R. (2016). "Effect of high graphite filler contents on the mechanical and tribological failure behavior of epoxy matrix composites." *Theoretical and Applied Fracture Mechanics*, 85, 113–124.

Bobbili Ravindranadh and Madhu V. (2016). "Sliding wear behavior of E-glass-epoxy/MWCNT composites: An experimental assessment." *Engineering Science and Technology*, 19, 8–14.

Bazrgari D., Moztarzadeh F., Sabbagh-Alvani A.A., Rasoulianboroujeni M., Tahriri M. and Tayebi L. (2018). "Mechanical properties and tribological performance of epoxy/Al_2O_3 nanocomposite." *Ceramics International*, 44, 1220–1224.

Bunsell A.R. and Renard J., Fundamentals of fiber reinforced composite materials, *Institute of Physics*, London, UK.

Cho Young-Tae, Choong-Ho Lee, Kwang-Hee Im and In-Nam Hwang. (2006). "Finite element analysis of contact stress for particle reinforced composites." *Key Engineering Materials*, Vol- 324-325, 1201-1204.

Chang Li and Friedrich Klaus. (2010). "Enhancement effect of nanoparticles on the sliding wear of short fiber-reinforced polymer composites: A critical discussion of wear mechanisms." *Tribology International*, 43, 2355–2364.

Chandramohan D., and J. Bharanichandar. (2013). "Natural fiber reinforced polymer composites for automobile accessories." *American Journal of Environmental Science*, 9 (6), 494-504.

Campbell F.C., Manufacturing processes for advanced composites, *Elsevier Advanced Technology*, Kidlington, Oxford, UK.

Chauhan Santram and Thakur Sunil. (2012). "Effect of micro size cenosphere particles reinforcement on tribological characteristics of vinyl ester composites under dry sliding conditions." *Journal of Minerals and Materials Characterization and Engineering*, 11, 938-946.

Dwyer-Joyce R. S. (1997). Tribological Design Data, Part 3: Contact Mechanics, University of Sheffield; *The Tribology Group of The Institution of Mechanical Engineers*, 1st Edition.

Daniel Nélias, Eduard Antaluca, Vincent Boucly and Spiridon Cretu. (2007). "A three-dimensional semianalytical model for elastic-plastic sliding contacts." *Journal of Tribology*, Vol. 129, 761-771.

Davim Paulo J. and Cardoso Rosaria. (2009). "Effect of the reinforcement (carbon or glass fibres) on friction and wear behaviour of the PEEK against steel surface at long dry sliding." *Wear*, 266, 795–799.

Dhieb H., Buijnsters J.G., Eddoumy F., Vázquez L. and Celis J.P. (2013). "Surface and sub-surface degradation of unidirectional carbon fiber reinforced epoxy composites under dry and wet reciprocating sliding." *Composites: Part A*, 55, 53–62.

Detomi Anine Cristina, Reniene Maria dos Santos and Sergio Luiz Moni Ribeiro Filho. (2014). "Statistical effects of using ceramic particles in glass fibre reinforced Composites." *Materials and Design,* 55, 463–470.

Fu Shao-Yun, Xi-Qiao Feng, Bernd Lauke and Yiu-Wing Mai. (2008). Effects of particle size, particle/matrix interface adhesion and particle loading on mechanical properties of particulate–polymer composites." *Composites: Part B*, 39, 933–961.

Fayyad Sayel M. (2013). "Analysis and Simulation of Contact Stresses of Convex Punch." *IOSR Journal of Engineering*, 3, Issue 12, 59-67.

Graham Darren L., Doug R. Forbes and Simon D. Smith. (2006). "Modeling the ready mixed concrete delivery system with neural networks." *Automation in Construction*, 15, 656 – 663.

Guo Qing Bing, Kin Tak Lau, Min ZhiRong and Ming Qiu Zhang. (2010). "Optimization of tribological and mechanical properties of epoxy through hybrid filling." *Wear,* 269, 13–20.

Gupta Vikrant, Singh Rama, Manoj Kumar Jha, and M. F. Qureshi. (2014). "ANFIS Prediction of the Polymer and Polymer Composite properties and its Optimization Technique." *AMSE JOURNALS –2014-Series: Modelling A*; Vol. 87; No- 2, 70-88.

Gao C.P., Guo G.F., Zhao F.Y., Wang T.M., Jim B., Wetzel B., Zhang G. and Wang Q. H. (2016). "Tribological behaviors of epoxy composites under water lubrication conditions." *Tribology International*, 95, 333–341.

Guo Lihe, Huimin Qi, Ga Zhang, Tingmei Wanga and Qihua Wanga. (2017). "Distinct tribological mechanisms of various oxide nanoparticles added in PEEK composite reinforced with carbon fibers." *Composites: Part A*, 97,19–30.

Hassan S.B., Oghenevweta J.E., Aigbodion V.S. (2012). "Morphological and mechanical properties of carbonized waste maize stalk as reinforcement for eco-composites." *Composites: Part B*, 43, 2230–2236.

Hu Zhong and Mohammad Robiul Hossan. (2012). "Strength evaluation and failure prediction of short carbon fiber reinforced nylon spur gears by finite element modeling." *Appl Compos Mater*, 9274-7, 1-15.

Hung Pui-yan, Lau Kin-tak, Cheng Lai-kwan, Leng Jinsong and Hui David. (2018). "Impact response of hybrid carbon/glass fibre reinforced polymer composites designed for engineering applications." *Composites Part B*, 133, 86-90.

Ihara T., Shaw M.C. and Bhushan B. (1986). "A finite element analysis of contact stress and strain in an elastic film on a rigid substrate—Part I: Zero Friction." *Journal of Tribology*, Vol. 108, 527-533.

Ismail Mohammed, Bheemappa Suresha and Rajendra N. (2012). "Investigations on mechanical and erosive wear behaviour of cenosphere filled carbon-epoxy composites." *International Conference on Mechanical, Automotive and Materials Engineering* (ICMAME'2012), 208-213.

Jang Jyh-Shing Roger. (1993). "ANFIS: Adaptive-Network-Based Fuzzy Inference System." *IEEE Transactions on Systems, Man, and Cybernetics*, Vol. 23, NO. 3, 665-685.

Jacobs O., Jaskulka R., Yang F., and Wu W. (2004). "Sliding wear of epoxy compounds against different counterparts under dry and aqueous conditions," *Wear*, Vol. 256, No. 1-2, 9–15.

Joshi H. C., Tiwari A. N. and Goyal R. K. (2010). "Improvement in thermal, mechanical and water resistance properties of epoxy/glass particulate composites." *Int. J. Plastic Technology*, 14(2):167–178.

Jin Hongyun, Yaoqing Wu, Shuen Hou Yunlong Li, Min Liu and Zhengjia Ji Jiao Yuan. (2013). "The effect of spherical silica powder on the tribological behavior of phenolic resin–based friction materials." *Tribology Letter*, 51, 65–72.

Jo Hyu Sang and Lee Gyo Woo. (2017). "Investigation of mechanical and thermal properties of silica-reinforced epoxy composites by using experiment and empirical model." *Materials Today: Proceedings*, 4 6178–6187.

Kishore, P. Sampathkumaran, S. Seetharamu, Thomas P. and Janardhana M. (2005). "A study on the effect of the type and content of filler in epoxy–glass composite system on the friction and slide wear characteristics." *Wear*, 259, 634–641.

Kharde Y.R. and Saisrinadh K. V. (2011). "Effect of oil and oil with graphite on tribological properties of glass filled PTFE polymer composites." *Bull. Mater. Sci.*, Vol. 34, No. 4, 1003–1012.

Kim Sung Soo, Min Wook Shin, Ho Jang. (2012). "Tribological properties of short glass fiber reinforced polyamide 12 sliding on medium carbon steel." *Wear*, 274– 275, 34– 42.

Kwon Dong-Jun, Pyeong-Su Shin, Jong-Hyun Kim, Yeong-Min Baek, Ha-Seung Park, K. Lawrence DeVries and Joung-Man Park. (2017). "Interfacial properties and thermal aging of glass fiber/epoxy composites reinforced with SiC and SiO$_2$ nanoparticles." *Composites Part B*, 130, 46-53.

Kumar Hemath G., Babuvishwanath H., Rajesh Purohit, Pramod Sahu and Rana R. S. (2017). "Investigations on mechanical properties of glass and sugarcane fiber polymer matrix composites." *Materials Today: Proceedings*, 4, 5408–5420.

Karami Pooria and Shojaei Akbar. (2017). "Improvement of dry sliding tribological properties of polyamide 6 using diamond nanoparticles." *Tribology International*, 115, 370–377.

Khan Ziaullah, Yousif B.F. and Mainul Islam. (2017). "Fracture behaviour of bamboo fiber reinforced epoxy composites." *Composites Part B*, 116, 186-199.

Li Xiubing, Yimin Gao, Jiandong Xing, Yu Wang and Liang Fang. (2004). "Wear reduction mechanism of graphite and MoS2 in epoxy composites." *Wear*, 257, 279–283.

Larsen Thomas Ø., Tom L. Andersen, Bent Thorning and Martin E. Vigild. (2007). "Comparison of friction and wear for an epoxy resin reinforced by a glass or a carbon/aramid hybrid weave." *Wear*, 262, 1013–1020.

Larsen Thomas Ø., Tom L. Andersen, Bent Thorning, Martin E. Vigild. (2008). "The effect of particle addition and fibrous reinforcement on epoxy-matrix composites for severe sliding conditions." *Wear*, 264, 857–868.

Li Du-Xin, Xin Denga, Jin Wangb, Jun Yangb and Li Xiangxiang. (2010). "Mechanical and tribological properties of polyamide 6–polyurethane block copolymer reinforced with short glass fibers." *Wear*, 269, 262–268.

Luo Y., Yu X. Y., Dong X. M., Rong M. Z. and Zhang M. Q. (2010). "Effect of nano-Si3N4 surface treatment on the tribological performance of epoxy composite." *eXPRESS Polymer Letters*, Vol.4, No.3, 131-140.

Mohan N., Natarajan S. and Kumaresh Babu S.P. (2011). "Abrasive wear behaviour of hard powders filled glass fabric–epoxy hybrid composites." *Materials and Design*, 32, 1704–1709.

Mohanty Akash and Srivastava V. K. (2012). "Compressive failure analysis of alumina nano particles dispersed short glass/carbon fiber reinforced epoxy hybrid composites." *International Journal of Scientific & Engineering Research*, Volume 3, Issue 11, 1-7.

Mesbahi Ali Haghighat, Dariush Semnani and Saeid Nouri Khorasani. (2012). "Performance prediction of a specific wear rate in epoxy nanocomposites with various composition content of polytetrafluoroethylen (PTFE), graphite, short carbon fibers (CF) and nano-TiO2 using adaptive neuro-fuzzy inference system (ANFIS)." *Composites: Part B*, 43, 549–558.

Mahato Kishore Kumar, Rathore Dinesh Kumar, Krishna Dutta and Bankim Chandra Ray. (2017). "Effect of loading rates of severely thermal-shocked glass fiber/epoxy Composites." *Composites Communications*, 3, 7–10.

Michael F Ashby and David R H Jones. Engineering Materials-1, An Introduction to their properties and application, (Second Edition) by, Butterworth-Heinemann, an imprint of *Elsevier Service* (pp.2-3)

.Matykiewicz D., Barczewski M., Knapski D. and Skorczewska K. (2017). "Hybrid effects of basalt fibers and basalt powder on thermomechanical properties of epoxy composites." *Composites Part B*, 125, 157-164.

144

Mazumdar Sanjay K., Composites manufacturing, *CRS Press*, Florida, USA

Merwin J. E. and Johnson K. L. (1963). "An analysis of plastic deformation in rolling contact." *Proceedings of the Institution of Mechanical Engineers*,177: 676.

Nirmal Umar, Jamil Hashim and Low K.O. (2012). "Adhesive wear and frictional performance of bamboo fibres reinforced epoxy composite." *Tribology International*, 47, 122–133.

Omrani Emad, Bamdad Barari, Afsaneh Dorri Moghadam, Pradeep K. Rohatgi and Krishna M. Pillai. (2015). "Mechanical and tribological properties of self-lubricating bio-based carbon-fabric epoxy composites made using liquid composite molding." *Tribology International*, 92, 222–232.

Parnaik Amar, Satapathy Alok and Mahapatra S.S. (2009). "Study on erosion response of hybrid composites using Taguchi experimental design." *Journal of Engineering Materials and Technology*, Vol. 131, 031011-1-16.

Patnaik Amar, Satapathy Alok and Biswas Sandhyarani. (2010). "Effect of particulate fillers on erosion wear of glass polyester composites: A comparative study using Taguchi approach." *Malaysian Polymer Journal*, Vol. 5, No. 2, 49-68.

Pettarin V., Churruca M. J., Felhos D., Karger-Kocsis J., and Frontini P. M. (2010). "Changes in tribological performance of high molecular weight high density polyethylene induced by the addition of molybdenum disulphide particles." *Wear*, Vol. 269, No. 1-2, 31–45.

Petkovic Dalibor, Mirna Issa, Nenad D. Pavlovic, Nenad T. Pavlovic and Lena Zentner. (2012). "Adaptive neuro-fuzzy estimation of conductive silicone rubber mechanical properties." *Expert Systems with Applications*, 39, 9477–9482.

Purushothaman Prabhakar and Thankachan Prashanth. (2014). "Hertz contact stress analysis and validation using finite element analysis." *IJRASET*, Volume 2, Issue XI, 531-538.

Patil Nitinchand and Prasad Krishna. (2015). "Effect of graphite and bronze on strength of chopped E-Glass fiber reinforced epoxy composites." *American Journal of Materials Science*, 5(3C): 121-125.

Patil N. and Prasad K. (2016). "Characterization of short E-Glass fiber reinforced graphite and bronze filled epoxy matrix composites." *Iranian Journal of Materials Science and Engineering*, Vol 13, Number 1, 28-36.

Patil Nitinchand and Prasad Krishna. (2017). "Effect of CuSn filler on tribological performance of glass fiber-epoxy composite." *International Journal of Mechanical Engineering and Technolog*y, Volume 8, Issue 7, 367-378.

Qing Bing Guo, Min Zhi Rong, Guo Liang Jia, Kin Tak Lau, Ming Qiu Zhang. (2009). "Sliding wear performance of nano-SiO_2/short carbon fiber/epoxy hybrid Composites." Wear 266 (2009) 658–665.

Qi Huimin, Ga Zhang, Bernd Wetzel, Werner Osterle, Tingmei Wang and Qihua Wang. (2016). "Exploring the influence of counterpart materials on tribological behaviors of epoxy composites." *Tribology International*, 103, 566–573.

Ru-Min Wang, Shui-Rong Zheng and Yujun Zheng. (2011). Polymer Matrix Composites and Technology, 1st Edition, eBook, *Woodhead Publishing*.

Raju Bhadrabasol Revappa, Bheemappa Suresha, Ragera Parameshwarappa Swamy and Bannangadi Swamy Gowda Kanthraju. (2013). "Investigations on mechanical and tribological behaviour of particulate filled glass fabric reinforced epoxy composites." *Journal of Minerals and Materials Characterization and Engineering*, 1, 160-167.

Rao Sudarshan K., Varadarajan Y. S., and Rajendra N. (2013). "Investigation of the abrasive wear behaviour of graphite filled carbon fabric reinforced epoxy composite - A Taguchi approach." *International journal of mechanical engineering And technology*, Volume 4, Issue 1, 101-108.

Ramesh C.S, Nirupama Mohan, Jain V.K.S and Gudi Harsha R. (2014). "Adaptive Neural network for estimation of sliding wear behaviour of Al6061-Carbon fiber Composites." *Applied Mechanics and Materials,* Vols. 592-594, 1267-1271.

Raja Satheesh R., Manisekar K. and Manikandan V. (2014). "Study on mechanical properties of fly ash impregnated glass fiber reinforced polymer composites using mixture design analysis." *Materials and Design*, 55, 499–508.

Rafiq Ahmad, Nesar Merah, Rachid Boukhili and Muneer Al-Qadhi. (2017). "Impact resistance of hybrid glass fiber reinforced epoxy/nanoclay Composite." *Polymer Testing*, 57, 1-11.

Suresha B., Chandramohan G., Prakash J. N., Balusamy V. and Sankaranarayanasamy K. (2006). "The role of fillers on friction and slide wear characteristics in glass-epoxy composite systems." *Journal of Minerals & Materials Characterization & Engineering*, Vol. 5, No.1, 87-101.

Suresha B., Chandramohan G., Samapthkumaran P., and Seetharamu S. (2007). "Investigation of the friction and wear behavior of glass-epoxy composite with and without graphite filler." *Journal of Reinforced Plastics and Composites*, Vol. 26, No. 1, 81–93.

Sua Feng-Hua, Zhao-Zhu Zhang and Wei-Min Liu. (2008). "Tribological behavior of hybrid glass/PTFE fabric composites with phenolic resin binder and nano-TiO2 filler." *Wear*, 264, 562–570.

Scarcella Jeffrey A. (2008). "Contact stress concentration due to surface irregularity in cylindrical rolling element bearings." *Masters of Mechanical Engineering thesis*, Rensselaer Polytechnic Institute Hartford, CT.

Sagbas A., Kahraman F. and Esme U. (2009). "Modeling and predicting abrasive wear behaviour of poly oxy methylenes using response surface methodology and neural networks." *Metabk*, 48(2), 117-120.

Singhal Manoj and Chawla Vikas. (2010). "Mechanical properties of epoxy resin-fly ash composite." *Journal of Minerals & Materials Characterization & Engineering*, Vol. 9, No.3, 199-210.

Siddhartha, Patnaik Amar and Bhatt Amba D. (2011). "Mechanical and dry sliding wear characterization of epoxy–TiO2 particulate filled functionally graded composites materials using Taguchi design of experiment." *Materials and Design*, 32, 615–627.

Subbaya K. M., Rajendra N., Varadarajan Y. S. and Suresha B. (2012). "Multiple response optimization of three-body abrasive wear behaviour of graphite filled carbon-epoxy composites using grey-based Taguchi approach." *Journal of Minerals and Materials Characterization and Engineering*, 11, 876-884.

Singh Bhoopal Rajpal, Ramvir Singh and Pradeep Kumar Sharma. (2012). "Adaptive neuro-fuzzy inference system for prediction of effective thermal conductivity of polymer-matrix composites." *Modeling and Numerical Simulation of Material Science*, 2, 43-50.

Siddhartha and Gupta Kuldeep. (2012). "Mechanical and abrasive wear characterization of bidirectional and chopped E-glass fiber reinforced composite materials." *Materials and Design* 35, 467–479.

Shivamurthy B., K. Bhat Udaya and Anandhan S. (2013). "Mechanical and sliding wear properties of multi-layered laminates from glass fabric/graphite/epoxy composites." *Materials and Design*, 44, 136–143.

Sudheer M., Karthik Madhyastha N., Kewin Amanna M., Jonthan B., and Mayur Jayaprakash K. (2013). "Mechanical and abrasive wear behavior of metal sulphide lubricant filled epoxy composites." *Polymer Science Volume*, Article ID 242450, 1-8.

Shaikh M. H., Pawar G. J., Sidh J. S. (2013). "Tribological characterisation and morphological study of epoxy composites filled with WS_2 under dry sliding" *International Journal of Science and Research* , Vol 2 Issue 6, 462-465.

Sudheera M., Hemantha K., Rajua K. and Bhat Thirumaleshwara. (2014). "Enhanced mechanical and wear performance of epoxy/glass composites with ptw/graphite hybrid fillers." *Procedia Materials Science*, 6, 975 – 987.

Sayer Metin. (2014). "Elastic properties and buckling load evaluation of ceramic particles filled glass/epoxy composites." *Composites: Part B*, 59, 12–20.

Shen J.T., Top M., Pei Y.T. and De Hosson J.Th.M. (2015). "Wear and friction performance of PTFE filled epoxy composites with a high concentration of SiO_2 particles." *Wear*, 322-323, 171–180.

Shuhimi Fairuz Fazillah, Mohd Fadzli Bin Abdollah, Md Abul Kalam, Masjuki Hassan, Ashafi'e Mustafa and Hilmi Amiruddin. (2016). "Tribological characteristics comparison for oil palm fibre/epoxy and kenaf fibre/epoxy composites under dry sliding conditions." *Tribology International*, 101, 247–254.

Song Fuzhi, Qihua Wang and Tingmei Wang. (2016). "Effects of glass fiber and molybdenum disulphide on tribological behaviors and PV limit of chopped carbon fiber reinforced Polytetrafluoroethylene composites." *Tribology International*, 104 392–401.

Saba N., Paridah M.T., Abdan K. and Ibrahim N.A. (2016). "Dynamic mechanical properties of oil palm nano filler/kenaf/epoxy hybrid nanocomposites." *Construction and Building Materials*, 124, 133–138.

Sun Yousong, Qiang Zhang, Lei Gao, Xianghui Zhou, Yongqi Cheng, Peng Zhang. (2016). "Experimental study on tribological properties of carbon/polytetrafluoroethylene hybrid fabric reinforced composite under heavy loads and oil lubrication." *Tribology International*, 94, 82–86.

Sepe R., Bollino F., Boccarusso L. and Caputo F. (2018). "Influence of chemical treatments on mechanical properties of hemp fiber reinforced composites." *Composites Part B*, 133, 210e217.

Suparta W.and Alhasa K.M., Chapter 2, *Modeling of Tropospheric Delays Using ANFIS*, *Springer Briefs in Meteorology*, DOI 10.1007/978-3-319-28437-8-2.

Suparta W.and Alhasa K.M., Chapter 2, *Modeling of Tropospheric Delays Using ANFIS*, *Springer Briefs in Meteorology*, DOI 10.1007/978-3-319-28437-8-2.

Tibor Goda, Karoly Varadi, Klaus Friedrich and Hermann Giertzsch. (2002). "Finite element analysis of a polymer composite subjected to a sliding steel asperity Part I Normal fibre orientation." *Journal of Materials Science*, 37, 1575 – 1583.

Tahir Noor Ayuma Mat, Mohd Fadzli Bin Abdollah, Rafidah Hasan and Hilmi Amiruddin. (2016). "The effect of sliding distance at different temperatures on the tribological properties of apalm kernel activated carbon–epoxy composite." *Tribology International*, 94, 352–359.

Torres Rubens Bagni, Julio Cesar dos Santos, Túlio Hallak Panzera, Andre Luis Christoforo, Paulo H. Ribeiro Borges and Fabrizio Scarpa. (2017). "Hybrid glass fibre reinforced composites containing silica and cement microparticles based on a design of experiment." *Polymer Testing*, 57, 87-93.

Ulus Hasan, Halil B Kaybal, Volkan Eskizeybek, Omer S Sahin and Ahmet Avc. (2018). "Static and dynamic mechanical responses of $CaCO_3$ nanoparticle modified epoxy/carbon fiber nanocomposites." *Composites Part B*, 12.013.

Varga C.S., Miskolczi N., Bartha L. and Lipoczi G. (2010). "Improving the mechanical properties of glass-fibre-reinforced polyester composites by modification of fibre surface." *Materials and Design*, 31, 185–193.

Varade B.V and Dr. Kharde Y.R. (2012). "Prediction of specific wear rate of glass filled ptfe composites by artificial neural networks and taguchi approach." *International Journal of Engineering Research and Applications (IJERA)*, Vol. 2, Issue 6, 679-683.

Venkata Krishna K. and, Kanny K. (2016). "The effect of treatment on kenaf fiber using green approach and their reinforced epoxy composites." *Composites Part B*, 104, 111-117.

Vijayakumar S. and Karunamoorthy L. (2016). "Modelling wear behaviour of Al–SiC metal matrix composites: soft computing technique." *Tribology - Materials, Surfaces & Interfaces*, 6:1, 25-30.

Wang Shibo, Qian Li, Sha Zhang and Li Pan. (2013). "Tribological behavior of poly (phenyl p-hydroxybenzoate)/polytetrafluoroethylene composites filled with hexagonal boron nitride under dry sliding condition." *Materials and Design*, 43, 507–512.

XU Wenjuan, Hong Gao, Li Lan Gao, Xu Chen and Yong Wang. (2013). "Tensile ratcheting behaviors of bronze powder filled Polytetrafluoroethylene." *Front. Chem. Sci. Eng.*, 7(1): 103–109.

Xing X.S. and Li R.K.Y. (2004). "Wear behavior of epoxy matrix composites filled with uniform sized sub-micron spherical silica particles." *Wear*, 256, 21–26.

Xu Songbo, Aydar Akchurin, Tin Liu, Weston Wood, X.W. Tangpong, Iskander S. Akhatov and Wei-Hong Zhong. (2012). "Wear and friction of carbon nanofiber reinforced HDPE composites." *Journal of Tribology*, Vol. 134, 1-7.

Yousif B.F. and El-Tayeb N.S.M. (2008). "Wear and friction characteristics of CGRP composite under wet contact condition using two different test techniques." *Wear*, 265, 856–864.

Yang Yu-lin, Zhi-ning jia, jin-jiang Chen and Bing-li Fan. (2010). "Tribological behaviors of PTFE-based composites filled with nanoscale lamellar structure expanded graphite." *Journal of Tribology*, Vol.132, 1-7.

Yousif B.F., A. Shalwan, C.W. Chin and K.C. Ming. (2012). "Flexural properties of treated and untreated kenaf/epoxy composites." *Materials and Design*, 40, 378–385.

You Yi-Lan, Du-Xin Li, Gao-Jie Si and Xin Deng. (2014). "Investigation of the influence of solid lubricants on the tribological properties of Polyamide 6 nanocomposite." *Wear*, Volume 311, Issues 1–2, 57-64.

Yesgat A.L. and Kitey R. (2016). "Effect of filler geometry on fracture mechanisms in glass particle filled epoxy composites." *Engineering Fracture Mechanics*, 160, 22–41.

Zhang Hui, Zhong Zhang and Klaus Friedrich. (2007). "Effect of fiber length on the wear resistance of short carbon fiber reinforced epoxy composites." *Composites Science and Technology*, 67, 222–230.

Zhang X. R., Pei X.Q., and Wang Q. H. (2008). "Tribological properties of MoS2 and carbon fiber reinforced polyimide composites," *Journal ofMaterials Science*, Vol. 43, No. 13, 4567–4572.

Zhang G., R. Sebastian, T. Burkhart and K. Friedrich. (2012). "Role of monodispersed nanoparticles on the tribological behavior of conventional epoxy composites filled with carbon fibers and graphite lubricants." *Wear*, 292–293, 176–187.

Zhao Gai, Irina Hussainova, Maksim Antonov, QihuaWang and Tingmei Wang. (2013). "Friction and wear of fiber reinforced polyimide composites." *Wear*, 301, 122–129.

Zhang Yongli, Yan Li, Hao Ma, Tao Yu. (2013). "Tensile and interfacial properties of unidirectional flax/glass fiber reinforced hybrid composites." *Composites Science and Technology*, 88, 172–177.

Zhao Fuyan, Guitao Li, Werner Osterle, Ines Häusler, Ga Zhang, Tingmei Wang and Qihua Wang. (2016). "Tribological investigations of glass fiber reinforced epoxy composites under oil lubrication conditions." *Tribology International*, 103, 208–217.

Zhang Ligang, Ga Zhang, Li Chang, Bernd Wetzel, Baicheng Jim and Qihua Wang. (2016). "Distinct tribological mechanisms of silica nanoparticles in epoxy composites reinforced with carbon nanotubes, carbon fibers and glass fibers." *Tribology International*, 104, 225–236.

Zhao Fuyan, Guitao Li, Ga Zhang, Tingmei Wang and Qihua Wang. (2017). "Hybrid effect of ZnS sub-micrometer particles and reinforcing fibers on tribological performance of polyimide under oil lubrication conditions." *Wear*, 380-381, 86–95.

Zhang Ligang, Huimin Qia, Guitao Li, Ga Zhang, Tingmei Wang and Qihua Wang. (2017). "Impact of reinforcing fillers' properties on transfer film structure and tribological performance of POM-based materials." *Tribology International*, 109, 58–68.

PUBLICATIONS

I. PAPERS PUBLISHED

1. Nitinchand Patil and Prasad Krishna (2015) "Effect of Graphite and Bronze on Strength of Chopped E-Glass Fiber Reinforced Epoxy Composites", *American Journal of Materials Science*, 5(3C): 121-125.

2. N. Patil and K. Prasad (2016) "Characterization Of Short E-Glass Fiber Reinforced Graphite and Bronze Filled Epoxy Matrix Composites", *Iranian Journal of Materials Science and Engineering*, Vol 13, Number 1, 28-36.

3. Nitinchand Patil and Prasad Krishna (2017) "Effect of CuSn Filler on Tribological Performance of Glass Fiber-Epoxy Composite", *International Journal of Mechanical Engineering and Technology*, Volume 8, Issue 7, 367-378.

II. INTERNATIONAL CONFERENCE

1. Nitinchand Patil and Prasad Krishna (2018) "Study of Wear Mechanism of Chopped Fiber Reinforced Epoxy Composite Filled with Graphite and Bronze" at International Conference on Design, Materials & Manufacture (IcDeM 2018), at NITK, Surathkal.

   (Citation: AIP Conference Proceedings 1943, 020112 (2018); doi: 10.1063/1.5029688)

III. POSTER PRESENTATION

1. "Prediction of mechanical properties of chopped E-Glass fiber reinforced epoxy composites" at COPEN-9 National conference, IIT, Bombay.

ACADEMIC CARRICULUM VITAE

Mr. Nitinchand Ramkrishna Patil

B/612, Ramakant Karnik Nagar,

Solapur-413006

Ph: (0217) 2391827

Cell: 9552529252   **e-mail: pnitin239@gmail.com**

Date of Birth   : 23rd September 1973

EDUCATIONAL QUALIFICATION:

Pursing PhD   NITK Surthakl

M.E. Mechanical- Design   PVPIT, Budhagaon.

B.E. Mechanical   WIT, Solapur.

Diploma in Automobile Engg.   SESP, Solapur.

DETAILS OF EDUCATIONAL QUALIFICATION:

Degree	University	Grades/Class
PhD	NITK, Surathkal	
ME (Design Engg)	Shivaji Uni., Kolhapur	Distinction
BE (Mechanical Engg)	Shivaji Uni., Kolhapur	First class
Diploma in Auto Engg	MSBTE, Mumbai	Distinction

PROJECT WORK:

Phd Thesis Title:

Characterization of Fiber Reinforced Epoxy Matrix Composites with Sintered Bronze and Graphite Fillers

ME Mechanical- Design

Designed a Cultivator for the farmer community, which weeds out the weed and helps

to grow the crop. This Cultivator works with an engine which is petrol start kerosene run. This cultivator is manually operated.

BE Mechanical

Designed a two row velocity compounded Steam Turbine working model for the Thermal Laboratory in WIT Solapur. It is operated by a boiler available in WIT.

WORK EXPERIENCE:

1. Worked as Auto Engine Technician at Solapur for Six months.
2. Worked as Lecturer for six years at SPM Polytechnic, Kumathe, Solapur.
3. Worked as Lecturer in College of Engg., Pandharpur for one year (UGC Selection).
4. Worked as Lecturer in BIG College of Engg., Kegaon, Solapur from July 2007 to July 2009
5. Currently working as Associate Professor at NK Orchid college of Engg., and Tech., Solapur since July 2009.

TRAINING PROGRAM ATTENDED:

1. TTTI training arranged by S.P.M.Polytechnic, Kumathe, Solapur
2. GDS-II training program for a week at Sou. Venutai Chavan Polytechnic, Sinhgad, Pune
3. DGS-II training program for Two Week at Apex Institute of Management, Pune.
4. Training at Kirloskar Oil Engines Ltd., Solapur.
5. One week STTP on Vibration & Noise Control at COE, Pandharpur.

I, hereby declare that the information given above is true to the best of my knowledge and belief.

Date:

Place: NITK, Surathkal   Mr. Nitinchand Ramkrishna Patil